Macrophage cell-autonomous adrenergic alpha 1 signaling mediated extracellular matrix remodeling in cardiac regeneration

Inaugural-Dissertation

to obtain the academic degree

Doctor rerum naturalium (Dr. rer. nat.)

submitted to the Department of Biology, Chemistry, Pharmacy

of Freie Universität Berlin

by

Onur APAYDIN

2023

This work was done between November 2017 and September 2023 at Max Delbruck Center for Molecular Medicine in the Helmholtz Association (MDC) in Berlin under the supervision of Dr. Suphansa Sawamiphak.

1st Reviewer: Dr. Suphansa Sawamiphak
2nd Reviewer: Prof. Dr. Petra Knaus

date of defense: 10.06.2024

Acknowledgment

I am deeply grateful to my advisors, Dr. Suphansa Sawamiphak and Dr. Alessandro Filosa, for granting me the chance to be a member of their excellent team and for their unwavering guidance as I navigated my PhD journey. Their expert counsel, continual support, and invaluable insights have been a constant source of inspiration and helped me to become a confident scientist. I couldn't have completed this academic journey without their constructive feedback and encouragement, and I sincerely hope that I will have a chance to work with them again in the future.

I am sincerely grateful to Prof. Dr. Petra Knaus for taking an interest in my project and for being my supervisor at the Freie Universität Berlin.

I would like to sincerely thank Prof. Dr. Michael Gotthardt and Prof. Dr. Dominik Müller for their participation in my committee meetings during my studies and for their invaluable feedback and excellent guidance, providing new perspectives for my work.

I would like to acknowledge the MDC Fish Facility, MDC Advanced Light Microscopy Facility, MDC Genomics Platform, and MDC Flow Cytometry Facility for their excellent support and contributions.

I would like to extend many thanks to all my group members, colleagues, and friends for the great and accommodating environment. I particularly extend my appreciation to Akerke for her incredible contributions to my project, her scientific insights and detail-oriented approach. I am thankful to Anne for her continuous support in providing us with an excellent working environment and for her technical help. To Bhakti and Paul, many thanks for your support in the laboratory in my occasional disoriented times. To my previous group member Laura, many thanks for all the fun memories in the lab and outside, for supporting me all the time.

I would like to thank my oldest friend Serkan Meydaneri for always being with me even when we are not even in the same country. Thanks for all the incredibly happy memories from Ankara to Berlin.

I owe my continuing academic career to my parents, Ferihan and Ahmet, and my sister Sinem. Their never-ending encouragement, love, and support, through good wishes and prayers, was

always felt, even when we are apart. Many thanks to my mother-in-law Ozgul, my sister-in-law and brother-in-law Ilayda and Halil for always providing encouragement and leaving me with happy memories.

Finally, I would like to thank my partner in every aspect of life, my beloved wife Dilem Ceren Apaydin. She is my friend, was my lab mate, was my roommate and she is and always will be the love of my life. Her never-ending love, encouragement, and cheer were the pillars that pushed me through thick and thin. Even in her sadness she was always there for me and always helped me to become the best version of myself. Thank you for being in my life.

Declaration of Independence

Herewith I certify that I have prepared and written my thesis independently and that I have not used any sources and aids other than those indicated by me.

Table of Contents

Abstract

Ischemic heart disease ranks among the leading causes of death worldwide. Following myocardial infarction, cardiomyocyte loss through necrosis leads to inflammation, fibrosis, and permanent scarring, impairing heart function and leaving it susceptible to failure. Clinical efforts employing progenitor or stem cell-derived cardiomyocyte transplantation or utilizing biomaterials to induce cardiomyocyte proliferation, have proven ineffective in renewing the myocardium due to the human heart's almost non-existent inherent self-renewal capacity. Unlike most adult mammals, neonatal mice and several non-mammalian vertebrates demonstrate the ability to regenerate cardiac tissue following myocardial infarction. Cardiac regeneration is a complex process, demanding a delicate orchestration of multiple cellular and molecular events. One fundamental aspect of regeneration is the resolution of scarring following injury and its replacement with new cardiomyocytes, partially attributed to fibroblast inactivation. However, a comprehensive understanding of the entire regeneration process is lacking, impeding the development of effective therapeutic strategies.

The immune response is a significant event following ischemic injury, with macrophages as primary effectors. These cells are implicated in various processes, from dead cell clearance to tissue remodeling. Their initial pro-inflammatory phenotype is critical for cell influx into the injury area, and their subsequent anti-inflammatory phenotype contributes to the activation of fibroblasts, facilitating collagen deposition for extracellular matrix organization. Consequently, exploring the mechanisms that govern macrophage functional diversification is vital for elucidating the regeneration process.

Additionally, the nervous system plays a pivotal role in immune modulation, with sensory neurons capable of relaying the immune state of peripheral locations to the central nervous system to regulate the immune response. Both sympathetic and parasympathetic signaling was shown to be critical for proper regenerative response. Transcriptomic studies in zebrafish have revealed that blocking cholinergic signaling post-cardiac injury impairs the immune response, and sympathetic signaling influences macrophage phenotype. The immunomodulatory capabilities of the nervous system, in conjunction with the multifaceted roles of macrophages, underscore the importance of neuro-immune interactions in cardiac regeneration.

This dissertation revealed previously unidentified neural modulation of myocardial regenerative response and delineated the distinct roles of a macrophage subset. Utilizing zebrafish, known for its robust regenerative capacity, genetic tractability, and larval translucency allowing real-time injury event tracing, to model human myocardial infarction, this study identifies adrenergic receptor alpha-1 (Adra1) as a potent modulator of regenerative response and macrophage diversification. Utilizing a macrophage-specific loss-of-function model for Adra1 signaling and single-cell transcriptomics, this study uncovered the activation of an 'extracellular matrix remodeling' macrophage population that regulates the extracellular matrix composition and turnover. *In vivo* and *ex vivo* validation of the in-silico analyses elucidated the Adra1-activated macrophages' roles in activating a pro-regenerative collagen XII-expressing fibroblast subset through Mdka-Lrp1aa crosstalk, regulating the cardiac regenerative niche, promoting vessel formation and cardiomyocyte proliferation.

In short, this project emphasizes the potential of Adra1-mediated neural input as a key regulator of macrophage function, unveiling a novel mechanism of neuro-immune interactions that modulate fibrosis and myocardial renewal during the regeneration process. The insights into nervous modulation of immune response to regulate cardiac fibrosis and facilitate myocardial self-renewal provide a substantial foundation for development of a much-needed therapeutic strategy for cardiac regenerative medicine.

Zusammenfassung

Ischämische Herzkrankheiten sind weltweit eine der häufigsten Todesursachen. Nach einem Myokardinfarkt führt der Verlust von Kardiomyozyten durch Nekrose zu Entzündung, Fibrose und dauerhafter Narbenbildung, was die Herzfunktion beeinträchtigt und das Herz anfällig für ein Versagen macht. Klinische Versuche, Kardiomyozyten aus Vorläufer- oder Stammzellen zu transplantieren oder Biomaterialien zu verwenden, um die Proliferation von Kardiomyozyten zu induzieren, haben sich als unwirksam erwiesen, da das menschliche Herz kaum über eine eigene Selbsterneuerungskapazität verfügt. Im Gegensatz zu den meisten erwachsenen Säugetieren zeigen neonatale Mäuse und einige Nicht-Säugetiere die Fähigkeit, Herzgewebe nach einem Herzinfarkt zu regenerieren. Die Regeneration des Herzens ist ein komplexer Prozess, der ein fein abgestimmtes Zusammenspiel zahlreicher zellulärer und molekularer Ereignisse erfordert. Ein grundlegender Aspekt der Regeneration ist die Auflösung der Narbenbildung nach einer Verletzung und deren Ersatz durch neue Kardiomyozyten, was teilweise auf die Inaktivierung von Fibroblasten zurückzuführen ist. Es fehlt jedoch ein umfassendes Verständnis des gesamten Regenerationsprozesses, was die Entwicklung wirksamer therapeutischer Strategien behindert.

Die Immunantwort ist ein wichtiges Ereignis nach einer ischämischen Verletzung, wobei Makrophagen als primäre Effektoren fungieren. Diese Zellen sind an verschiedenen Prozessen beteiligt, die von der Beseitigung abgestorbener Zellen bis zum Gewebeumbau reichen. Ihr anfänglicher proinflammatorischer Phänotyp ist entscheidend für den Einstrom von Zellen in den verletzten Bereich, und ihr späterer antiinflammatorischer Phänotyp trägt zur Aktivierung von Fibroblasten bei, die die Ablagerung von Kollagen für die Organisation der extrazellulären Matrix erleichtern. Die Erforschung der Mechanismen, die die funktionelle Diversifizierung der Makrophagen steuern, ist daher für das Verständnis des Regenerationsprozesses von entscheidender Bedeutung.

Darüber hinaus spielt das Nervensystem eine entscheidende Rolle bei der Immunmodulation. Sensorische Neuronen sind in der Lage, den Immunstatus peripherer Orte an das zentrale Nervensystem weiterzuleiten, um die Immunantwort zu regulieren. Es konnte gezeigt werden, dass sowohl die sympathische als auch die parasympathische Signalübertragung für eine adäquate Regenerationsantwort entscheidend sind.

Transkriptomische Studien am Zebrafisch haben gezeigt, dass die Blockade der cholinergen Signalübertragung die Immunantwort nach einer Herzverletzung beeinträchtigt, während die sympathische Signalübertragung den Phänotyp von Makrophagen beeinflusst. Die immunmodulatorischen Fähigkeiten des Nervensystems in Verbindung mit den vielfältigen Funktionen der Makrophagen unterstreichen die Bedeutung der Neuro-Immun-Interaktionen für die Herzregeneration.

In dieser Dissertation wurde eine bisher unbekannte neuronale Modulation der myokardialen Regenerationsantwort aufgedeckt und die differenzielle Rolle einer Makrophagen-Subgruppe beschrieben. Unter Verwendung des Zebrafisches, der für seine robuste Regenerationsfähigkeit, seine genetische Rückverfolgbarkeit und seine larvale Transparenz bekannt ist, die es erlaubt, Verletzungen in Echtzeit zu verfolgen, wurde in dieser Studie der adrenerge Rezeptor alpha-1 (Adra1) als potenter Modulator der Regenerationsantwort und der Makrophagen-Diversifizierung identifiziert, um einen menschlichen Myokardinfarkt zu modellieren. Mit Hilfe eines Makrophagen-spezifischen Funktionsverlustmodells der Adra1-Signaltransduktion und der Einzelzell-Transkriptomik konnte die Aktivierung einer Makrophagenpopulation für den Umbau der extrazellulären Matrix nachgewiesen werden, die die Zusammensetzung und den Umsatz der extrazellulären Matrix reguliert. Die in vivo- und ex vivo-Validierung der in silico-Analysen zeigte, dass Adra1-aktivierte Makrophagen über den Mdka-Lrp1aa-Crosstalk eine pro-regenerative, Kollagen XII-exprimierende Fibroblasten-Subpopulation aktivieren, die die kardiale Regenerationsnische reguliert und die Vaskularisierung und Proliferation von Kardiomyozyten fördert.

Zusammenfassend unterstreicht dieses Projekt das Potenzial des Adra1-vermittelten neuronalen Inputs als Schlüsselregulator der Makrophagenfunktion und deckt einen neuartigen Mechanismus der Neuro-Immun-Interaktionen auf, der die Fibrose und die Erneuerung des Herzmuskels während des Regenerationsprozesses moduliert. Die Erkenntnisse über die nervale Modulation der Immunantwort zur Regulation der kardialen Fibrose und zur Erleichterung der myokardialen Selbsterneuerung bilden eine wesentliche Grundlage für die Entwicklung einer dringend benötigten therapeutischen Strategie für die kardiale Regenerationsmedizin.

1 Introduction

1.1 Myocardial infarction

Heart failure remains a leading cause of death and morbidity worldwide despite the vastly improved prompt revascularization techniques and increased prevalence rates after an acute ischemic event [1–5]. Critical factors contributing to heart failure include hypertension, acute myocardial infarction (MI), and any ischemic event that leads to blood flow obstruction in parts of the heart, resulting in ischemic damage and death of millions of cardiomyocytes [2,4]. Even with the magnitudes of leaps made in detection and treatment techniques for such events that result in cardiomyocyte loss, MI remains the culprit of more than 30% of deaths attributable to heart failure [1–3]. MI leads to heart failure through the persistent scarring caused by the loss of cardiomyocytes [1,2]. Infarcted regions with scarring result in desynchronization during the beating and impaired cardiac output. This increases left ventricular wall stress, triggering morphological changes that compromise overall heart function and eventually lead to heart failure [1,3].

Being one of the significant weights on the global health system with over 190 million cases in recent years, ischemic heart diseases like MI have attracted extensive research interest over the years [1,2,5]. Various strategies have been investigated over 40 years to prevent or reverse the progression to heart failure following MI [1,2,5]. Most of these approaches have targeted left ventricular pathological remodeling after MI or adjusting a person's daily habits or precursor cardiovascular parameters through pharmaceutical interventions [1,2,5]. From renin-angiotensin system blockers such as angiotensin II converting enzyme (ACE) inhibitors to sympathetic nervous system signaling regulators such as beta-blockers, several pharmacological methods exist among these treatment options. Although beta-blockers can reduce recurrent MI risk by 30% and angina risk by 10%, they also have side effects such as worsening heart failure by 10% or increasing cardiogenic shock risk. ACE inhibitors can also improve post-MI survival or reduce the risk of MI. However, they have systemic effects and were shown to worsen renal function. Furthermore, to achieve increased efficiency, combinatorial treatments were shown to be necessary, which increases the load on systemic health. Therefore, a definitive solution to pathological conditions after ischemic injuries has yet to be elucidated [1–4,6,7].

Another major field of research aims to uncover more precise and effective treatments to sustain post-MI damage. This endeavor's straightforward yet challenging question is how to replace the lost cardiomyocytes following MI. To address this, various implantation strategies have emerged. These involve the use of harvested natural or engineered cell types or synthesized biomaterials, which are implanted into the injured heart after MI to replace the lost cardiomyocytes [1,4,8], to compensate for impaired heart function, or induce cardiomyocyte proliferation [1,4,9]. However, several challenges remain, such as optimizing adverse immune responses to implanted cells or biomaterials and achieving sufficient cell renewal or colonization of implanted cells.

The replacement of cardiomyocytes is challenging due to their terminal differentiation and inability to re-enter the cell cycle [1,2,4]. Even though it was shown that humans and other mammals have around 50% cardiomyocyte turnover throughout life [4,10], a timely increase in the insignificant proliferation rate of cardiomyocytes following MI is needed to restore the lost ones. On the other hand, it has been discovered that some organisms, such as amphibians and teleost fish, and even early post-natal mammalians like mice, can replace the damaged tissue after MI with fully functional cardiomyocytes. Given this distinction in proliferative capacity among species, a new and promising field of research has emerged, aiming to combat MI-induced heart failure by regenerating damaged hearts to their fully functional state. [1,2,4,10,11].

1.2 Cardiac regeneration

Among several studies aimed at remedying pathological changes following MI, the repair and regeneration of damaged tissue was particularly focused on. Investigations led to the revealing of events following MI to a certain degree **(Fig. 1.1)**. Currently, MI is seen as an irreversible injury to the myocardium when sustained ischemia, imbalanced perfusion, and altered supply-demand dynamics of blood and oxygen [1,2,4,10,12–15]. Following an MI, the lack of oxygen damages the ventricle, leading to the loss of millions of cardiomyocytes [1,2,4,10]. Necrotic cardiomyocytes trigger an immune response and attract the first line of defense, mononuclear leukocytes, to clear the debris and molecules that could exacerbate pathological levels of immune response [1,2,4,15,16]. This initial response usually lasts 3-7 days post-MI and results in the clearance of necrotic and apoptotic cells and inflammatory particles from the microenvironment, leading to the resolution of the immune response [1,15,16] **(Fig. 1.1)**.

Subsequently, fibrosis is initiated to replace the lost tissue and repair the injury. This process involves deposition and remodeling of the extracellular matrix (ECM) and eventually results in scar formation in the injury area [1,2,4,10,15,17] **(Fig. 1.1)**. Typically, the repair process takes around 5-6 weeks [1,4,10]. The scar formed during this process is persistent and usually followed by another remodeling round, leading to interstitial fibrosis. This fibrotic tissue alters heart muscle contractility, eventually leading to heart failure [1,4,10].

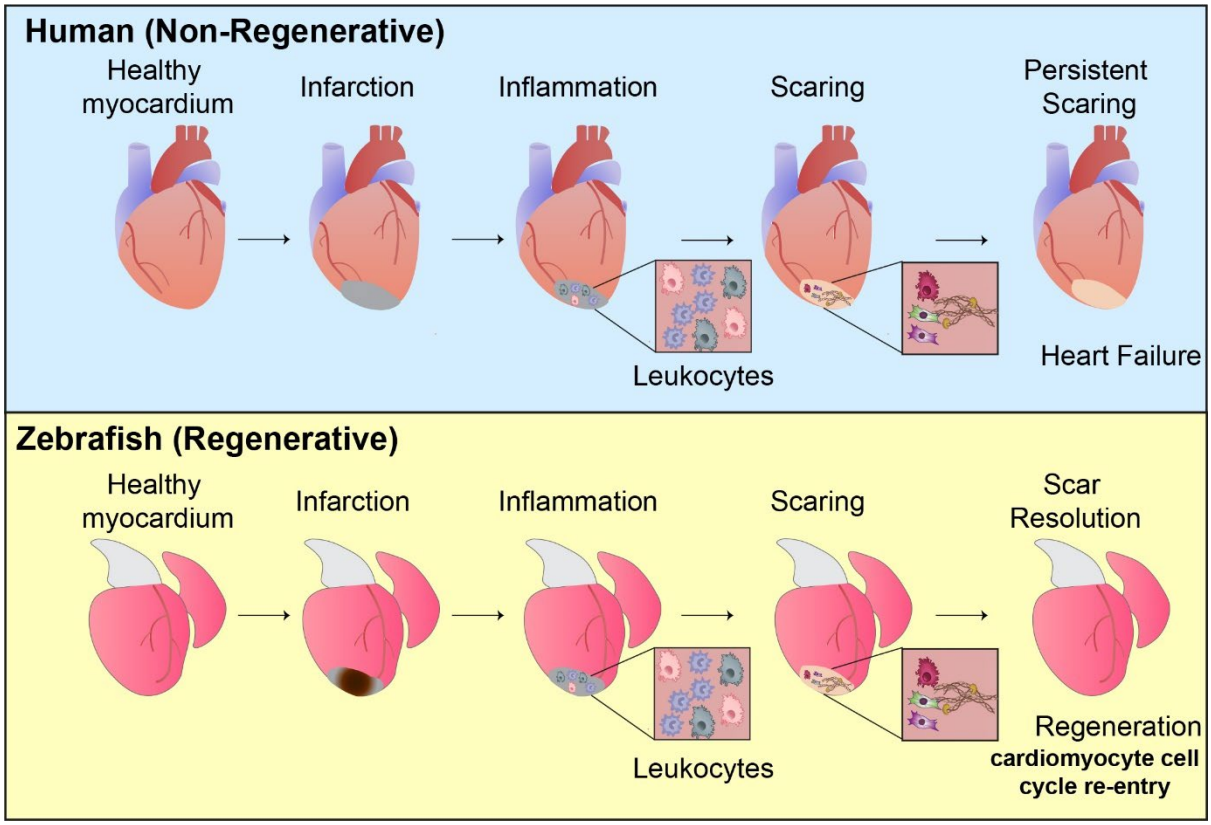

Figure 1.1 Myocardial infarction and following events in non-regenerative (human) and regenerative (zebrafish) hearts. Human and zebrafish heart repair processes are depicted. Post-injury, hearts undergo similar inflammatory phases and form scars in both organisms. In the final phase, the human heart is left with persistent scarring, leading to heart failure. In contrast, the zebrafish heart resolves the scar tissue and replaces it with functional cardiomyocytes, restoring itself to a healthy state. Adapted from Ryan et al. 2020.

Regeneration studies aim to restore the heart function to its initial state after MI. Considering the general stages following MI **(Fig. 1.1)**, the removal of scar tissue and its replacement with functional cardiomyocytes, as well as physiological restoration of the heart microenvironment components, including blood vessels, the lymphatic system, and nerves, is

the primary goal in this field [1,4,12]. Negligible mitotic activity of cardiomyocytes in the human heart was identified as one of the primary reasons behind the failure to regenerate to a fully functional heart [4,10]. Cardiomyocytes, during development, may go through cytokinesis and karyokinesis, but soon after birth, they cease to divide either cytoplasm or nucleus, despite ongoing DNA replication leading to polyploidy [1,4,10,18]. This phenomenon is also observed in other mammals like mice or rodents [1,4,10,18]. Studies suggest that this shared inability for cell cycle re-entry is one of the significant reasons behind the lack of regenerative capacity in mammals [10,18].

Over the years, it was discovered that early post-natal mammals possess an intrinsic regenerative capacity after MI but lose this ability early after birth.[1,2,4,10]. Studies investigating the reasons for this have found that certain amphibians and some teleost fish, such as zebrafish, maintain the ability to regenerate such injuries throughout adulthood **(Fig. 1.1)** [2,4,11,19]. For example, while the initial stages following MI in zebrafish are similar to those in mammals-including the removal of apoptotic cells, fibrosis, and varying levels of inflammatory response-scar tissue in zebrafish is eventually replaced by fully functional cardiomyocytes, and re-vascularization and re-innervation occurs [2,4,10,19]. A critical factor contributing to this regenerative capacity in zebrafish, contrary to mammals, is the continued ability of their cardiomyocytes to re-enter the cell cycle [4,19]. One hypothesis is that the maintenance of both cytokinesis and karyokinesis in zebrafish cardiomyocytes, leading to mononucleated diploid cells, is a key difference between mammals and zebrafish that enables regeneration as these mechanisms irreversibly change in mammals shortly after birth [1,2,4,10,19]. However, a more detailed understanding of the exact mechanisms underlying regeneration remains to be elucidated.

The changes to the heart environment after an ischemic damage and repair process affect not only cardiomyocytes but also fibroblasts, endothelium, and interstitium. Therefore, several strategies have targeted different cell/tissue types to achieve regeneration [1,4,12] and basic research to understand the exact mechanism behind the regenerative function of teleost fish or amphibians [1,4,11,20,21]. Therapeutic approaches often focus on reestablishing blood flow to the injured area or balancing the microenvironment to manage unregulated immune responses. Some examples include methods such as coronary artery bypass grafting surgery (CAGB) [1,22], as well as treating possible blood clotting and imbalanced microenvironment to alleviate non-regulated immune response through pharmacotherapy or thrombolytic therapy [1,3,12,16]. On top

of this, research into the regenerative capacity of organisms such as zebrafish uncovered several critical factors such as content of mono-nucleated cardiomyocytes, collagen content in the fibrotic tissue, ECM regulation and content such as Agrin and Dag1 levels, and metabolic pathway regulation, that differentiate regenerative animals from mammals to adapt new therapeutic approaches [4,10,19,23,24], yet there is still no definitive treatment to fully restore MI damaged heart to its full potential.

Apart from the ability of cardiomyocytes in regenerative animals to re-enter the cell cycle, other systems and cell types were shown to be critical for adequate regenerative capacity. For example, the importance of the immune system through the removal of macrophages (MPs) via clodronate-loaded liposomes [4,25], of fibroblasts through suppression or activation via the manipulation of secreted ECM components such as collagen I-V or matrix metalloproteases (MMPs)[4,17,26], of nerves through chemical sympathectomy or pharmacological inhibition of selective signaling pathways [4,27], and of endothelial cells through lineage tracing and differentiation studies [4,28,29] were established for proper regenerative response. Most of these factors are also vital in early post-natal mammals, which exhibit transient regenerative abilities [2,21,30–32]. However, some of these factors undergo changes shortly after birth, similar to the cardiomyocyte proliferative capacity, resulting in an irreversible shift from regenerative function to mere repair and scar formation [1,2,21].

Overall, the current synopsis on regeneration suggests key differences in several stages of post-MI repair between mammals and regenerative animals like zebrafish. The promise of converting irreversible injury into reversible damage still seemingly hinges on fully understanding these regenerative functions and their underlying mechanisms. In this endeavor, exploring the role of other systems involved in regeneration and communication among them is crucial.

1.3 Immune system in cardiac regeneration

In the intricate spatiotemporal orchestration of events during cardiac repair and regeneration, one of the critical systems involved is the immune system [2,4,15,33,34]. The heart environment has been shown to include several types of immune cells both during physiological conditions and following cardiac injury. MPs, monocytes, neutrophils, dendritic cells (DCs), T and B cells, and mast cells reside in the cardiac environment either through

permanently occupying space since development, namely hematopoiesis, or infiltration later, depending on the situational demand. [2,4,15,33,34].

The immune system is critical for maintaining homeostasis and as the first line of defense; for instance, neutrophils are initial responders to injury or infection, and together with already residing mast cells, they are the first to organize the initial immune response [15,33,34]. In injury cases, for example, neutrophils are attracted to the injury site by damage-associated molecular patterns (DAMPs) released from the necrotic cells, initiating the clearance of the dead cells [4,33–35]. These cells also set the environment as more pro-inflammatory through the secretion of cytokines, including Tumor Necrosis Factor (TNFα) and Interleukin (IL) 6, which orchestrate subsequent immune responses from other immune cell types [4,33–35]. The ensuing pro-inflammatory microenvironment activates both resident and recruited MPs and monocytes [4,33,34]. Natural killer (NK) cells help regulate the initial immune response by limiting the infiltration of pro-inflammatory cells through anti-inflammatory cytokine secretion [33]. Adaptive immune cells are also involved in mounting the immune response and its resolution. Initially, DCs activate the CD8+ T cells, leading to a pro-inflammatory response. Subsequently, CD4+ T cells infiltrate the injury area to regulate MP activity [15,16,33,34]. T regulatory cells contribute to the resolution of the immune response, whereas B cells are found to be essential for pro-inflammatory response by promoting infiltration of pro-inflammatory monocytes and MPs [15,16,33,34]. MPs are critical for multiple functions, including tissue repair, dead cell clearance, killing bacteria, and organ growth from early developmental stages [15,33,34]. Findings on the diverse roles of immune cells—particularly MPs—at different stages of the immune response post-MI and implications of these discoveries for adaptation of regenerative function to mammals attracted more focus onto the role of MPs in regeneration. Despite the leaps made in this field, the exact roles of MPs in regeneration and a detailed understanding of differences between regenerative animals such as zebrafish and mammals require more work for a definitive answer.

1.4 Macrophage diversity and role in regeneration

1.4.1 Macrophage origin and heterogeneity

MPs are found in all tissues and represent a heterogeneous population with diverse roles, ranging from immunity to tissue repair [33,36–38]. Despite years of research attempting to elucidate the various types of MPs, their origin, and their functions in the body [33,36–38], many questions remain unanswered. As a broad definition, they are phagocytic mononuclear cells responsible for tasks such as clearing necrotic debris following injury or responding to pathogens. However, this general definition falls short of capturing their intricate functionalities as well as their origin and mechanism of persistence within tissues [33,36–38]. The traditional view that all MPs arise solely from the bone marrow through circulating blood monocytes has dramatically shifted with the observation that MPs from embryonic progenitors can persist into adulthood and self-maintain by local proliferation. Emerging evidence proposes that MPs may originate from three possible sources: the yolk sac, fetal liver, and hematopoietic stem cells (HSCs) [33,37–39]. During development, organs are populated by other progenitors like erythroid-myeloid-progenitor and, slightly coinciding with these HSCs, both of which can give rise to monocyte and MPs[40–42]. The early-appearing, yolk sac-derived MPs are commonly referred to as 'primitive MPs', whereas MPs appearing later (in mice around E13.5) are believed to stem from erythroid-myeloid-progenitors found in the fetal liver [40–42]. However, the contribution of HSC to these MPs cannot be ruled out. Mature MPs in certain organs were shown to replace the primitive ones or reside with them in those organs [40,42,43]. These are non-fetal liver-derived MPs produced from circulating monocytes, HSCs, and they are either circulating or residing in tissues during development [40–43]. The combination of cardiac MPs from varying origins has a marked effect on cardiac repair. Embryonic MPs play a crucial role in replenishing cardiomyocytes in neonatal mouse hearts, while circulating monocyte-derived MPs typically display an inflammatory phenotype that hinders the repair process [44–46]. A decline in the self-renewal capability of embryonic MPs, along with their gradual replacement by monocyte-derived MPs, has been suggested as a factor contributing to the diminished regenerative capacity found in adult mammalian hearts [47]. Interestingly, the immune responses in zebrafish, both innate and adaptive, are quite comparable to those in higher vertebrates[48]. The

heterogeneous origin of MP populations identified in mammals can also be observed in zebrafish [49–51].

In addition to their origin, MPs are also heterogeneous in terms of their functions, and exert these diverse functions by changing their phenotype in response to different environmental stimuli [36,38,52–58] **(Fig. 1.2).** Classically activated MPs, commonly referred to as 'type 1' or 'M1' MPs, promote the secretion of pro-inflammatory cytokines [38,52,59,60]. On the other hand, alternatively activated MPs, known as 'type 2' or 'M2' MPs, counteract inflammation [38,59–61]. Additionally, M2 MPs play a role in tissue repair, ECM regulation, and wound healing [46,53,56,57,62]. It is important to note that these subtypes serve as simplified models to capture the complexity and plasticity of MP activation. The M1/M2 classification is not a dichotomy but a spectrum [63,64].

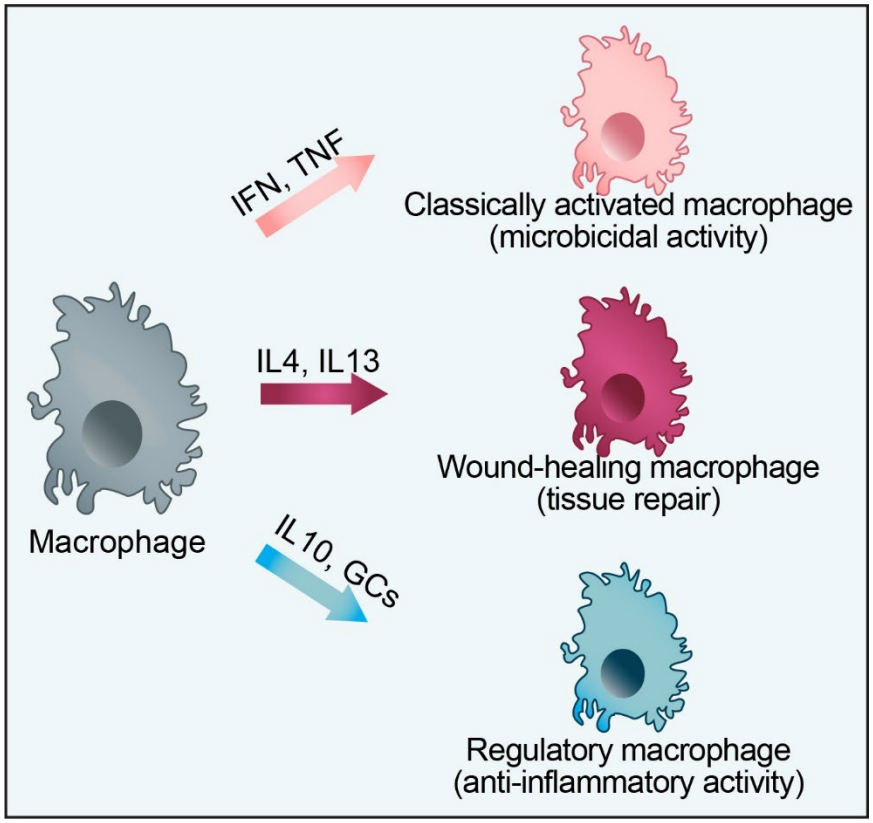

Figure 1.2 MP polarization in response to environmental stimuli. MPs respond to pro-inflammatory stimuli such as IFN and TNF by becoming 'classically activated' with inflammatory and microbicidal functions. They respond to stimuli such as IL4 and IL13 by becoming 'wound healing' MPs with roles in tissue repair, and they respond to stimuli such as IL10 and GCs by becoming 'regulatory' with anti-inflammatory functions.

Another key aspect of MP diversity is their spatial distribution within a fully developed organism. Spatial distribution within various heart regions, such as myocardium, perivascular spaces, and endocardium, can significantly influence their phenotype and function [41,46,58,64–67]. Recent transcriptomic studies unveiled a spectrum of MP subsets within the cardiac tissue, each potentially possessing distinct roles in homeostasis, disease progression, and tissue repair [68–71].

Despite the earlier dogma that MPs residing in the cardiac niche are derived from circulating monocytes, emerging evidence suggests that the presence of a distinct population of resident MPs in the heart that are embryonically derived and capable of self-renewal without a significant contribution from circulating monocytes [45,70–72]. For example, studies involving *Cx3cr1* knockout mice showed that a resident MP pool in the heart originating from embryonic precursors can persist even without hematopoiesis [73]. Transcriptomic analyses deepened our understanding by revealing that this cardiac resident MP pool with embryonic origin expresses specific marker genes, such as *Timd4* and *MHC-II*, albeit at lower levels compared to other MP populations[72]. Furthermore, C-C Motif Chemokine Receptor 2 (Ccr2) negative MPs within this resident pool were shown to sustain themselves through local proliferation rather than relying on monocyte input from the circulation[70,74].

Thus, a comprehensive understanding of the dynamics of MPs, including their origin, localization, and function in the heart, is crucial for developing targeted therapeutic strategies for treating cardiac diseases and injuries.

1.4.2 Role of macrophages in cardiac regeneration

Although studies underlined the importance of MPs during regeneration [37,38,56], conflicting reports make it challenging to comprehend the whole immune response tapestry [36–38,53,55–57,75,76]. MP ablation through knock-out of the *irf8* gene, essential for MP maturation, or chlodronate liposome injection in zebrafish, for instance, has led to impaired regenerative responses such as lower cardiomyocyte proliferation or larger scar size after injury [75,76]. However, excessive expansion of MPs leading to prolonged inflammatory response was also detrimental to proper repair response in mice [77]. These findings so far point towards the need for fine-tuned control of inflammatory/anti-inflammatory response for the apt regeneration process.

MPs are classically activated and pro-inflammatory in the initial phases following cardiac injury [77–79]. Initially, resident MPs respond first to cell debris and DAMPs from the necrotic tissue [38,56,79]. Later, from the spleen and bone marrow, circulating Ly6C-expressing monocytes replace this population [42,70,79–81]. These monocytes infiltrate the tissue and differentiate into MPs with diverse functions [42,81,82]. In this initial pro-inflammatory phase, the secretion of cytokines and chemokines such as TNFα, IL1β, IL6, or Chemokine (C-C motif) ligand 2

(CCL2) help maintain the required proper inflammatory response in the environment [79,81,83]. They contribute to necrotic debris clearing via phagocytosis [79,81]. Phagocytosis leads to upregulation of anti-inflammatory and pro-fibrotic genes such as Transforming Growth Factor β (TGF-β), IL-4, and IL-10 [36–38,54]. This marks the shift towards an anti-inflammatory profile in the injury microenvironment [2,19,36,84,85]. Studies showed the presence of anti-inflammatory MPs in this second phase of regeneration that are involved in tissue remodeling functions [2,11,84,85]. MPs were shown to be involved in the activation of pro-fibrotic myofibroblasts and even contribute to the deposition of ECM components [20,53,84–87]. They balance the MMPs and their inhibitors in the microenvironment, thus allowing ECM turnover to stabilize the injury in non-regenerative models [20,57,87,88]. Their role in ECM regulation, thereby influencing subsequent regenerative processes such as revascularization, was also shown to be critical in regenerative organisms[11,19,57,88–91]. This modulation is critical for non-contractile scar tissue resolution and myocardium renewal[11,19,89–91].

Studies elucidating functional differences and similarities between regenerative and non-regenerative hearts underlined the importance of strict spatiotemporal regulation of the immune response for regeneration [24,51,68,92,93]. Imbalance in this dynamic, for example, an excessive or prolonged 'M1' response could lead to exacerbated tissue damage, fibrosis, and maladaptive cardiac remodeling, potentially culminating in heart failure [2,11,36–38,81,84]. On the other hand, an imbalance favoring an overly dominant 'M2' response could lead to insufficient debris clearance and suboptimal scar formation, thus compromising the structural integrity of the heart [36–38,53,55,57,67,94,95]. For instance, even though the initial stages are similar in regenerative animals, evidence points towards minor but critical differences in immune cell activities that are vital for adequate regenerative capacity [2,4,33,34]. In zebrafish, the absence of MPs impairs regeneration after MI [33,34,76]. MPs that are *Tnfa* +/+ in the early stages post-MI were shown to be essential for proper ECM remodeling and collagen deposition [57,68,69,96,97] whereas *Tnfa*-/- MPs were shown to be critical for scar resolution via ECM turnover [33,57,72,96,97]. These MP functions also influence the subsequent re-vascularization and cardiomyocyte proliferation [11,34,52,67,98–100]. Overall, MPs and monocytes are instrumental in orchestrating the response to cardiac injury [8,11,33,34,67,81]. However, the extent and direction of their influence and the role of diverse subsets and underlying mechanisms are still elusive.

1.4.3 Macrophage interaction with injury microenvironment

MPs are also heterogeneous regarding interaction partners, affecting their functionality through environmental cues [65,81,82,101–103]. Such cues can include various growth factors, cytokines, ECM components, and cell-cell interactions [33,65,101–103] **(Fig. 1.3)**. These elements modulate the behavior of MPs, driving them toward either pro-inflammatory or reparative states, depending on the context[33,65,101–103]. In the cardiac microenvironment, for example, unique factors such as myocardial-derived exosomes, tissue oxygenation levels, and mechanical forces from the beating heart can direct MP polarization [33,65,101–104]. These interactions heavily influence the post-MI outcomes.

The cardiac microenvironment undergoes several changes with activation state transitions of residing cell types. The initial inflammatory phase involves infiltration of immune cell types, recruited by cell debris and signaling molecules increasing in the environment due to dying cells. Fibroblasts are becoming activated, contributing to the initial remodeling of the ECM, making it inducive for further recruitment of required cells. MPs contribute to cell debris clearance through phagocytosis. In the following proliferative phase, distinct fibroblast populations emerge, regulating ECM remodeling by collagen-rich contribution. MPs start to become more anti-inflammatory by signaling mediators in the environment. In this phase, ECM provides a signaling hub for directing residing cells to required functions. In the final maturation phase, fibroblasts and MPs start to return to their homeostatic states, recruited MP numbers subside, ECM becomes more rigid with interstitial fibrosis, and a mature scar is formed (Fig. 1.3).

One of the major interaction groups for MPs is fibroblasts, and their primary regulation targets ECM [20,36,57,67,86,94]. For instance, studies in axolotl showed that MP depletion leads to impaired fibrosis [20,105]. MPs were shown to secrete collagen components such as collagen I or collagen IV in zebrafish after injury, and it was shown in vitro that human MPs could secrete type VIII collagen [33,56,68,106]. The interaction of MPs with ECM and fibroblasts is also diverse depending on the MP subtype[57,67,107–109]. In line with this information, M1-like MPs were shown to be able to upregulate several MMPs, such as MMP1, 3, 10, 13 [57,67,107–109]. This is thought to be facilitative of necrotic debris cleaning and establishing the wound area for the upcoming remodeling events [33,34,38,57,110]. In the anti-inflammatory reparative phase, MPs are shown to upregulate genes such as vascular endothelial growth factor (VEGF), myeloid-

derived growth factor, collagen V and XII, which are in various studies shown to be facilitative of neo-vascularization, proliferation of neighboring cells or remodeling of scar tissue [75,100,111–116]. It was shown that in neonatal mice, depletion of MPs leads to impaired neo-vascularization [24,44,46]. In zebrafish, it was revealed that MPs act as chaperons for capillary network formation after injury [117]. They are also shown to express factors like TGF-β and IL10, known activators of pro-fibrotic fibroblasts [36,67,94]. A mouse model cardiac injury study demonstrated that type V collagen deficiency in pro-fibrotic fibroblasts leads to increased scar size, and several single-cell RNA-sequencing (scRNAseq) studies showed that MPs could also express collagen V in zebrafish [71,116,118]. All the findings so far showing MPs with fibroblast-like expression profiles in some cases lead researchers to hypothesize that MPs might undergo fibroblast-like transition [86]. However, conflicting findings didn't provide a conclusive result yet [36,67,87,94]. Therefore, even though both ECM deposition/turnover and activation of critical fibroblast types require MP involvement, the underlying mechanisms of this involvement are still unclear.

Another role of MPs is to support the transition from a pro to an anti-inflammatory profile in the environment [33,36–38,91]. MPs start to switch their profile to more anti-inflammatory through the expression of TGF-β and IL10[33,34,36,38]. On top of this, other mechanisms were shown to be potentially crucial for the microenvironmental change in inflammatory profile[9,15]. For instance, LDL receptor-related protein 1 (LRP1), a scavenger receptor involved in mostly regulation of diverse molecule availability in the microenvironment, was shown to be potentially involved in the recruitment of M2-like activated MPs[107,108,119,120]. LRP1 deletion or inhibition was implicated in the upregulation of IL1b, TNFa, and CCL2, known pro-inflammatory genes, upregulated in the initial phases after injury[120–122]. TGF-β signaling, on top of changing the MP phenotype, is also vital for fibroblast activation and fibrosis regulation[20,36,67,87,94]. LRP1 depletion was also shown to reduce TGF-β response in myoblasts[123]. In a murine skeletal muscle damage model, for instance, it was demonstrated that the LRP1/decorin modulatory pathway increases in correlation with TGF-β and connective tissue growth factor, which are essential for proper regeneration and fibronectin accumulation[124]. LRP1 was shown to promote fibroblast survival, proliferation, and activation, which sets the environment for following scar formation[121]. Even though the exact mechanisms of how MPs contribute to inflammatory profile change of the microenvironment, it is undeniable that they are critical for this process.

Overall, there is a plethora of evidence about the interaction of MPs with other actors in the cardiac regeneration niche, pointing out the critical role of diverse MP subsets. However, a clear picture of the multi-system interactions and underlying mechanisms regulating the general regenerative response is still missing.

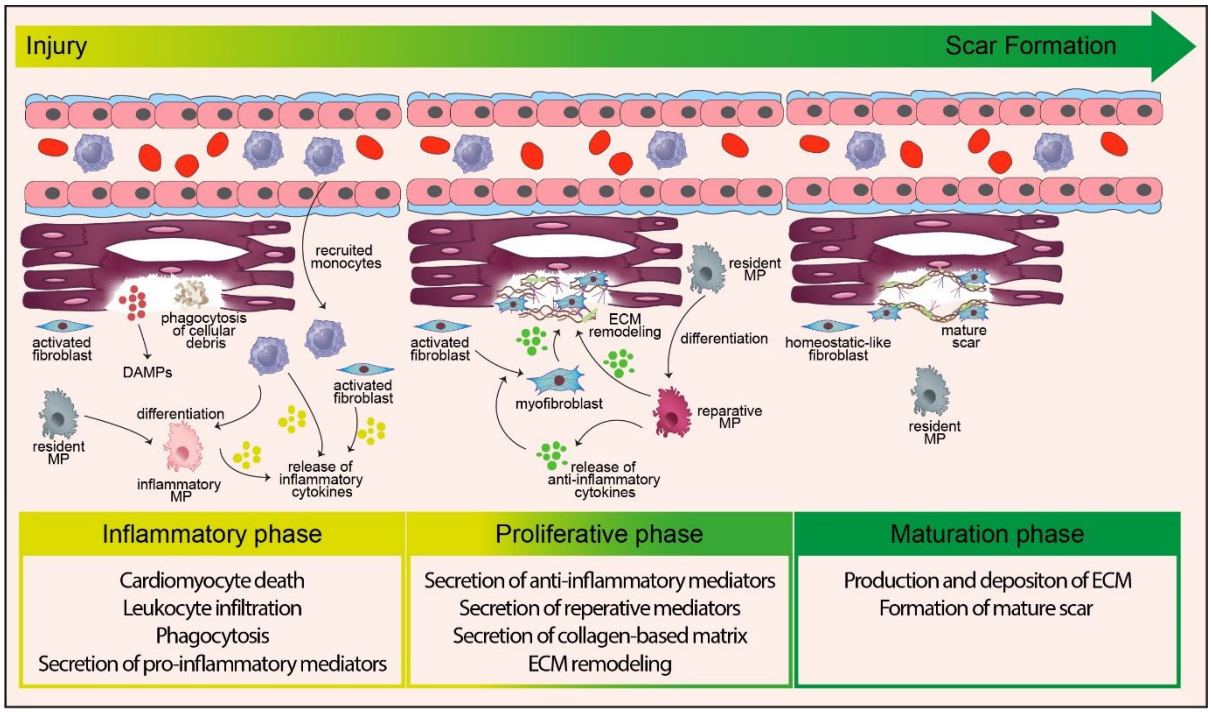

Figure 1.3 Cardiac microenvironment phases following myocardial infarction. Dynamic changes occur within the cardiac microenvironment during tissue repair, delineating three distinct but interrelated phases: inflammatory, proliferative, and maturation. In the initial inflammatory phase, immune cells infiltrate the damaged area, drawn by increased levels of cell debris and signaling molecules. Concurrently, fibroblasts become activated and start remodeling the ECM to facilitate the recruitment of additional cells. MPs contribute to clearing cellular debris through phagocytosis. The proliferative phase sees a shift in fibroblast populations that produce collagen-rich ECM, while MPs take on an anti-inflammatory role influenced by local signaling mediators. The ECM serves as a crucial signaling hub during this stage, directing cell behavior for tissue repair. Finally, the maturation phase marks a return to homeostasis: fibroblasts and MPs revert to their baseline states, the number of recruited MPs decreases, the ECM stabilizes into a more rigid structure through interstitial fibrosis, and a mature scar is formed.

1.5 Fibroblasts and ECM in regeneration

1.5.1 Fibroblast role in cardiac regeneration

Traditionally perceived as a homogenous milieu, the cardiac environment is now recognized to harbor a remarkable heterogeneity of fibroblast populations, each with distinct origins, markers, and functions [17,87,125]. The appreciation for this intricacy emanated from lineage tracing and single-cell transcriptomic analyses[17,87,125,126]. For instance, utilizing the Postn-CreER system to trace fibroblasts, it became evident that different fibroblast subpopulations emerge at various developmental stages, originating from the epicardium and endocardium[127,128]. Additionally, the advent of scRNAseq unveiled distinct transcriptional profiles among cardiac fibroblasts, highlighting differences in ECM component synthesis, receptor expression, and growth factor production[17,87,127,128]. Collagen diversity is an example of the distinct functions of fibroblasts. Specific subpopulations were shown to have elevated expression of collagen XII and collagen V, which are believed to contribute to the intricate architecture of the cardiac ECM and modulate fibroblast-collagen interactions[17,111–113,116]. Therefore, it is imperative to appreciate the importance of the heterogeneity of fibroblasts and their role in the modulation of the cardiac microenvironment **(Fig. 1.3)**.

Fibroblasts are the primary cell type that regulates ECM after MI in mammalian and zebrafish hearts, and they exert their influence by transitioning between quiescent and activated states in response to environmental cues[17,86,87] **(Fig. 1.3)**. They are mostly inactive in homeostasis conditions with minimal proliferative and ECM regulatory activity[17,129–131]. Hypoxia conditions, growth factors, or tissue injury can trigger their activation[17,129–131]. For instance, in post-cardiac injury, a distinct subset of fibroblasts undergoes activation, transitioning to myofibroblasts characterized by the expression of alpha-smooth muscle actin (α-SMA) and the enhanced production of ECM proteins[94,129,130,132]. While initially beneficial for tissue stability, the resultant fibrotic response can impede functional cardiac regeneration in non-regenerative organisms such as adult mammals[17,24,131,133]. Conversely, fibroblast activity in regenerative organisms like zebrafish is precisely modulated, ensuring transient scar formation followed by complete cardiac tissue restoration[17,24,129–131,133,134].

The functional regulation process of fibroblasts, driven by factors such as TGF-β and mechanical stress, is essential for initial wound closure but can precipitate pathological fibrosis

if unchecked [17,129–131]. MPs were shown to be one of the primary activators, resulting in fibroblast differentiation to myofibroblasts [17,94,129–131]. Experiments utilizing murine models with targeted deletion of the *Tgfb1* gene showed attenuated fibroblast activation and reduced scar formation post-MI [135,136]. On top of this, indicating the involvement of MPs in the activation of fibroblast subsets, a study with *Ccl2*, the ligand for *Ccr2*, knockout mice, which have impaired MP infiltration post-MI, displayed diminished fibroblast activation and reduced scar formation, underscoring the importance of both MP and fibroblast heterogeneity [137]. MP input can be attributed mainly to the shift in the expression profile after the debris clearance following injury [38,81]. Phagocytic debris clearance leads to TGF-β upregulation, activating fibroblasts, resulting in abundant ECM component deposition or ECM regulatory enzyme secretion [36,38,67,81,94]. Concurrently, fibroblasts can secrete chemokines, such as CCL2, promoting MP recruitment and polarization [137]. In regenerative species, MP-fibroblast interactions appear transient and controlled, fostering a milieu conducive to regeneration [20,36,94]. In contrast, in non-regenerative models, persistent activation of this crosstalk can exacerbate fibrosis, compromising cardiac function [36,67,94].

Understanding the regulatory networks guiding cardiac fibroblasts and MP behavior in distinct organisms can provide pivotal insights for therapeutic advancements in cardiac regeneration.

1.5.2 Extracellular matrix remodeling role in cardiac regeneration

Regulation of ECM components plays a pivotal role in cardiac regeneration[88]. Following cardiac injury, a swift deposition of ECM components, predominantly driven by collagen isoforms such as COL1A1 and COL3A1, stabilizes the damaged tissue, and this early response is governed by resident fibroblasts and infiltrating immune cells, particularly MPs[1,10,57,67,94,131]. Notably, specific collagens exhibit dynamic changes: Collagen V and Collagen XII are involved in the initiation and organization of the fibrillar structure of the ECM and provide the developing ECM with elasticity[111–113,116,138]. At the same time, Collagen IV establishes the basement membrane architecture[139]. Responding to cues such as TGF-β, Midkine (MDK), reactive oxygen species, and metabolic changes in the microenvironment, resident fibroblasts modulate these ECM transitions, affecting subsequent fibroblast proliferation and migration[17,87,129,130]. MPs, on the other hand, play dual roles: secreting matrix components and

cues, including MDK, a heparin-binding growth factor that influences cellular adhesion and migration, and regulating fibroblasts through growth factors like TGF-β[36,57,67,68,94,140,141]. The physical properties of the ECM, like stiffness, evolve as the injury progresses and directly influence resident cardiac cell behaviors [36,88,131] **(Fig. 1.3)**.

In regenerative organisms like the zebrafish, efficient removal of these ECM components, orchestrated by MMPs such as MMP9, facilitates cardiomyocyte proliferation and heart muscle regeneration[17,71,129,131,142,143]. Contrastingly, in non-regenerative organisms like adult mammals, persistent activation of fibroblasts and sustained MP signaling often leads to pathological fibrosis, with the ECM failing to return to its homeostatic composition, thus impeding regeneration[24,129,131,142]. The differential regulation of the ECM in tandem with MP behavior underscores the complexity of cardiac repair mechanisms and highlights the divergence between regenerative and non-regenerative organisms in addressing cardiac injury.

1.6 Autonomic nervous system in regeneration

The autonomic nervous system (ANS) serves as a regulatory conduit between the central nervous system (CNS) and peripheral organs across vertebrates, with both zebrafish and mammals exemplifying its foundational architecture [144–146]. In each, the ANS bifurcates into the sympathetic and parasympathetic divisions, orchestrating an array of involuntary physiological processes[144,146] **(Fig. 1.4)**. In the context of neurochemical signaling, both zebrafish and mammals deploy catecholamines, including norepinephrine, for sympathetic communication, targeting a spectrum of α- and β-adrenergic receptors like ADRA1 and ADRB2[144,146–148]. Conversely, the parasympathetic dialogue is primarily mediated by acetylcholine, interacting with muscarinic and nicotinic receptors in both organisms[144,146–148]. However, the common point of both ANS branches is that all the receptors are G protein-coupled[149–151]. G protein-coupled receptors (GPCRs) represent one of the most extensively studied and diversified protein families, pivotal in transmitting extracellular signals into cells[149,150]. Downstream activation mechanisms for GPCRs of sympathetic signaling can be summarized as follows; the α-adrenergic receptors, comprising of ADRA1 and ADRA2, predominantly activate phospholipase C (PLC) through the Gq protein, leading to inositol triphosphate (IP3) production and consequent intracellular calcium mobilization[151,152] **(Fig. 1.5)**. In contrast, β-adrenergic receptors, notably ADRB1, ADRB2, and ADRB3, are mainly

coupled to Gs proteins, which stimulate adenylate cyclase, augmenting cyclic AMP (cAMP) levels and activating protein kinase A (PKA)[151,152] **(Fig. 1.5)**. Other G proteins, notably Gi and Go, can act diversely by inhibiting adenylate cyclase, reducing cAMP[150,152,153] **(Fig. 1.5)**. Parasympathetic signaling receptors such as muscarinic acetylcholine receptors, are a classic example of utilizing these G proteins[149,150,153,154]. Notably, the M2 receptor, when activated, couples to Gi, attenuating heart rate and myocardial contractility[149,150,154]. On the other hand, the M3 receptor, prominent in smooth muscle, engages Gq, promoting muscle contraction[149,155]. Additionally, some receptors can couple with multiple G proteins. The muscarinic M3 receptor, besides engaging Gq, can also activate Go in specific contexts[149,155].

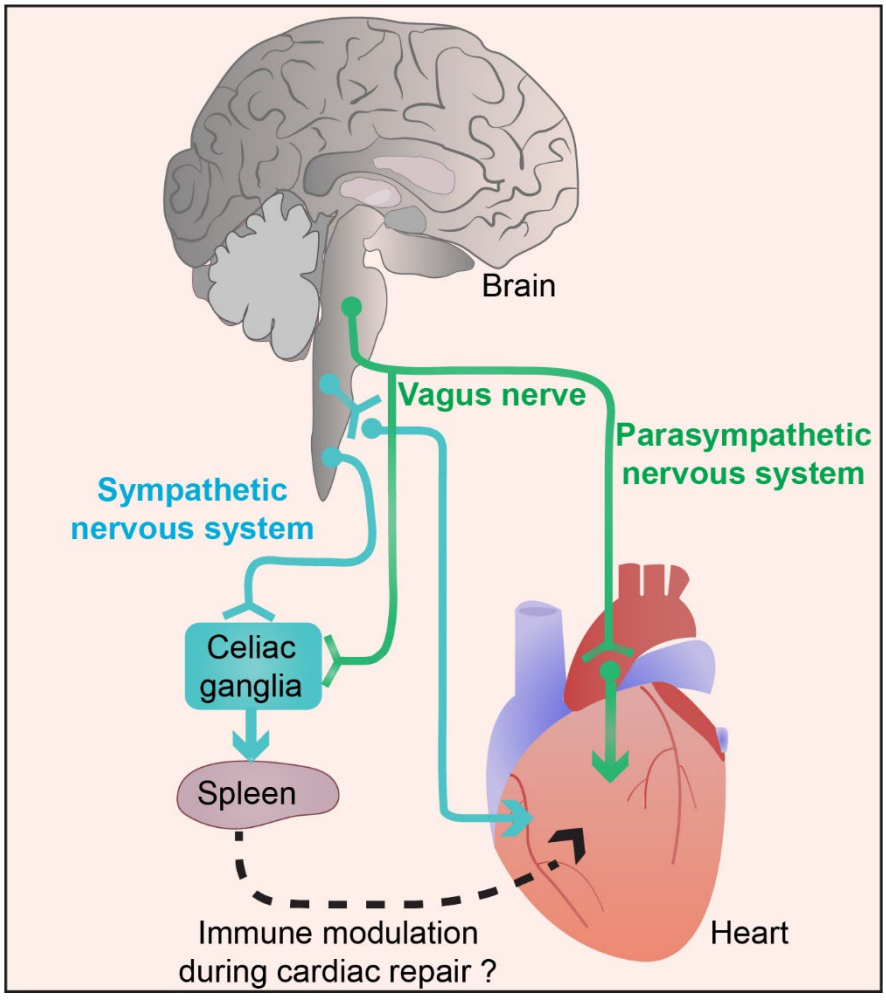

Figure 1.4 Autonomic nervous system and its interaction with the heart. Schematic representation of two branches of the ANS, sympathetic and parasympathetic, and the primary pathways through which they can interact with the heart. Both sympathetic and parasympathetic input were shown to effect the cardiac repair. They may influence immune response by an impact on spleen, probably through celiac ganglia, or locally in the heart through signaling mediators. The nervous system has a multifaceted interaction scheme. However, the mechanisms underlying its ultimate influence on cardiac repair still require elucidation. Adapted from Filosa and Sawamiphak 2021.

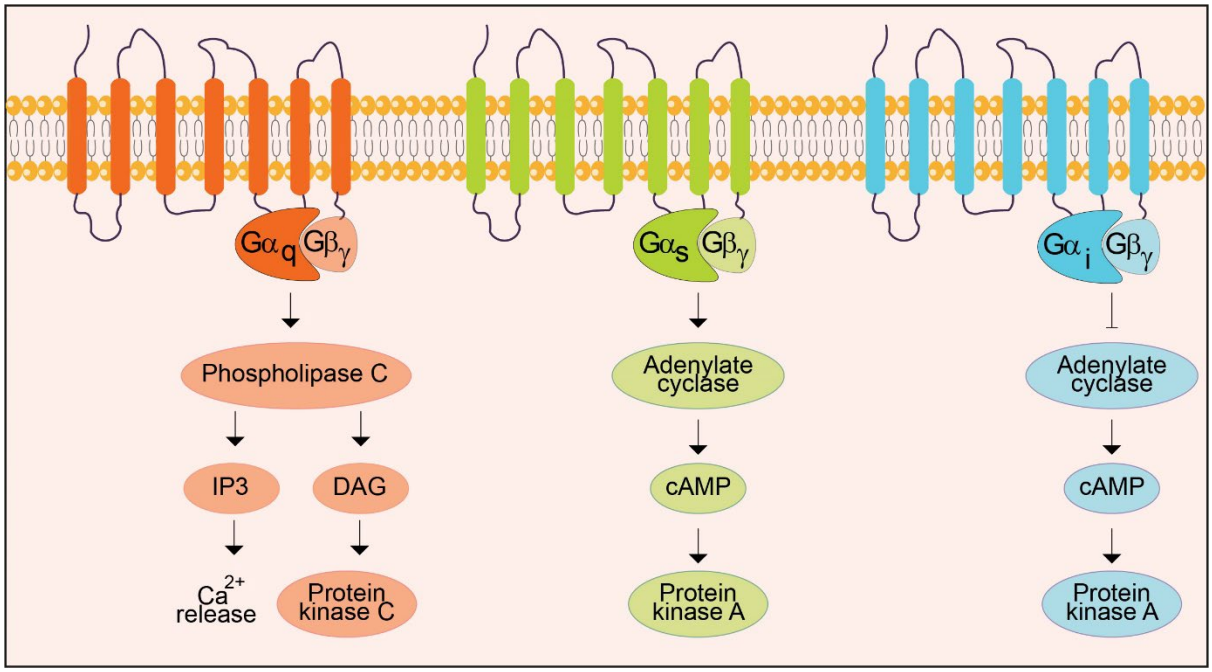

Figure 1.5 G protein-coupled receptor signaling pathway. Diagram showing the downstream signaling pathways of different G protein subtypes coupled receptors. Gq-coupled receptors signal through PLC and subsequent IP3 production. Diacylglycerol (DAG) leads to protein kinase C (PKC) activation. Gs-coupled receptors signal through adenylate cyclase activation and cAMP production, leading to PKA activation. Contrary to Gs, Gi-coupled receptors can inhibit adenylate cyclase and downstream cAMP production. All G protein types and coupled receptors ultimately lead to diverse consequences in the cell.

The ANS and its intricate molecular signaling cascades are critical in cardiac repair and regeneration regulation[27,30,145,156,157]. Several studies underlined their importance in both regenerative and non-regenerative organisms [27,30,145,156,157]. For instance, a salamander study showed that nerve signals are required for proper regenerative response after limb loss [27,158]. Furthermore, studies in zebrafish showed that blocking sympathetic signaling through adrenergic signaling antagonists impairs the regenerative response of the heart [27,156]. Further studies showed the requirement of cardiac innervation for regenerative response in zebrafish and proper reparative response in mice following MI [30,156]. When sympathetic nerves degenerated, both responses were impaired, indicated by increased scar size in zebrafish and increased fibrosis and cardiac function in mice [27,30,156]. Furthermore, it was shown that with chemical sympathectomy in neonatal mice hearts, regeneration was impaired[30]. Although several studies indicate a critical role for neuronal influence on the regenerating heart, the underlying mechanism for how ANS exerts this influence still needs to be elucidated.

1.6.1 Neuro-immune interactions in cardiac regeneration

Emerging evidence provides insights into the mechanistic underpinning of neuronal influence on regeneration by showing the inflammatory dynamics as one of the primarily affected processes [149,157,159,160]. The dynamic interplay of these systems in physiological and regenerative contexts presents divergences. Notably, zebrafish harness their ANS in facilitating robust regenerative processes, especially in cardiac tissues, whereas mammalian counterparts exhibit more restrained regenerative outcomes, albeit with ANS still modulating tissue remodeling responses[77,149,157,159–162].

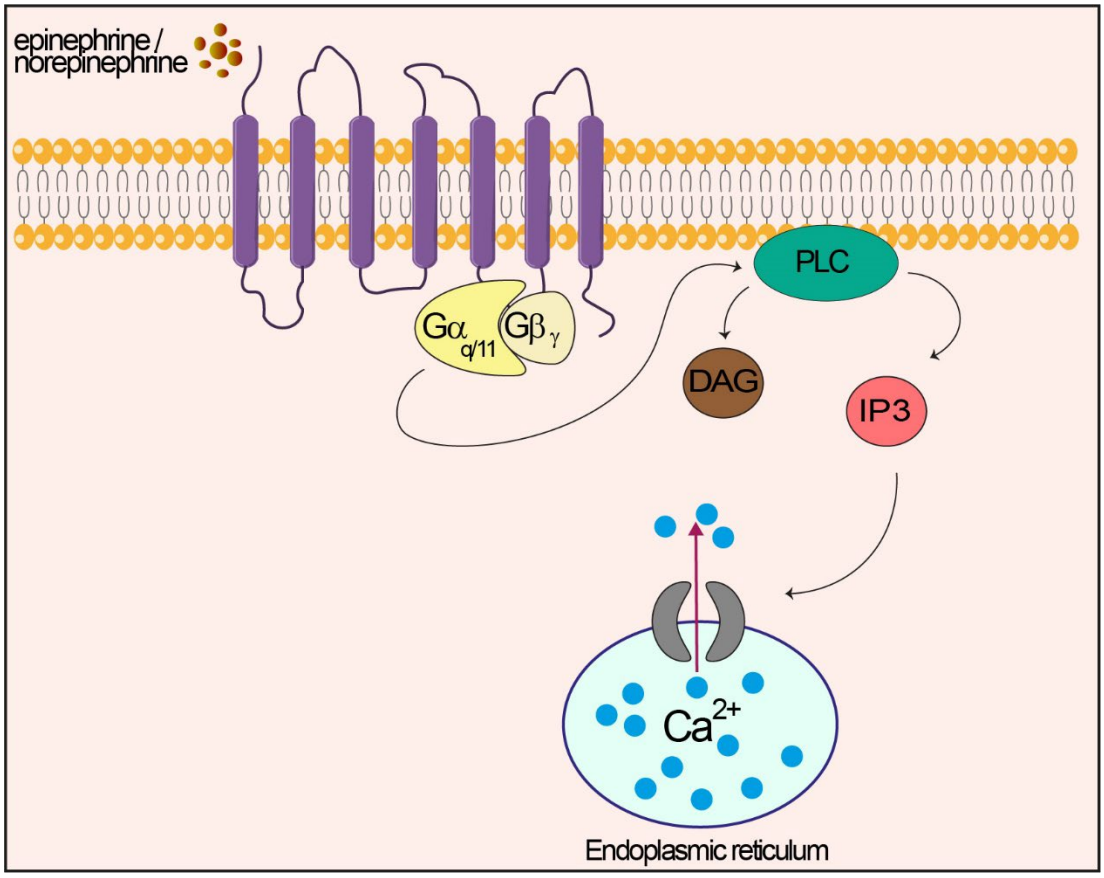

Figure 1.6 Gq-coupled receptor signaling induced by catecholamines. Diagram showing the downstream pathway of Gq-coupled receptor signaling. When induced by epinephrine or norepinephrine, phospholipase C (PLC) and subsequent IP3 production occurs. IP3 releases calcium from intracellular stores, such as endoplasmic reticulum. Activation of the Gq-coupled receptor signaling was shown to rely on the interaction of 3rd intracellular loop of the receptor and Gq protein subunit.

Focusing on ANS branches separately, sympathetically driven processes are diverse; for instance, stimulation of the ADRB2 receptor triggers a cascade involving cAMP and downstream protein kinases, modulating cardiomyocyte function and survival [151,152,163,164]. Additionally, the ADRA1 receptor activates PLC through Gq protein-mediated pathways, leading to the production of IP3 and DAG [151,152,163–165]. This elevation in IP3 triggers calcium release from intracellular stores and influences cellular processes, including those in MPs [163,164,166] **(Fig. 1.6)**. It was observed that ADRA1 stimulation can have nuanced effects. Some studies suggest that activation of ADRA1 might promote pro-inflammatory M1 MP polarization, characterized by increased production of inflammatory cytokines like IL-6 and TNFα [163,166,167]. At the same time, ADRA1 activation is also linked to a shift toward a pro-fibrotic phenotype, characterized by the augmented secretion of factors such as TGF-β that are central to ECM synthesis and fibrosis initiation [163,165,166]. As such, the ADRA1 pathway in MPs has garnered attention as a potential therapeutic avenue to fine-tune tissue repair mechanisms in response to injury; however, it still lacks a complete understanding.

The parasympathetic arm, acting mainly through acetylcholine acting on muscarinic receptors, exerts a scope of anti-inflammatory actions, which are crucial in tempering the post-injury inflammatory response [27,157,168]. For instance, cholinergic signaling blocking was shown to impair regeneration through an excessive inflammatory response in zebrafish [27]. Also, in mice, it was shown that the cholinergic receptor nicotinic alpha 7 subunit (CHRNA7) promotes inflammation suppression through MP phenotype modulation [168–170]. This regulation was shown to be important for the prevention of excessive fibrosis [27,31]. Other studies showed that lymphocytes from spleens of vagotomy-applied mice had increased pro-inflammatory phenotype marked by high IFNγ and TNFα expression [171,172]. Moreover, when specific pathways involving IP3 and calcium modulation were targeted, this further illuminated the nuances of how ANS signaling intersects with cardiac and immune responses [173–175]. However, due to the intricacy of signaling networks involved in this interaction and the global effect of nervous signaling on other cell types and primarily on cardiac function, it was not possible to develop a targeted therapy with a compound effect [31,156]. Therefore, despite the provided insights, the role of neuro-immune interactions in cardiac regeneration still requires further research.

1.7 Zebrafish as a model organism

The zebrafish (*Danio rerio*) has steadily ascended as a preferred model organism in cardiovascular research, especially in the study of cardiac injury and repair mechanisms [91,133,176–178]. Its transparent embryos, coupled with its rapid developmental pace, make it an ideal candidate for real-time visualization of cardiogenesis and injury dynamics [11,91,92,133,176,178]. At the molecular level, zebrafish possess a high degree of genetic conservation with mammals, facilitating the translation of findings [91,92,147,176–178]. A hallmark study by Poss et al. unveiled the zebrafish's astonishing capacity to regenerate its heart after apex resection, a phenomenon largely absent in adult mammals [90]. This regenerative process is underpinned by the reactivation of the myocardial program, with genes such as *gata4*, *hand2*, and *tbx5* playing instrumental roles [179–181]. Genetic lineage tracing experiments have shown that pre-existing cardiomyocytes, rather than a progenitor population, are the primary source of new cardiac tissue following injury [89,179,182]. Moreover, the zebrafish model has also elucidated the intricate interplay between cardiomyocytes and the immune system during regeneration [33,183,184]. Notably, a study by Huang et al. highlighted the essential role of MPs in clearing necrotic debris post-injury, with subsequent experiments revealing complex signaling crosstalk involving factors like TNFα that promote cardiomyocyte proliferation [185]. Given its unparalleled regenerative capabilities and genetic tractability, the zebrafish will undoubtedly continue to shed light on cardiac repair's molecular and cellular orchestration, offering potential therapeutic insights for mammalian heart diseases.

1.8 Aim of the thesis

Ischemic heart disease is a predominant global health concern, with the central issue being the irreversible loss of cardiomyocytes, leading to fibrotic scar formation, which impairs cardiac function. While certain organisms inherently possess cardiac regenerative capabilities after injury, the human heart demonstrates limited self-renewal ability, emphasizing the importance of understanding regenerative mechanisms. As crucial mediators in both inflammatory and reparative responses, MPs exhibit distinct subsets with varied roles in heart repair. This phenotypic diversity, observed in mammals, is also evident in regenerative organisms like zebrafish, where MPs regulate fibroblast differentiation and contribute to fibrosis through collagen deposition. The nervous system, which maintains immune

homeostasis, interacts profoundly with the immune response, especially MPs, to efficiently regulate inflammation and subsequent repair. Recent studies indicate the intrinsic role of both the sympathetic and parasympathetic branches of the ANS in heart regeneration. However, targeted therapies with isolated effects are hard to develop due to the varying effects of nervous signaling on cardiac function or wide expression of some of the receptors involved in these signaling in multiple cell types. Thus, it is pivotal to grasp the multifaceted influence of specific MP pools in this nexus, as their capacity to orchestrate temporally precise and harmoniously balanced inflammatory and fibrotic responses on top of their modulation by ANS interactions, holds the key to innovative therapeutic interventions. Studies so far provide some insights into the critical role of the players in this nexus, either separately or partially in relation to others. However, comprehension of the whole regenerative tapestry is still missing a lot of links. Therefore, a deeper understanding of neuro-immune interactions in cardiac repair is imperative for advancing cardiac regenerative medicine. Accordingly, the primary objective of this dissertation was to explore how diverse MP subsets orchestrate the neuronal influence on the regenerating heart, particularly through interactions with other cardiac niche components, leading to scar-free myocardial repair.

More specifically, the project focused on the following points.

1. Examining the neural signaling pathways pivotal to the regenerative response, probing the extent to which MPs mediate these effects on the recuperating heart.
2. Deciphering the ways distinct MP subpopulations influence and adjust regenerative outcomes in response to neuronal input.
3. Investigating subsequent biological processes to gain insights into the mechanisms underlying the MP modulation of regenerative responses and delineating their interactions with other cardiac niche residents, namely fibroblasts, to pinpoint pathways that might redefine therapeutic interventions for cardiac injuries.

2 Materials and Method

2.1 Materials

2.1.1 Laboratory devices

	SUPPLIER	CAT NUMBER
Agarose Gel Chamber	Thermo Scientific	Owl Easycast B1
Bacteria Incubator	Infors HT	N/A
Cell Culture Incubator	Binder	CB210
Centrifuge	Eppendorf	5417R
Cryostat Microtome	Leica	N/A
Electrophoresis Power Supply	BioRad	PowerPac Basic
Fluorescence-Activated Cell Sorting	BD Biosciences	Aria II
Fluorescent Microscope	Olympus	SZX16
Heating Block	Eppendorf	5382000015
Illumina NovaSeq 6000	Illumina	N/A
Incubator Zebrafish	Velp Scientifica	FOC215L
Incubator 37°C	LLG Labware	uni INCU 20
Leica DM6 CFS confocal microscope	Leica	DM6 CFS
Steamer	WMH	N/A
Magnetic Stirrer	VWR	VMS-C7
Magnetic Stir Bar	Carl Roth	X171.1
Microscale	Fisher Scientific	PAS214
Microinjector	World Precision Instr.	PV820
Microinjection Molds	MDC, self-made	N/A
Microwave	Exquisit	N/A
Mini Centrifuge	Santa Cruz	N/A
Mini Vortex	Carl Roth	HXH6.1
Nano Drop / Photometer	Eppendorf	D30
Needle Puller	Narishige	PC-100
Pipette 10, 100, 200, and 1000 µl	Eppendorf	Research Plus
Pipetboy	Integra	Acu 2
PCR Machine	Eppendorf	6337000019
Ph-Meter	Mettler-Toledo	Five Easy
Real-Time PCR Machine	Thermo Fisher	Step One Plus

Shaker (Rotator)	Stuart	SRT6
Stereomicroscope	Leica	S6
Tecan Spark 20m plate reader	Tecan	N/A
Thermo Block	Eppendorf	5382000015
Transmitted Light Microscope	Zeiss	Axiovert 40CFL
UV Transilluminator	Alpha Imager HP	N/A
Vortex Device	Grant Bio	PV-1
Water Bath	GFL	11347017J
Weighing Balance	Kern	EW4200
Zeiss LSM 800 confocal microscope	Zeiss	LSM 800

2.1.2 Laboratory materials

	SUPPLIER	CAT NUMBER
Bacterial culture tubes	TPP	352059
Cell Strainer 40µm	Neolab	352340
Cell culture plate, 24 well	Sarstedt	83.3922.005
Centrifuge tubes (15 and 50 ml)	TPP	91015, 91050
Flow cytometry tubes	Falcon	352058
Forceps	Dumont	N/A
Gauge needle	B.Braun	4657705
Glass Capillaries	Science Products	GB120F-8P
Microcentrifuge tubes (1.5 and 2 ml)	Sarstedt	72.706.400, 72.695.400
qPCR plates (Fast Optical 96-Well Reaction Plate)	Life Technologies	4346907
Pellet Pestle, 1.5 ml	Fisher Scientific	11872913
Petri dish (35, 60, and 100 mm)	Sarstedt	82.1135.500, 83.3901, 82.1473
Plastic pipette 3 mL	Pastette	LW4111
PCR tubes	Sarstedt	72.991.002
pellet pestle	Fisher Scientific	11872913
pellet pestle gun	Fisher Scientific	12-141-361
Pipette tips (10, 200, and 1000 µl)	Sarstedt	701130, 70.760.002, 70.1186
Serological pipette tips (10 and 25 ml)	Sarstedt	86.1254.001, 86.1685.001
Syringes	B.Braun	9161406V
Ultrasonic cell distruptor	VWR	N/A

2.1.3 Solutions and Buffers

30x Danieau's medium

Reagent	Final concentration	Amount
NaCl	1740 mM	101.7 g
KCl	21 mM	1.56 g
MgSO4	12 mM	2.96 g
Ca(NO3)2	18 mM	4.25 g
HEPES	150 mM	35.75 g
MilliQ H_2O		Add to 1 L
Total		1 L

1x PTU

Reagent	Final concentration	Amount
N-Phenylthiourea (PTU)	0.003%	30 mg
1x Danieau's medium	1x	Add to 1 L
Total		1 L

1xPBS

Reagent	Final concentration	Amount
PBS	1x	5 tablets
MilliQ H2O		Add to 1 L
Total		1 L

1xPBST

Reagent	Final concentration	Amount
Triton X-100	0.1%	500 µl
1xPBS		Add to 500 mL
Total		500 ml

4% PFA + 0.03% TritonX-100

Reagent	Final concentration	Amount
PFA 16%	4%	10 ml
Triton X-100	0.03%	12 µl
1xPBS		Add to 40ml
Total		40 ml

10 % KOH

Reagent	Final concentration	Amount
KOH 10%	10 %	10 g
MilliQ H_2O		Add to 100 ml
Total		100 ml

Bleaching solution

Reagent	Final concentration	Amount
H_2O_2 30%	3%	100 µl
KOH 10%	0.5%	50 µl
PBST		850 µl
Total		1 ml

0.3% Tween20

Reagent	Final concentration	Amount
Tween20	0.3 %	300 µl
PBS		Add to 100 ml
Total		100 ml

0.1% Tween20

Reagent	Final concentration	Amount
Tween20	0.1 %	100 µl
PBS		Add to 100 ml
Total		100 ml

1% BSA in HBSS

Reagent	Final concentration	Amount
BSA	1%	0.1 g
HBSS	1%	Add to 10 ml
Total	1x	10 ml

0.05 % BSA in HBSS

Reagent	Final concentration	Amount
BSA %1	0.05 %	500 µl
HBSS	1%	Add to 10 ml
Total	1x	10 ml

Explant medium

Reagent	Final concentration	Amount
FBS	10%	5 ml
MEM-NEAA (100X)	1x	500 µl
Penicillin-Streptomycin (10.000 U/ml)	100 ug/ml	500 µl
Primocin (50 mg/ml)	100 µg/ml	100 µl
2-mercaptoethanol (50mM)	50 µM	50 µl
DMEM		Add to 50 ml

5x SSCT

Reagent	Final concentration	Amount
Tween 20	0.1 %	10 µl
Sodium chloride sodium citrate (20X)	5X	2.5ml
Water		Add to 10 ml
Total	1x	10 ml

Tricaine

Reagent	Final concentration	Amount
Tricaine	4 mg/mL	2 g
1x Danieau's medium	1x	Add to 500 ml
Total		500 mL

1.5 % agarose

Reagent	Final concentration	Amount
Agarose, NEEO	1.5%	1.5 g
MilliQ H_2O		Add to 100 ml
Total		100 mL

Immunostaining blocking solution for larvae

Reagent	Final concentration	Amount
Goat serum	5%	500 µl
BSA	1%	0.1 g
1xPBS		Add to 10 ml
Total		10 ml

Immunostaining blocking solution for adult

Reagent	Final concentration	Amount
Goat serum	5%	500 µl
BSA	10%	1 g
1xPBS		Add to 10 ml
Total		10 ml

2.1.4 Chemicals and Reagents

	SUPPLIER	CAT NUMBER
Acetic Acid	Carl Roth	6755.1
Acid fuchsin	Carl Roth	T128.1
Agarose, Low Melting Point	Sigma	A4018
Agarose NEEO Ultra Qualität	Carl Roth	2267.3
Ampicillin	Sigma	A9518
Aniline Blue	Santa Cruz	28631-66-5
Atropine sulfate salt monohydrate	Sigma	A0257
Bacterial LB Agar	Carl Roth	X969.2
Bacterial LB Medium	Carl Roth	964.2
Bovine Serum Albumin	Serva	11943.02
Calcium Nitrate ($Ca(NO_3)_2$)	Honeywell	C1396
Carvedilol	Sigma	3993
Chloroform	Fisher Chemical	C/4960/15
Citric acid	Serva	38640

Collagen Hybridizing Peptide, 5-FAM Conjugate	3-Helix	FLU300 / FLU60
Competent E. coli 5-alpha (High Efficiency)	NEB	C2987H
DAPI	Sigma	D9542-5MG
DAPI staining solution for FACS	Milteny Biotec	130-111-570
Dimethyl Sulfoxide (DMSO)	Th. Geyer	23419.3
DNaseI	Roche	10104159001
Dulbecco's Modified Eagle Medium, high glucose, GlutaMAX	GIBCO	31966021
Entellan	Sigma	1.07960
Ethanol	Carl Roth	9065.2
5-Ethynyl-2′-deoxyuridine (EdU)	Santa Cruz	61135-33-9
Fetal Bovine Serum	GIBCO	10270106
Fibronectin Bovine Protein, Plasma	Thermo Fisher	33010-018
Fluoromount Aqueous Mounting Medium	Sigma	F4680
Formamide	Thermo Fisher	17899
Gel Red Nucleic Acid Stain	Linaris	41003
GeneRuler 1kb DNA Ladder	Thermo Fisher	SM0311
Glycogen	Serva,	23550
Goat serum	Sigma	G6767
Hank's Balanced Salt Solution	LIFE Technologies	14175095
HCR™ IF + HCR™ RNA-FISH Products	Molecular Instruments	
Hydrochloric Acid (HCl)	Sigma	H1758
Hydrogen Peroxide (H2O2) 30%	ChemCruz	sc-203336A
HEPES	Carl Roth	9105.4
Isopropanol	Carl Roth	7343.2
Liberase TL Research Grade	Roche	5401020001
Loading Dye (Orange G)	Carl Roth	0318.2
Magnesium Sulfate (MgSO4)	ChemCruz	sc-211764
Master Mix Taq 2x	New England Biolabs	M0270
MEM Non-Essential Amino Acids Solution (100X)	Thermo Fisher	11140050
2-Mercaptoethanol	Sigma	M3148
Methanol	Roth	4627.1
Methoxamine hydrochloride	Sigma	M6524
Morphine	Ratiopharm	N/A
N-Phenylthiourea (PTU)	Sigma	P7629
Orange G	Santa Cruz	1936-15-8
Penicillin-Streptomycin (10.000 U/ml)	Thermo Fisher	15140122
Paraformaldehyde (PFA)	Sigma	P6148

Phenol/Chloroform/Isoamyl alcohol	Roth	A156.2
Phenol Red	Sigma	P0290
Phosphate-Buffered Saline (PBS)	Sigma	P4417
Pluron F-68 polyol, 100 ml	MP Biomedicals	092750049
Potassium Chloride (KCl)	ChemCruz	sc-203207
Potassium Hydroxide (KOH)	Alfa Aesar	A16199
Prazosin hydrochloride	Sigma	P7791
Primocin	InvivoGen	ant-pm-2
Propranolol hydrochloride	Sigma	P0884
Recombinant zebrafish LRPAP1 protein	This study	
RNase H	Life Technologies	EN0201
SOC-Medium	New England Biolabs	B9020S
Sodium Acetate	Calbiochem	567418-500GM
Sodium Chloride (NaCl)	Serva	39781.02
SYBR Safe DNA Gel Staining Solution	Life Technologies	S33102
O.C.T Compound	Sakura Tissue Tek	4583
Tricaine	PHARMAQ	N/A
Tris	Sigma	T1503
TRIzol	Life Technologies	15596026
Trypsin-EDTA	Sigma	T4049
Triton X-100	Carl Roth	3051.3
Trizma hydrochloride	Sigma	T2694
Tween 20	Santa Cruz	SC-29113
Water H2O RNase/DNase free	LIFE Technologies	R0581

2.1.5 Critical Commercials/Kits

	SUPPLIER	CAT NUMBER
Chromium Next GEM Single Cell 3′ GEM, Library & Gel Bead Kit v3.1	10x Genomics	PN-1000121
Chromium Next GEM Chip G Single Cell Kit	10x Genomics	PN-1000120
Click-iT™ EdU imaging kit	Thermo Fisher	C10640
In-Fusion® Snap Assembly Master Mix	Takara-Bio	638948
IP3(Inositol Triphosphate) ELISA Kit	Biocat	E-EL-0059-ELS
Phusion High-Fidelity PCR Kit	Life Technologies	F553L
NucleoSpin Gel and PCR Clean-up	Macherey-Nagel	740609.250
NucleoSpin Plasmid kit	Macherey-Nagel	740588.250
Single Index Kit T Set A	10x Genomics	PN-1000213

SuperScript III First Strand Kit	Life Technologies	18080051
Qubit dsDNA HS Assay Kit	LIFE Technologies	Q32851

2.1.6 Antibodies

	SUPPLIER	CAT NUMBER
Rabbit anti-MEF-2 Antibody (C-21)	Santa Cruz	sc-313
Rat anti-mCherry Antibody (16D7)-100µl	LIFE Technologies	M11217
Mouse anti-PCNA antibody [PC10]	Abcam	ab18197
Chicken anti-GFP antibody	LIFE Technologies	A10262
Goat anti-Chicken IgY (H+L) Secondary Antibody, Alexa Fluor 488	LIFE Technologies	A11039
Goat Anti-rat IgG (H+L), (Alexa Fluor(R) 555 Conjugate)	Cell Signaling	4417S
Rabbit anti-cd31 antibody	Abcam	ab28364
Rabbit anti-Collagen I antibody	Abcam	ab233639
Mouse anti-alpha smooth muscle Actin antibody [1A4]	Abcam	ab7817
Mouse anti-Tubulin, Acetylated antibody [6-11B-1]	Sigma	T6793
Mouse anti-TNF alpha antibody [52B83]	Abcam	ab1793
Rabbit anti-Col1a1a antibody	GeneTex	GTX133063
Goat anti-mouse IgG (H+L), (Alexa Fluor(R) 488 Conjugate)	Cell Signaling	4408S
Goat anti-mouse IgG (H+L), F(ab')2 Fragment (Alexa Fluor(R) 647 Conjugate)	Cell Signaling	4410S
Goat anti-rabbit IgG (H+L),(Alexa Fluor(R) 488 Conjugate)	Cell Signaling	4412S

2.1.7 RT-PCR Primers

Forward primer adra1 3i loop	5'-CACACGAATTCGCCGCCACCATGGTGGCCAAAATGACCACTAA-3'

Reverse primer 1 for adra1 3i loop	5'-CGTCACCGCATGTTAGAAGACTTCCTCTGCCCTCACCAGATCCTTTCTTTTCCCTGGAAAACTTG-3'
Reverse primer 2 for adra1 3i loop	5'-AGCTCTTCACCCTTGCTGACAGGGCCGGGATTCTCCTCCACGTCACCGCATGTTAGAAG-3'
Forward primer for CFP	5'-TGGAGGAGAATCCCGGCCCTGTCAGCAAGGGTGAAGAGC-3'
Reverse primer for CFP	5'-TATGATCTAGAGTCGCGGCCGCTCACTTATACAGTTCGTCCATACCC-3'
Forward primer for adra1aa	5'-TATCGTGGTGGGATGCTTCG-3'
Reverse primer for adra1aa	5'-CGTTGGGAAGATGGAACCGAT-3'
Forward primer for adra1bb	5'-TTTGCCAATTGTTTCATTCAACACC-3'
Reverse primer for adra1bb	5'-AGCAGGGGTAGATGATGGGA-3'
Forward primer for adrb1	5'-GGGTTACTGGTGGTGCCATT-3'
Reverse primer for adrb1	5'-GCGTGACGCAAAGTACATC-3'
Forward primer for adrb2a	5'-GCTTCCAGCGTCTTCAGAAC-3'
Reverse primer for adrb2a	5'-CCGAAGGGAATCACTACCAA-3'
Forward primer for adrb2b:	5'-CTCGTTCCTACCCATCCACA-3'
Reverse primer for adrb2b	5'-ATGACCAGCGGGATGTAGAA-3'

2.1.8 Software and Algorithms

	SOURCE	IDENTIFIER
CellChat package v1.6.1	https://github.com/sqjin/CellChat	RRID:SCR_021946
ClusterProfiler package v4.6.2	http://bioconductor.org/packages/release/bioc/html/clusterProfiler.html	RRID:SCR_016884
Fiji/ImageJ	http://fiji.sc	RRID:SCR_002285
Imaris v9.5.0	Oxford Instruments	RRID:SCR_007370
Graphpad Prism 8.0	GraphPad Software, San Diego, California USA, www.graphpad.com	RRID:SCR_002798
FlowJo	BD (Becton, Disckinson & Company), https://www.flowjo.com/solutions/flowjo	N/A
MAST package v1.24.1	https://bioconductor.org/packages/release/bioc/html/MAST.html	RRID:SCR_016340
scvelo v0.2.5	https://github.com/theislab/scvelo	RRID:SCR_018168
Scanpy v1.9.1	https://github.com/theislab/scanpy	RRID:SCR_018139
Seurat package v4.1.0	https://satijalab.org/seurat/get_started.html	RRID:SCR_016341
Velocyto	http://velocyto.org/	RRID:SCR_018167
ZEN software	Zeiss	N/A

2.2 Methods

2.2.1 Animal care and strains

Zebrafish maintenance and all associated experimental protocols were rigorously executed in compliance with the ethical and animal welfare guidelines set by the Max Delbrück Center for Molecular Medicine, Landesamt für Gesundheit und Soziales Berlin (LAGeSo Berlin), and German federal regulations. Standardized environmental conditions were maintained for zebrafish husbandry, including a water temperature of 28.5°C and a 14-hour light/10-hour dark photoperiod. Both embryos and larvae were maintained in Danieau's medium, composed of 58 mM NaCl, 0.7 mM KCl, 0.4 mM MgSO4, 0.6 mM Ca(NO3), and 2.5 mM HEPES, with the pH adjusted to 7.0. Gender differentiation among the zebrafish was not a parameter considered in this study. Adult specimens aged between one and two years and larval specimens aged up to either 5dpf or 7dpf were utilized as detailed in specific experimental sections.

Transgenic zebrafish lines previously established and used in this research include Tg(myl7:H2B-GFP)^{zf521}, TgBAC(csf1ra:Gal4-VP16)^{i186}, Tg(UAS:NTR-mCherry)^{c264}, Tg(14xUAS:GCaMP6s)^{mpn101}, Tg(tbp:Gal4,myl7:Cerulean)^{f13}, and Tg(tnfa:EGFPF)^{ump5}.

2.2.2 Microinjections in zebrafish embryos

For the creation of injection plates, a 2% agarose solution in Danieau's medium was prepared through microwave-assisted heating. The melted agarose was subsequently dispensed into a 10 cm diameter Petri dish, onto which a specialized multi-lane mold was laid. Upon solidifying the agarose, the mold was carefully removed to reveal the lanes for embryo placement. These plates were stored at 4ºC until use and equilibrated to room temperature prior to any injection procedures. For breeding setups, adult male and female zebrafish were co-housed in breeding tanks but separated by a transparent partition overnight. The intervening barrier was taken away the following morning, allowing for breeding. Eggs were harvested from the base of the breeding tanks within a 20-minute interval post-barrier removal. Microneedles for injection were made from glass capillaries using a needle-pulling device. The needles were subsequently loaded with the designated injection solution. A fine-tipped forceps

was utilized to fracture the needle tip, ensuring a precise aperture for injection. Zebrafish embryos at the 1-2 cell stage were methodically aligned within the lanes of the prepared injection plates. The injection solution was then microinjected directly into the cells. Post-injection, the embryos were maintained in fresh Danieau's solution. Later in the day, a stereomicroscopic examination was carried out to identify and remove any non-viable or unfertilized embryos.

2.2.3 Generation of constructs and transgenic animals

The *UAS:adra1-3i-T2A-CFP* construct was generated through amplification of the encoding sequences of 3rd intracellular loop of *adra1bb*, corresponding to the 231st to 291st amino acids, T2A self-cleaving peptide, and CFP. Primers used, listed in the materials section, also added the sequence for the T2A linker peptide to the amplified oligonucleotides, and they were:

Forward primer adra1 3i loop 5'-CACACGAATTCGCCGCCACCATGGTGGCCAAAATGACCACTAA-3'

Reverse primer 1 for adra1 3i loop 5'-CGTCACCGCATGTTAGAAGACTTCCTCTGCCCTCACCAGATCCTTTCTTTTCCCTGGAAAACTTG-3'

Reverse primer 2 for adra1 3i loop 5'-AGCTCTTCACCCTTGCTGACAGGGCCGGGATTCTCCTCCACGTCACCGCATGTTAGAAG-3'

Forward primer for CFP 5'-TGGAGGAGAATCCCGGCCCTGTCAGCAAGGGTGAAGAGC-3'

Reverse primer for CFP5'-TATGATCTAGAGTCGCGGCCGCTCACTTATACAGTTCGTCCATACCC-3'.

To generate the *Tg(UAS:adra1-3i-T2A-CFP)* line, the *UAS:adra1-3i-T2A-CFP* construct was injected into embryos at the 1-cell stage, along with mRNA encoding the Tol2 transposase. Injected embryos were sorted for CFP signal under a fluorescence microscope and raised. Grown zebrafish were crossed again to identify the founders with stable integration of the

transgene, and their offspring were raised to expand the transgenic line and establish F2 generation.

2.2.4 Imaging techniques

Confocal microscopy was employed for the imaging of both live and fixed specimens, utilizing either a Zeiss LSM 880 confocal microscope or a Leica DM6 CFS confocal microscope. For the specific task of capturing Acid Fuchsin Orange G (AFOG) stained samples, an Olympus SZX16 stereo microscope was used. For real-time imaging, zebrafish larvae were immobilized using 1.5% low-melting-point agarose in petri dishes.

2.2.5 Myocardial infarction models

In larval models, focal ventricular necrosis was induced via the application of a two-photon laser. Larvae were anesthetized with tricaine and immobilized in petri dishes containing 1.5% low-melting-point agarose dissolved in Danieau's medium. A region of the agarose overlaying the heart was carefully excised. Five pulses of a 920 nm wavelength laser, each with a duration of approximately 0.8 ms, were then focused on the ventricle using a Zeiss W Plan-APOCHROMAT 20x/1.0 DIC (UV) VIS-IR dipping lens. Post-injury, larvae were freed from the agarose and transferred to fresh Danieau's medium.

For adult models, anesthesia was applied with Danieau's medium containing 0.168 mg/ml tricaine. Fish were positioned on a sponge featuring a small, medium-soaked groove. Following an incision in the body wall and the pericardium to reveal the heart, the ventricular apex was subjected to cryoinjury via a cryoprobe pre-chilled in liquid nitrogen. After the procedure, fish were transferred to system water containing 1.5 μg/ml morphine. Morphine treatment was terminated at 6 hours post-injury (dpi), after which fish were either left to recover under standard conditions or received additional pharmacological intervention up to 7dpi.

2.2.6 Pharmacological Interventions

Following the 2-photon laser-induced necrosis in larval zebrafish, pharmacological inhibitors of neurotransmitters were administered for a 24-hour period. These compounds, all

dissolved in Danieau's medium, included carvedilol, propranolol, atropine, and prazosin at concentrations of 50 μM, 50 μM, 50 μM, and 100 μM, respectively. Control groups received the solvent (vehicle) alone in equal volumes. To assess cellular proliferation, 500 μM of EdU was added to the medium at 6hpi. Following the 24-hour incubation period, larvae were anesthetized with tricaine, euthanized, and fixed overnight in a 4% PFA solution containing 0.03% Triton X-100 at 4°C. For adult specimens, prazosin was supplied at a concentration of 100 μM in the system water post-injury, with daily water changes up to 7 dpi.

2.2.7 Heart dissection and cryosectioning

In adult zebrafish, euthanasia was induced through hypothermic immersion in ice-cold water (0-4°C) for a minimum duration of 20 minutes. Post-euthanasia, decapitation was carried out from the base of the pectoral fin using a surgical razor blade, followed by heart excision. The extracted hearts were fixed overnight in a 4% PFA solution containing 0.03% Triton X-100 at 4°C. Following fixation, the hearts were washed in PBS with 0.1% Triton X-100 (v/v) (PBST). For long-term storage, the hearts were preserved in methanol at -20°C or left overnight in the same solution at 4°C prior to subsequent steps. For cryosectioning, the hearts were rehydrated by decreasing concentrations of methanol solutions diluted in PBS, ending with a PBS wash. The hearts were then submerged in 15% sucrose solution for a period of 3-5 hours, followed by immersion in 30% sucrose solution overnight for cryopreservation. The specimens were embedded in molds filled with OCT and stored at -80°C. Cryosections of 10 μm thickness were obtained for subsequent histological and immunofluorescence analyses.

2.2.8 Tissue dissociation

Tissues were transferred to a dissociation buffer comprising 0.26 U/ml Liberase^{TM} enzyme mixture and 1X Pluronic F-68 in Hank's Balanced Salt Solution (HBSS). Tissues were incubated at 37°C with shaking at 750 rpm for 30 minutes, with intermittent pipetting executed at 5-minute intervals. The dissociation process was halted by adding an equal volume of 1% bovine serum albumin (BSA) in HBSS, followed by centrifugation at 200xg at 4°C. The isolated cells were washed in a 0.05% BSA in HBSS solution, resuspended, and filtered through a 40 μm cell strainer.

2.2.9 Recombinant Lrpap1 protein production

The zebrafish Lrpap1 gene sequence, retrieved from the UniProt protein database under the accession number Q7ZW96, was synthesized and subcloned into a pET-24(+) expression vector. The construct, under the transcriptional regulation of the T7 promoter, was transfected into Escherichia coli (E. coli). The resulting recombinant protein was isolated using 6xHis affinity chromatography. Post-purification, the histidine tag was cleaved by TEV protease. The purity, size, and mass of the protein were verified using sodium dodecyl sulfate-polyacrylamide gel electrophoresis (SDS-PAGE) and liquid chromatography/time-of-flight mass spectrometry (LC/MS TOF).

2.2.10 Explant culture and cryoinjury

Heart explant cultures were established with hearts from euthanized zebrafish, as described earlier. The hearts were cultured in explant medium comprising DMEM, 10% fetal bovine serum (FBS), 1% MEM-NEAA, 100 U/ml penicillin, 100 µg/ml streptomycin, 100 µg/ml primocin, and 50 µM 2-mercaptoethanol. The cultures were maintained in 24-well plates at 28°C. Ex vivo cryoinjury was administered by applying a precooled cryoprobe to the ventricular wall for a 20-second duration. Following cryoinjury, the hearts were transferred to a fresh explant medium and returned to the incubator for 7 days. Lrpap1 protein, at a concentration of 10 µg/µl, was added to the culture medium starting from the first day post-cryoinjury. To activate α1-adrenergic receptors, which would otherwise be absent in explanted hearts, 500 µM methoxamine was supplemented starting from the fourth day post-injury and continued until the seventh day. Explant medium, LRPAP1, and methoxamine were refreshed daily following their respective times of initial administration.

2.2.11 Enzyme-linked immunosorbent assay (ELISA)

Transgenic zebrafish larvae of strains Tg(tbp:Gal4, myl7:Cerulean)^{f13}; Tg(UAS:adra1-3i-T2A-CFP) and as control group Tg(tbp:Gal4, myl7:Cerulean)^{f13} at 5dpf were treated with either vehicle, 200 µM methoxamine, or 100 µM prazosin. Additionally, wild-type 5dpf larvae were exposed to 50 µM carvedilol, 200 µM methoxamine, a combination of both, or a vehicle.

Subsequent to these treatments, the intracellular levels of IP3 were assessed using the IP3 ELISA kit as per the manufacturer's instructions. Treated groups of larvae were pooled and subjected to tissue dissociation, as previously explained. The cells were subsequently lysed using an ultrasonic cell disruptor. Following lysis, the samples were centrifuged at 5000xg at 4°C for 10 minutes, and the supernatants were collected for analysis. Both standard solutions and the prepared samples were added to the ELISA plate wells. Biotinylated detection antibody solution and horseradish peroxidase (HRP) conjugate working solutions, supplied with the kit, were also added as per the protocol. Signal intensities were measured using a Tecan Spark 20m plate reader at specified incubation times recommended by the manufacturer.

2.2.12 Calcium measurements

Transgenic zebrafish larvae strains TgBAC(csf1ra:Gal4)^{i186}; Tg(UAS:NTR-mCherry)^{c264}; Tg(UAS:adra1-3i-T2A-CFP; Tg(14xUAS:GCaMP6s)^{mpn101} were utilized for calcium measurement. The larvae were immobilized in 1.5% low-melting-point agarose. Baseline calcium signaling in CFP-negative and CFP-positive MPs within the same larvae was captured at a frequency of every 0.2 seconds for a total duration of 3 minutes. Subsequently, a 200 μM methoxamine solution was added, and imaging continued at the same frequency for an additional 10 minutes. GCaMP6s fluorescence was quantified using the ImageJ [186] software. MPs expressing both mCherry and GCaMP6s were manually selected as regions of interests. These MPs were categorized as either CFP-positive or CFP-negative. The fluorescence intensity changes ΔF/F0 ((F – F0)/F0) were calculated for individual cells, where F0 represents the average baseline fluorescence intensity, and F denotes the average fluorescence intensity following the addition of methoxamine.

2.2.13 Immunofluorescence and other histological staining protocols

Whole mount zebrafish larvae immunofluorescence staining

For the immunofluorescence staining of zebrafish larvae, I adhered to an established whole-mount immunostaining procedure [187]. Following fixation, specimens were gradually transitioned to 100% methanol and subjected to overnight incubation at -20°C. Subsequently, they were rehydrated into PBST. For non-PTU treated samples, pigmentation of the skin was

quenched via a 30-minute exposure to a bleaching solution of 3% hydrogen peroxide and 0.5% potassium hydroxide at room temperature, followed by PBST rinsing. Antigen retrieval was conducted via a 5-minute room temperature incubation in 150 mM Tris buffer (pH 5.0), followed by a 15-minute incubation at 70°C with shaking at 600 rpm. To enhance membrane permeability, samples were treated with a 1:20 dilution of Trypsin-EDTA (500 BAEE units) in PBST for 35 minutes on ice. A blocking buffer consisting of 5% (v/v) goat serum and 1% (w/v) BSA in PBS was used to reduce non-specific binding with 1 hour room temperature incubation. The larvae were then subjected to primary and secondary antibody (dissolved in blocking solution) incubation, both for 72 hours at 4°C and shielded from light. EdU labeling was performed post-permeabilization, as per the Click-iT™ Plus EdU Cell Proliferation Kit Alexa 647 instructions. The following primary antibodies were used for larval zebrafish staining: rat anti-mCherry (1:300) and chick anti-GFP (1:500). The following secondary antibodies were used for larval zebrafish staining: Alexa Fluor 488 anti-chicken (1:1000), Alexa Fluor 555 anti-rat (1:500). DAPI (1:300) was added during the secondary antibody incubations. Finally, specimens were mounted using Fluoromount aqueous mounting medium for subsequent imaging.

Immunofluorescence staining of adult heart sections

Cryosections from adult zebrafish were initially fixed in ice-cold acetone for 10 minutes at -20°C and then washed thrice with PBS. Permeabilization was achieved via a 10-minute treatment with 0.2% Triton X-100 in PBS, followed by another triple wash in PBS. Sections were blocked using a solution of 5% (v/v) goat serum and 10% (w/v) BSA in PBS. Primary antibody incubations were done overnight at 4°C, with a subsequent triple wash using PBS with 0.3% Tween 20. After secondary antibody incubation, sections were washed and mounted in Fluoromount aqueous mounting medium for imaging. DAPI was added during the secondary antibody incubation. The following primary antibodies were used: rabbit anti-Mef2 (1:300), mouse anti-PCNA (1:300), rabbit anti-CD31 (1:300), rabbit anti-Col1 (1:300), mouse anti-a-SMA (1:150,), mouse anti-acTub (1:300), rat anti-mCherry (1:300), chick anti-GFP (1:500), mouse anti-Tnfa (1:200), rabbit anti-col1a1a (1:100). The following secondary antibodies were used: Alexa Fluor 488 anti-chicken (1:1000), Alexa Fluor 555 anti-rat (1:500), Alexa Fluor 647 anti-mouse (1:500), Alexa Fluor 488 anti-mouse (1:500), Alexa Fluor 647 anti-rabbit (1:500), Alexa Fluor 488 anti-rabbit (1:500). Integration of collagen hybridizing peptide (CHP) into the cryosection immunofluorescence staining was performed by first heating the CHP at

80°C for 5 minutes and quenching it to room temperature in ice water quickly before using it, in line with manufacturer's instructions. Subsequently, during the secondary antibody incubations, 30 μM of CHP solution was added to the samples.

Acid Fuchsin Orange G staining

For fixation in Bouin's solution, cryosections were incubated at 58°C for two hours and then at room temperature for an additional hour. After a 20-minute rinse under tap water, 1% phosphomolybdic acid and 0.25% phosphotungstic acid solution was applied to sections for 5 minutes, followed by an AFOG staining solution containing 1g Aniline Blue, 3g acid Fuchsin, 2g Orange G in distilled water (pH adjusted to 1.1). Samples were then washed with water, dehydrated through a series of ethanol and xylene baths, and mounted with Entellan.

Hybridization Chain Reaction (HCR) Fluorescent In Situ Hybridization (FISH)

The mRNA expressions of *postnb*, *col12a1a*, *cxcl12b*, *lrp1aa*, *mdka*, *lyve1*, *col5a1*, and *sdc2* genes were evaluated using HCR-FISH staining in accordance with supplier's protocols. Following immunofluorescence, sections were post-fixed with 4% PFA for 10 mins at room temperature and washed with PBS containing 0.1% (V/V) Tween 20 for 5 minutes twice and with 5x SSCT solution containing sodium chloride sodium citrate (SSC) and 0.1% (V/V) Tween 20 for 5 minutes, both at room temperature. Subsequently, sections were incubated with probe hybridization buffer for 10 minutes at 37°C and left for overnight incubation with appropriate 16mM probe solutions at 37°C. Afterward, they were subjected to a series of washes, each lasting 15 minutes in this order: 75% of probe wash buffer / 25% 5× SSCT, 50% of probe wash buffer / 50% 5× SSCT, 25% of probe wash buffer / 75% 5× SSCT, and 100% 5× SSCT. Sections were incubated with amplification buffer at room temperature for 30 minutes and left to overnight incubation with amplification buffer containing 60 n M of appropriate hairpins at room temperature in the dark. Hairpins were snap-cooled by heating at 95°C for 90 seconds and cooling at room temperature before application to sections. The sections were washed with 5x SSCT for 2x5 minutes, 2x15 minutes, and 1x5 minutes at room temperature and mounted using Fluoromount aqueous mounting medium for subsequent imaging.

2.2.14 Image analysis methodology

To evaluate the recruitment of MPs to the site of cardiac injury, I employed a transgenic zebrafish line with *csf1ra:Gal4; UAS:NTR-mCherry; UAS:adra1-3i-CFP; tnfa:EGFPF*. To quantify the involvement of Adra1 signaling-deficient MPs (CFP+mCherry+) in comparison to the control MPs (mCherry+), in both *tnfa* expressing (EGFPF+) and non-*tnfa* expressing (EGFPF-) MP subpopulations post 2-photon laser-induced necrosis, time-lapse imaging was performed from 30 minutes post-injury (mpi) to 24hpi. At each designated time point, MP subpopulations situated within a 100 μm radius from the point of injury were counted.

To assess the proliferation rate of cardiomyocytes in the larval hearts, I counted the nuclei demonstrating colocalization of H2B-GFP and EdU in individual z-planes acquired through confocal microscopy, which spanned the entire ventricular region. The counting of these nuclei was conducted using ImageJ [186] software. Imaris software was employed to assess the total number of cardiomyocytes. Furthermore, both the total and proliferating MP content, marked with NTR-mCherry and EdU, respectively, were quantified within an area extending 100 μm from the demarcated injury zone. MPs expressing either or both adra1-3i-T2A-CFP and tnfa were categorized and counted based on the respective fluorescence markers.

For adult cardiac tissue sections, cell counting was performed within the injury site and the adjoining 100 μm zone proximal to the injury border zone. Comparative evaluations were also carried out in sham-operated hearts by assessing a similarly sized ventricular apex region. Each data point represents the mean value derived from a minimum of three tissue sections per heart specimen. Levels of Collagen I, CD31, acTub, and CHP were determined through image thresholding techniques using ImageJ [186], and the extent of area occupied by the respective signals was assessed. Proportional areas in both the injured and sham-operated specimens were subsequently calculated. For the quantification of collagen content, detected through AFOG staining, I employed the color threshold tool in ImageJ [186] to measure the percentage of collagen (represented in blue) covered area within the injured region or the similar sized apex region in sham-operated specimens. For HCR-FISH quantifications, the area for measurement was defined as previously stated. Cells displaying positive signals were counted, and the integrated density of HCR-FISH staining signals were quantified using ImageJ [186], followed by normalization against the measurement area.

2.2.15 Fluorescence activated cell sorting (FACS)

Tissue samples from either dissociated whole larvae or adult hearts were subjected to cell sorting using a BD FACSAria II machine. To be utilized in scRNAseq, cells were pre-stained with DAPI to provide the distinction between viable and non-viable cells. The initial gating strategy involved employing forward scatter area (FSC-A) versus side scatter area (SSC-A) plots to account for the variables of cellular size and granularity. This step was crucial for the exclusion of both cellular debris and aggregated cells. Subsequent gating was executed through the examination of FSC-Height (FSC-H) versus FSC-Width (FSC-W) and SSC-Height (SSC-H) versus SSC-Width (SSC-W) plots. These plots enabled the isolation of single cells that fell within the expected physiological size range. Cells conforming to these initial gating criteria were then subjected to further downstream gating procedures. These subsequent steps were designed to either isolate live cells or specifically focus on cells expressing either mCherry or CFP markers whenever appropriate. Gating for cells based on mCherry or CFP fluorescence was carried out using reference samples lacking any transgenes, which served as negative controls for background fluorescence signals.

2.2.16 Single-cell RNA sequencing protocol and analysis

Hearts from zebrafish *csf1ra:Gal4; UAS:NTR-mCherry; UAS:adra1-3i-T2A-CFP* and their control counterparts *csf1ra:Gal4; UAS:NTR-mCherry* were harvested at 7dpi following cryoinjury and dissociated as previously described. Live cell populations were isolated via FACS and subsequently loaded onto a Chromium 10x Genomics instrument for encapsulation into droplets. Library construction ensued, guided by the Chromium Single Cell 3' Reagent Kits User Guide (v3.1 Chemistry) CG000204. Concentrations of cDNA and the resulting library were quantified utilizing a Qubit dsDNA HS Assay Kit and analyzed on a high-sensitivity DNA tape-station. Sequencing was executed on an Illumina NovaSeq6000 system, configured for 400 million reads per lane with 50 bp paired-end read lengths.

For data alignment and custom reference genome assembly, Cell Ranger software (v6.0.1) was deployed. The zebrafish reference genome Danio_rerio.GRCz11 (release 104) obtained from the Ensembl database was modified to include the CFP sequence through the mkgtf function. Subsequent data processing was performed using the R package Seurat

(version 4.1.0). Filtering parameters were applied to exclude cells with less than 200 genes and more than 2500 genes and cells that have more than 15% mitochondrial content. Following normalization and variable gene selection (2500 genes), principal component analysis (PCA) and Louvain clustering were conducted using default settings, with K-nearest neighbor graph with a resolution of 1.0 for whole heart clustering and 0.5 for MP and fibroblast population clustering. The dimensionality of the data was further reduced through t-Stochastic Neighbor Embedding (t-SNE). Differentially expressed genes within each cell cluster were identified employing the MAST algorithm within Seurat. This yielded insights into monocytes/MPs, which were further subdivided based on CFP expression for additional clustering and differential expression analysis. An analogous approach, barring the MP/monocyte subdivision, was employed for control heart samples. The same approach was also utilized for fibroblast population analysis in both datasets. Heatmaps, scatter plots, and violin plots were created via vlnPlot, doHeatmap, and DimPlot functions in Seurat. Gene ontology (GO) overrepresentation analysis was performed with clusterProfiler package in R. GO terms with more than 5 and less than 500 annotated genes from the DEG list were taken into account and filtered according to Bonferroni-Holm adjusted p values (0.05 cutoff). For cellular interaction analysis, the CellChat package in R was employed. Interactions and their respective strengths were initially tabulated for all MP and fibroblast clusters. Subsequently, significant interactions involving the 'ECM remodeling' cluster were highlighted. RNA velocity analysis was conducted utilizing scanpy (v1.9.1) and scvelo (v0.2.5), incorporating PAGA for trajectory inference. Velocity data were sourced from the datasets, Cell Ranger-aligned reads mapped to the Danio_rerio.GRCz11 (release 104) genome. RNA velocity values were quantified using default parameters of stochastic model scvelo (v0.2.5) and plotted on to uniform manifold approximation and projection (UMAP) representation of the cell populations.

2.2.17 Quantification and Statistical Analysis

Initial evaluation of all collected datasets involved administering the Shapiro-Wilk test to ascertain normal distribution. The outcome revealed that the datasets conformed to normal distribution parameters. Subsequently, statistical significance was gauged via the implementation of two-tailed Student's t-tests, executed in GraphPad Prism software. To evaluate the variance of datasets, whether they are equal or unequal, Fisher's F test was employed. Should datasets display unequal variances, t-tests incorporating Welch's correction

were conducted. In instances requiring the comparison of multiple datasets, p-values were adjusted in compliance with the Holm-Bonferroni correction method. Statistical significance was acknowledged for p-values less than 0.05. Detailed statistical annotations, inclusive of the specific tests applied, sample dimensions, and parameters for center and dispersion, are documented within the figures and corresponding figure legends.

3 Results

This study was accepted to be published as the article titled 'Alpha-1 adrenergic signaling drives cardiac regeneration via an extracellular matrix remodeling transcriptional program in zebrafish macrophages' in the journal Developmental Cell on its 20th November 2023 issue. All experiments and results were performed by Onur Apaydin unless otherwise stated in the figure legends.

3.1 Pharmacological blockage of α1 adrenergic receptor signaling disrupts regenerative response of cardiomyocytes and macrophages to laser-induced necrosis in the larval zebrafish heart.

To identify the neurotransmitter receptors pivotal for myocardial regeneration via immune modulation, with an emphasis on MP functional dynamics, I employed a two-photon laser technique to produce localized necrosis in the ventricle of *myl7:H2B-GFP* zebrafish larvae where the cardiomyocyte nuclei exhibit GFP fluorescence at 7dpf **(Fig. 3.1)**. I then used this larval cardiac necrosis model for pharmacological experiments investigating the role of MP-neuron interactions in myocardial repair. This methodology facilitates targeted and consistent cardiac injury in a small, transparent organism. Such characteristics make the zebrafish model exceptionally suitable for pharmacological assessments, given its amenability to real-time visual observations and drug interactions.

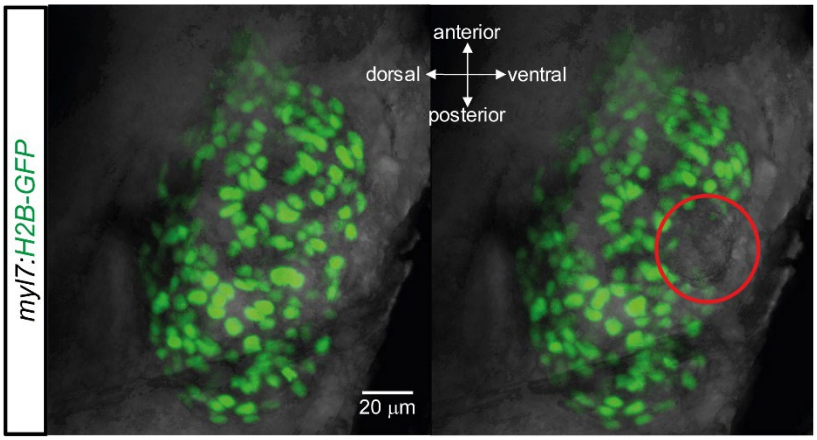

Figure 3.1 2-photon laser-induced necrosis of the larval heart. Confocal images showing the heart of a 7dpf zebrafish larva before (left) and after (right) 2-photon laser pulses were delivered to the ventricle. Cardiomyocyte nuclei are shown in green. The reporter line, *myl7: H2B-GFP*, expresses histone 2B fused to GFP under the control of a cardiomyocyte-specific *myl7* promoter. Scale bar is 20 μm.

After the injury, *myl7:H2B-GFP* larvae were exposed to either control (vehicle) or a range of sympathetic and parasympathetic neurotransmitter receptor antagonists for 24 hours. Along with the pharmacological signaling blockers, larvae were treated with EdU from 8hpi to 24hpi. This allowed me to quantify the mitotic activity of cardiomyocytes at 24hpi. At the end of the treatment, 24hpi, larvae were stained for EdU to assess proliferation and immunostained with anti-GFP antibody to label cardiomyocytes **(Fig. 3.2a)**. Notably, inhibiting adrenergic pathways via carvedilol, a comprehensive antagonist for α1, β1, and β2 adrenoreceptors, diminished the proliferation of cardiomyocytes within the injured myocardial tissue relative to the control treatment **(Fig. 3.2a-c).** Although carvedilol is widely recognized as a beta-blocker, it also exerts inhibitory effects on α1 adrenoreceptors. To assess the extent of carvedilol's ability to block the adrenergic α1 receptor (Adra1) signaling in zebrafish, I examined its impact on the activation of downstream elements of the Adra1 signaling. For this, I used ELISA for IP3, a secondary messenger downstream of this receptor. By also using methoxamine, an agonist of Adra1, I found that the Adra1 activation, induced by methoxamine, was attenuated in the presence of carvedilol in zebrafish larvae. **(Fig. 3.2d)**.

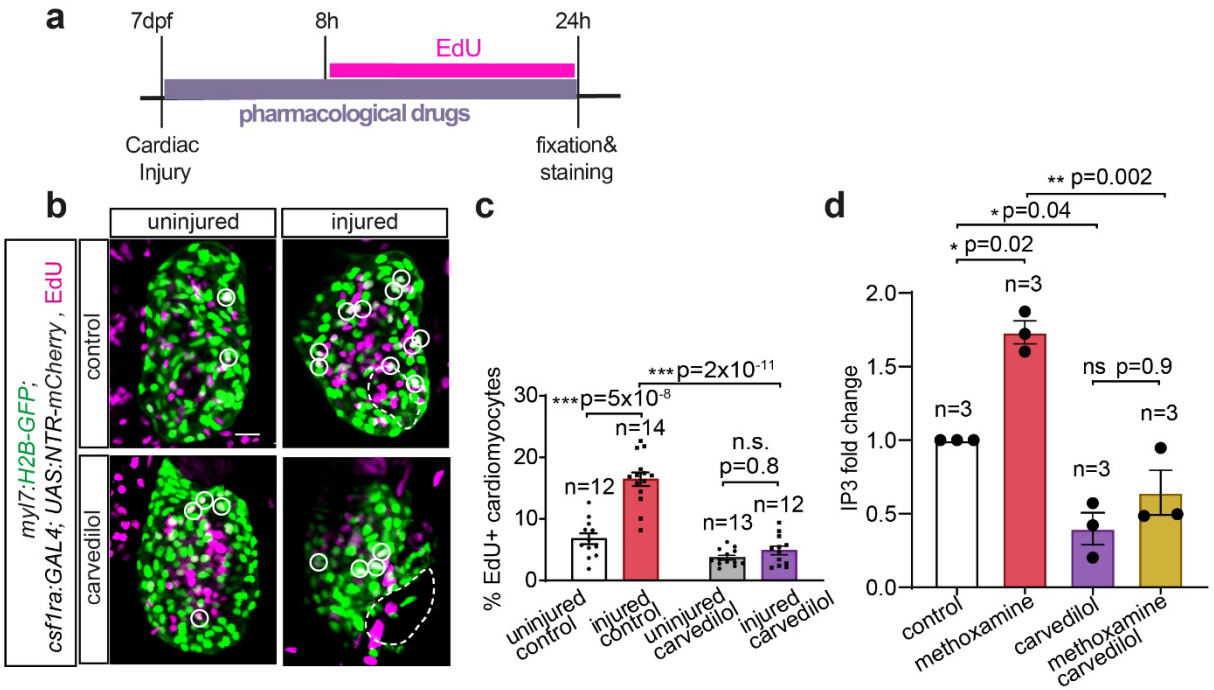

Figure 3.2 Alpha 1 and beta-adrenergic receptor blockage by carvedilol impairs cardiomyocyte proliferation after 2-photon laser-induced necrosis in larval zebrafish and inhibits Alpha-1 adrenergic receptor signaling. (a) Scheme of experimental setup representing the timepoints of 2-photon laser-induced cardiac necrosis of 7dpf *myl7:H2B-GFP*; *csf1ra:Gal4*; *UAS:NTR-mCherry* larvae, their treatment with the appropriate drug until 24hpi, and with EdU from 8 to 24hpi, their fixation

and staining at 24hpi. (b) Confocal images showing the 2-photon laser applied and control sibling hearts from control (vehicle) and carvedilol treated larvae at 24hpi. CMs are immunostained for GFP shown in green, and proliferating cells are marked by EdU shown in magenta. Dashed lines mark the injured area, white circles mark the colocalization of GFP and EdU signals, indicating proliferating CMs. Scale bar is 20 μm. (c) Bar graph depicting the percentage of proliferating CMs as Edu+ CMs over total CMs in cardiac ventricles of uninjured and injured control or carvedilol treated larvae. Data points indicate individual animals and n numbers denote the number of animals used for each group. (d) Bar graph depicting the IP3 levels relative to unstimulated control in lysates of whole 5dpf larvae treated with, methoxamine, carvedilol, and methoxamine + carvedilol. Data points indicate average values of individual experiments with 30 pooled larvae and n numbers denote the number of individual experiments used for each group. All data are presented as mean ± S.E.M. * $p<0.05$, ** $p<0.01$, *** $p<0.001$, n.s. not significant, two-tailed t-test.

Similarly, propranolol, a β-blocker, and prazosin, an α1-blocker, also hindered the post-injury proliferative response of cardiomyocytes **(Fig. 3.3a-d)**. On the other hand, atropine, which blocks muscarinic receptor signaling, had a lesser impact on cardiomyocyte proliferation **(Fig. 3.3a-b, e)**.

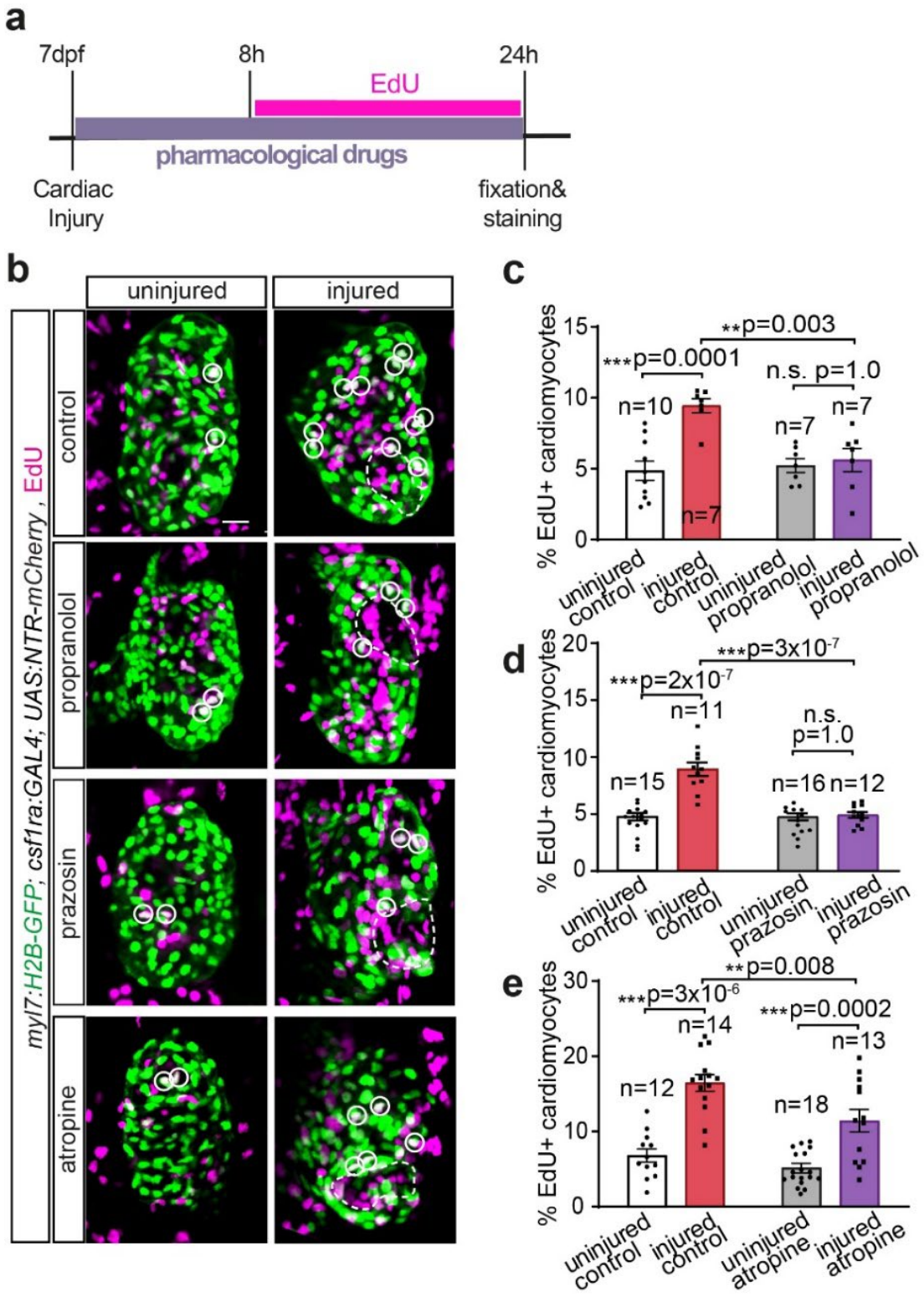

Figure 3.3 Alpha 1-adrenergic receptor is a robust regulator of cardiomyocyte response to 2-photon laser-induced necrosis in larval zebrafish. (a) Scheme of experimental setup representing the timepoints of 2-photon laser-induced cardiac necrosis of 7dpf *myl7:H2B-GFP*; *csf1ra:Gal4*; *UAS:NTR-mCherry* larvae, their treatment with the appropriate drug until 24hpi, and with EdU from 8 to 24hpi,

their fixation and staining at 24hpi. (b)Confocal images showing the 2-photon laser applied and control sibling hearts of control (vehicle), propranolol, prazosin, and atropine treated larvae at 24hpi. CMs are immunostained for GFP shown in green, and proliferating cells are marked by EdU shown in magenta. Dashed lines mark the injured area, white circles mark the colocalization of GFP and EdU signals indicating proliferating CMs. (c, d, e) Bar graphs depict the percentage of proliferating CMs as Edu+ CMs over total CMs in cardiac ventricles of the 2-photon laser applied and control siblings treated with propranolol (c), prazosin (d), and atropine (e) compared to control (vehicle) treated groups. Data points indicate individual animals and n numbers denote the number of animals used for each group, scale bar is 20 μm. All data are presented as mean ± S.E.M. * $p<0.05$, ** $p<0.01$, *** $p<0.001$, n.s. not significant, two-tailed t-test.

Regenerative response after injury heavily depends on the immune system. Thus, in addition to cardiomyocyte proliferation, I examined whether inhibition of adrenergic and cholinergic pathways influence MP recruitment to the injury site in 7dpf *myl7:H2B-GFP; csf1ra:Gal4; UAS:NTR-mCherry* larvae labeling cardiomyocytes with GFP and MPs with mCherry. In control conditions, MP numbers increased after injury **(Fig. 3.4).** Blockage of adrenergic β, α1, or β/α1 receptor signaling strongly reduced numbers of MPs **(Fig. 3.4b-e)** infiltrating the injured heart compared to cholinergic signaling **(Fig. 3.4b, f)**. Importantly, the data here showed that blocking the Adra1 pathway alone induced a reduction of both cardiomyocyte proliferation and MP accumulation after cardiac injury comparable to the effect of carvedilol, the drug with broader adrenergic inhibitory action, suggesting that the adra1 pathway is a significant modulator of cardiac regenerative response.

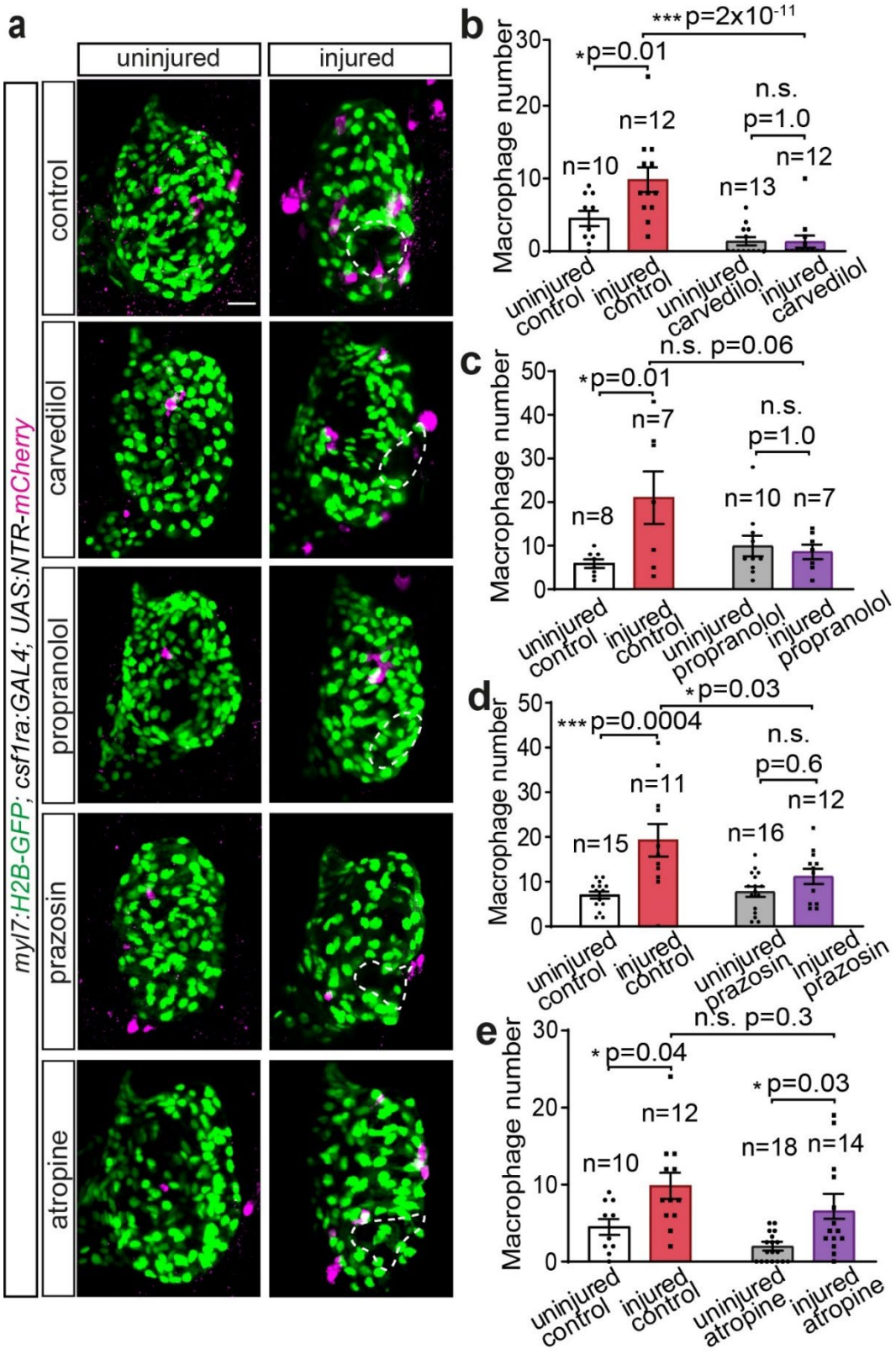

Figure 3.4 Alpha 1-adrenergic receptor is a robust regulator of macrophage response to 2-photon laser-induced necrosis in larval zebrafish. (a) Confocal images showing the 2-photon laser applied and control sibling hearts of 7dpf *myl7:H2B-GFP*; *csf1ra:Gal4*; *UAS:NTR-mCherry* larvae treated with

control (vehicle), carvedilol, propranolol, prazosin, and atropine until 24hpi, same experimental setup as in **Fig. 3.3a**. CMs are immunostained for GFP shown in green, and MPs are immunostained for mCherry shown in magenta. Dashed lines mark the injured area. (b, c, d, e) Bar graphs depict the numbers of MPs recruited to the injury area in ventricles of the 2-photon laser applied and control siblings treated with carvedilol (b), propranolol (c), prazosin (d), and atropine (e) compared to control (vehicle) treated groups. Data points indicate individual animals and n numbers denote the number of animals used for each group, scale bar is 20 μm. All data are presented as mean ± S.E.M. * $p<0.05$, ** $p<0.01$, *** $p<0.001$, n.s. not significant, two-tailed t-test.

To investigate whether the impaired MP accumulation results from reduced MP proliferation, I assessed the mitotic rate in MPs using *csf1ra:Gal4; UAS:NTR-mCherry* larvae upon 2-photon laser application followed by 24h prazosin treatment **(Fig. 3.5a)**. Proliferating MPs in larval hearts were labeled with anti-PCNA and anti-GFP antibodies by immunostaining **(Fig. 3.5b)**. I found that the treatment did not affect MP proliferation, indicating that the effect of Adra1 signaling on MP response is not through the local expansion but rather through regulation of their phenotypic or recruitment dynamics **(Fig. 3.5c)**.

These findings suggest that adrenergic signaling is crucial in proper MP response and cardiomyocyte renewal during regeneration after myocardial injury. As Adra1 signaling alone critically affects cardiomyocyte proliferation and MP accumulation profoundly, I further explored its influence on cardiac regeneration by elucidating neuro-MP interactions and how MPs mediate this influence.

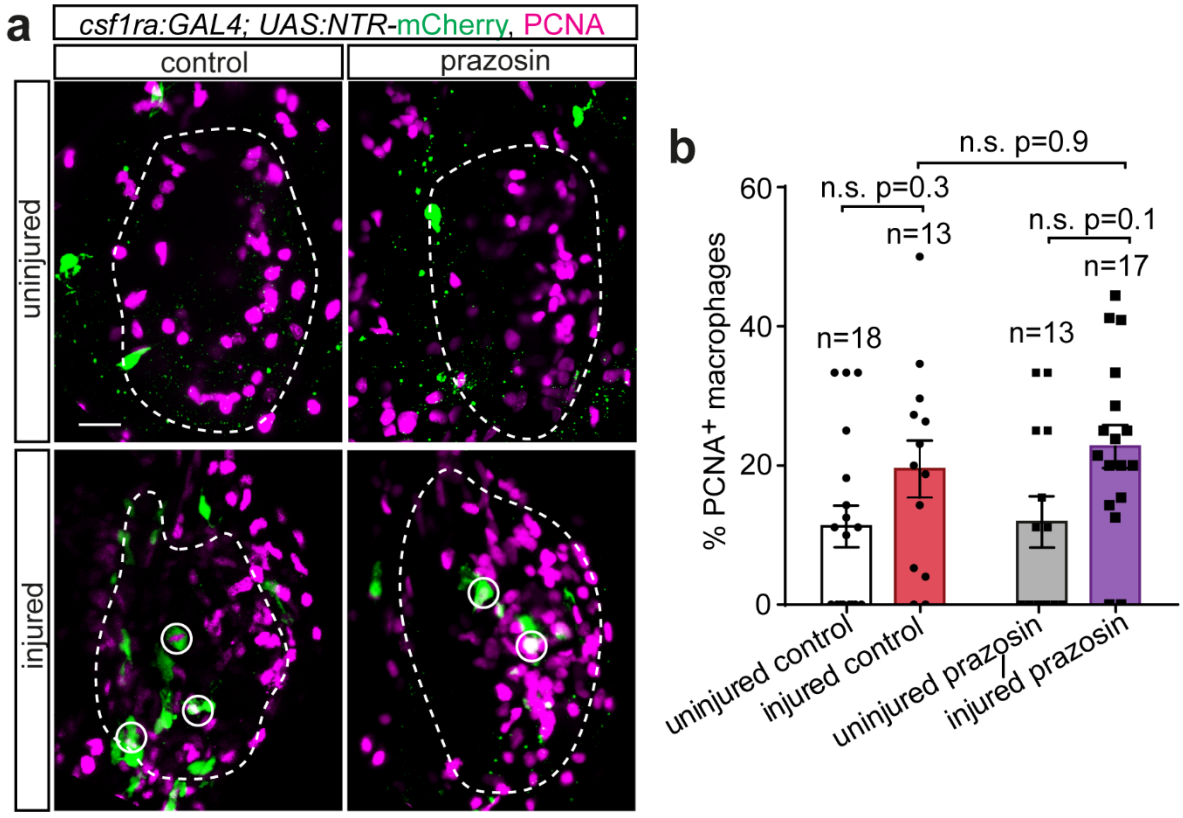

Figure 3.5 Macrophage proliferation is not affected by alpha 1-adrenergic receptor signaling inhibition after 2-photon laser-induced necrosis in larval zebrafish. (a) Confocal images showing the 2-photon laser applied and control sibling hearts of 7dpf *csf1ra:Gal4*; *UAS:NTR-mCherry* larvae treated with control (vehicle) or prazosin until 24hpi, same experimental setup as in **Fig. 3.3a**, except the EdU treatment. MPs are immunostained for mCherry shown in green, and proliferating cells are marked by EdU shown in magenta. Dashed lines mark the ventricle, white circles mark the colocalization of GFP and EdU signals indicating proliferating MPs. (b) Bar graph depicts the percentage of proliferating MPs as Edu+ MPs over total MPs in cardiac ventricles of the 2-photon laser applied and control siblings treated with prazosin compared to control (vehicle) treated groups. Data points indicate individual animals and n numbers denote the number of animals used for each group, scale bar is 20 μm. All data are presented as mean ± S.E.M. * $p<0.05$, ** $p<0.01$, *** $p<0.001$, n.s. not significant, two-tailed t-test.

3.2 Establishment and characterization of macrophage-specific adra1 loss of function model

To investigate if MPs are the mediators of Adra1 signaling influence on the regenerative response of the heart, we developed a MP specific loss-of-function model. This loss-of-function model is designed to interfere with the signal transduction pathway of the Adra1 receptor. Adra1 belongs to the class of GPCRs and operates through Gq/11 type G proteins [188]. It was shown that the majority of GPCRs engage with G proteins via their third intracellular loops, and expressing this segment as a mini-gene can hinder downstream pathway activation [188–190]. This strategy was previously employed to impede the downstream signaling pathway of the receptor in a dominant negative manner [188,191,192]. This mechanism potentially involves an interaction between the third intracellular loop and the intracellular domain of the parent receptor. This interaction has the capacity to sustain the receptor in an inactive conformation, thus culminating in a specific inhibition of the receptor's functionality.

The adrenergic α1 receptor has three subtypes: α1A, α1B, and α1D. These are Gq/11-coupled receptors that primarily signal through PLC activation. This activation elevates IP3 and intracellular Ca^{2+} levels [193]. Among the five zebrafish orthologs corresponding to these receptors—namely adra1aa, adra1ab, adra1ba, adra1bb, and adra1d—only adra1d and adra1bb demonstrate notable expression in the regenerating zebrafish heart, as evidenced by available databases http://zebrafish.genomes.nl/tomoseq/ and http://www.zfregeneration.org/ [194,195]. In the early pro-inflammatory phase, adra1d expression was observed to increase temporarily but quickly diminished by 3dpi. In contrast, adra1bb expression seemed to be sequentially initiated and sustained through the later stages of cardiac repair. Given this expression pattern, I chose to focus on the role of the adra1bb receptor in neuro-MP interactions modulating cardiac repair.

First, I aimed to examine the expression of adrenergic receptors in MPs. For this purpose, I isolated MPs from *csf1ra:Gal4; UAS:NTR-mCherry* larvae by fluorescence-activated cell sorting (FACS) and detected mRNA encoding adrenergic receptors by real-time reverse transcription-PCR (RT-PCR) **(Fig. 3.6)**. This showed that indeed adra1bb was expressed in MPs.

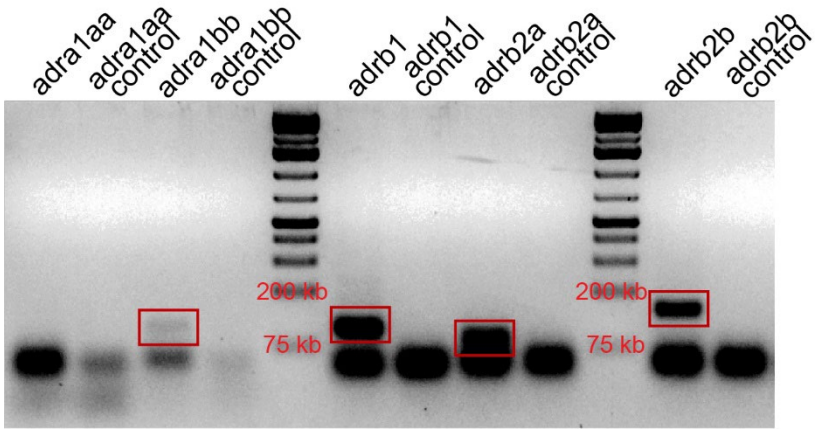

Figure 3.6 Expression of adrenergic receptors in macrophages. Agarose gel electrophoresis image showing the RT-PCR detected mRNAs encoding adrenergic receptors in MPs isolated by FACS from *csf1ra:Gal4; UAS:NTR-mCherry* larvae. Control lanes contain samples in which RT-PCR was performed without cDNAs.

In order to inhibit the adra1bb pathway, I engineered a genetic tool utilizing the third intracellular loop of the adra1bb receptor, fused with the fluorescent protein CFP (*adra1-3i-T2A-CFP*), and inserted it under the control of the *UAS* promoter (transgene hereinafter referred to as *adra1-3i)*. This construct enables specific expression within MPs using the *csf1ra:Gal4* driver line **(Fig. 3.7).**

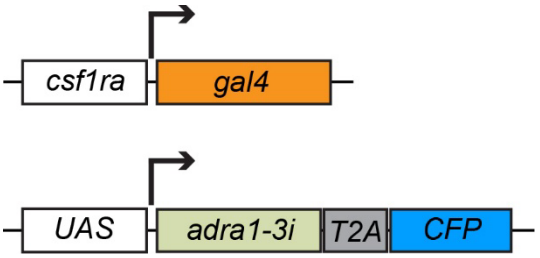

Figure 3.7 Macrophage specific expression design of alpha 1-adrenergic receptor Bb. Scheme of the *UAS:adra1-3i-T2A-CFP* construct, when paired with the *csf1ra:Gal4 line***,** ensures its expression specifically in MPs.

To characterize the loss-of-function model, I first examined the expression pattern in the *csf1ra:Gal4; UAS:adra1-3i-T2A-CFP; UAS:NTR-mCherry* zebrafish line both as whole larvae **(Fig. 3.8a-b)** and adult hearts **(Fig. 3.8c-d)**, which demonstrated a mosaic expression of *adra1-3i* with around 45% **(**Q2 in **Fig. 3.8b, d)** of all MPs **(**Q1+Q2 in **Fig. 3.8b, d)**, identifiable by NTR-mCherry labeling. To test the effect of the dual UAS system on the resulting MP populations, I compared the MP populations from the hearts of adult fish with *csf1ra:Gal4; UAS:adra1-3i-T2A-CFP; UAS:NTR-mCherry* and *csf1ra:Gal4; UAS:NTR-mCherry*. I found that similar amounts of total MPs **(**Q2+Q3 in **Fig. 3.8e-h)**, indicated by NTR-mCherry labeling, are present in both hearts **(Fig. 3.8e-h)**. The observed mosaicism, which might be accentuated by the competitive nature of the dual UAS system, enables the evaluation of functional changes in MPs expressing the *adra1-3i* transgene relative to control MPs without the *adra1-3i* expression within the same hearts.

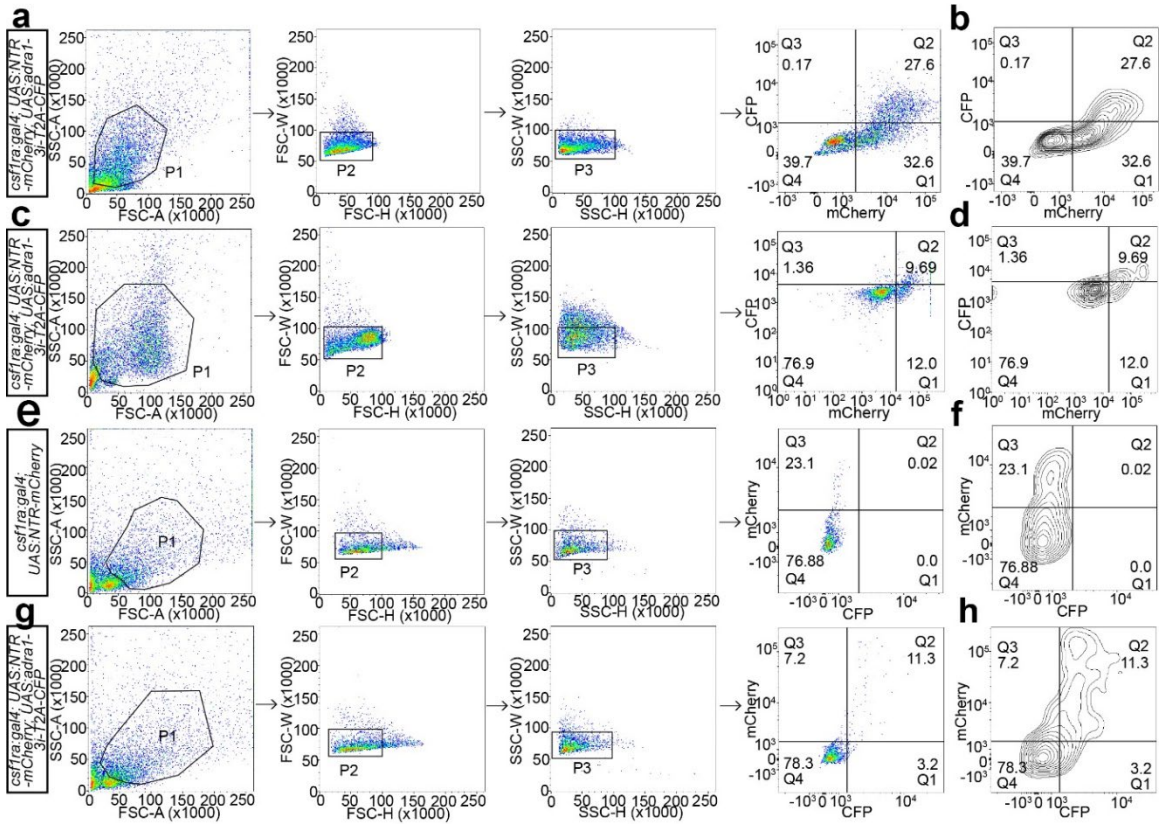

Figure 3.8 Mosaicism of *adra1-3i-T2A-CFP* expression in macrophages of *csf1ra:Gal4; UAS:adra1-3i-T2A-CFP; UAS:NTR-mCherry* transgenic line. (a-d) Plots depict the gating strategy for flow cytometry analysis of Adra1 signaling deficient cells (CFP+) in the whole MP population (mCherry+) from a pool of 50 dissociated 5dpf larvae (a, b) and pool of 3 adult hearts (c, d), shown as dot (a, c) and contour plots (b, d). In both larvae and adult hearts, CFP+ (Q2 in b and d) MPs are approximately 45% of the total (mCherry+) MP population (Q1 + Q2 in b and d). (e-h) Plots depict the gating strategy for flow cytometry analysis of cells from dissociated adult hearts of *csf1ra:Gal4; UAS:NTR-mCherry* (e, f) and *csf1ra:Gal4; UAS:adra1-3i-T2A-CFP; UAS:NTR-mCherry* (g, h) zebrafish shown as dot (e, g) and contour plots (f, h). mCherry+ MPs are approximately 23% and 19% (Q2 + Q3 in f and h) in *csf1ra:Gal4; UAS:NTR-mCherry* and *csf1ra:Gal4; UAS:adra1-3i-T2A-CFP; UAS:NTR-mCherry*, respectively.

To validate the impairment of MP-specific Adra1 signaling in the loss-of-function model, I initially quantified the transient intracellular calcium surges in MPs post-activation, as activation of Adra1 receptors prompts the release of calcium from intracellular reservoirs [196]. I adopted calcium imaging techniques, leveraging the genetically encoded calcium indicator, GCaMP6s in 5dpf *csf1ra:Gal4; UAS:NTR-mCherry; UAS:adra1-3i-T2A-CFP; 14XUAS:GCaAMP6s* larvae [197]. The *csf1r:gal4* transgene was used to direct the expression of *GCaMP6s*, *adra1-3i-T2A-CFP*, and *mCherry*, specifically in MPs **(Fig. 3.9a)**. Introducing

methoxamine triggered a transient rise in intracellular calcium within control MPs, which are not expressing *adra1-3i*. Expression of *adra1-3i-T2A-CFP* notably diminished the amplitude of this calcium surge **(Fig. 3.9a)**. This evidence shows that the *adra1-3i-T2A-CFP* expression effectively obstructs signaling downstream of the Adra1 receptor in MPs.

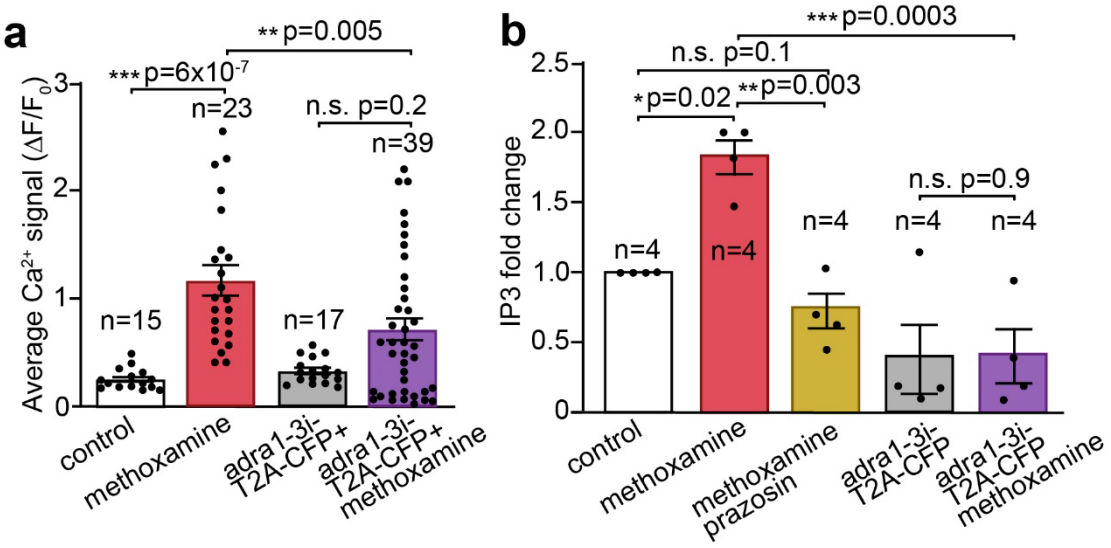

Figure 3.9 *adra1-3i-T2A-CFP* expression effectively inhibits Adra1 signaling indicated by calcium levels and IP3 production. (a) Bar graph depicts the impairment of calcium signaling mediated by *adra1-3i* expression in 5dpf c*sf1ra:Gal4; UAS:NTR-mCherry; UAS:adra1-3i-T2A-CFP; 14XUAS:GCaMP6s* larvae before and after application of the Adra1 agonist methoxamine. Calcium signals were measured by time-lapse imaging of control *adra1-3i–* and *adra1-3i+* MPs in the same *csf1ra:Gal4; UAS:NTR-mCherry; UAS:adra1-3i-T2A-CFP; 14XUAS:GCaMP6s* larvae and represented on the graph as change of fluorescent intensity (ΔF) relative to fluorescence intensity in resting condition (F0) Data are presented as mean ± S.E.M with data points of individual cells, and n numbers denoting the number of cells from 12-15 larvae per treatment group. (b) Bar graph depicts the impairment of IP3 production mediated by *adra1-3i* expression in 5dpf *tbp:Gal4* (control) and *tbp:Gal4; UAS:adra1-3i-T2A-CFP* whole larvae before and after application of the Adra1 agonist methoxamine. IP3 amounts were measured by ELISA using the lysates from all groups and presented as fold change relative to unstimulated controls. Data are presented as mean ± S.E.M with data points of independent experiments and n numbers denoting the biological replicates, each containing 30 pooled larvae per group.

To further characterize the loss-of-function approach, I assessed other critical outcomes of Adra1 signal transduction via IP3 measurement. I utilized 5dpf *tbp:Gal4; UAS:adra1-3i-T2A-CFP* larvae, where the majority of cells are expressing *adra1-3i*, as the experiment group and 5dpf *tbp:Gal4* larvae as control group. I measured the amount of IP3 after activating or inhibiting the Adra1 pathway with methoxamine and prazosin, respectively, using ELISA. In

control fish, methoxamine triggered an elevation in IP3 levels **(Fig. 3.9b)**. This elevation was abolished by the presence of the prazosin, showing that it is mediated by Adra1 receptors **(Fig. 3.9b)**. Significantly, the rise of IP3 amount was hindered in *adra1-3i* larvae, further confirming efficient inhibition of Adra1 signaling by *adra1-3i* expression **(Fig. 3.9b)**. These results suggest that deploying *adra1-3i* in a cell type specific manner is a reliable and efficient loss-of-function approach.

3.3 Adra1 signaling in macrophages reduces macrophage recruitment to the injured heart in larval zebrafish

After evaluating the efficacy of the loss-of-function tool in inhibiting adra1 signaling, I explored whether disrupting Adra1 signaling, specifically in MPs, could affect their accumulation at cardiac injury sites. I conducted live imaging on 7dpf *csf1ra:Gal4; UAS:NTR-mCherry; UAS:adra1-3i-T2A-CFP* larvae upon cardiac necrosis induced by a 2-photon laser. This line displays mosaic expression of the *adra1-3i-T2A-CFP.* Therefore, it allowed me to investigate *adra1-3i+* and *adra1-3i-* MPs in the same sample, providing a better comparison of their behaviors. At 24hpi, the hearts contained fewer *adra1-3i+* MPs compared to *adra1-3i-* **(Fig. 3.10)**. This indicates that specific inhibition of the Adra1 pathway in MPs influences their accumulation at the injury site, mirroring results from the pharmacological approach.

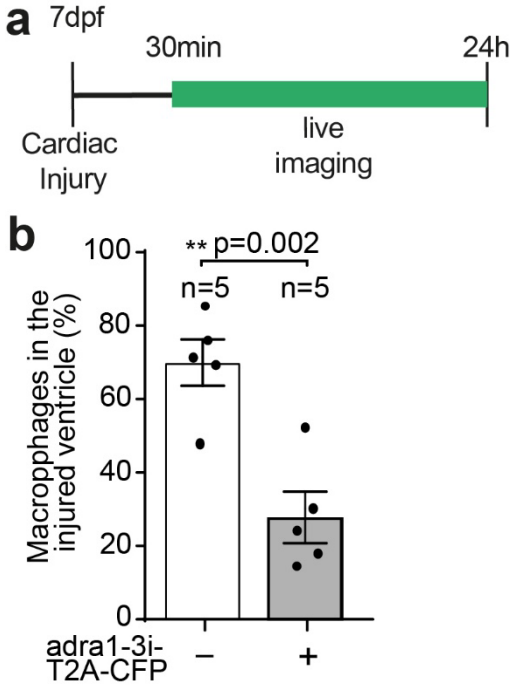

Figure 3.10 Cell-type specific effect of Adra1 signaling on macrophage response after cardiac injury. (a) Scheme of experimental setup representing the timepoints of 2-photon laser-induced cardiac necrosis of 7dpf *csf1ra:Gal4; UAS:adra1-3i-T2A-CFP; UAS:NTR-mCherry* larvae, and their time-lapse imaging from 30mpi to 24hpi. (b) Bar graph depicts the percentages of *adra1-3i+* and *adra1-3i-* MPs among the total MP population recruited to the cardiac lesion, assessed at 24hpi timepoint only. Data points indicate individual animals and n numbers denote the number of animals used for each group. All data are presented as mean ± S.E.M. * $p<0.05$, ** $p<0.01$, *** $p<0.001$, n.s. not significant, two-tailed t-test.

3.4 Cell-autonomous Adra1 signaling impacts macrophage polarization after cardiac injury in larval zebrafish

I wanted to further investigate the influence of Adra1 signaling on distinct MP subpopulations. MPs are known to execute a two-phase response following MI: initially adopting a pro-inflammatory phenotype during recruitment to the site of injury, followed by a phenotypic shift to anti-inflammatory status as the local environment transitions to an anti-inflammatory state. Both phases are pivotal for effective cardiac regeneration. Relying on this information, to distinguish between pro-inflammatory and anti-inflammatory MPs, I employed a transgenic reporter line, *tnfa:EGFP*, which labels cells expressing the pro-inflammatory cytokine TNFα. It has been previously established that tnfa expression serves as a reliable marker for pro-inflammatory MPs and can be utilized to differentiate between pro- and anti-inflammatory MP phenotypes in both zebrafish and mammalian models. By combining *tnfa:EGFP* with *csf1ra:Gal4; UAS:NTR-mCherry; UAS:adra1-3i-T2A-CFP* transgenes in the same zebrafish larvae, I was able to simultaneously evaluate the role of Adra1 signaling on both pro- and anti-inflammatory MPs post-injury **(Fig. 3.11a)**. Time-lapse imaging was performed starting at 30mpi and continued until 24hpi **(Fig. 3.11b)**.

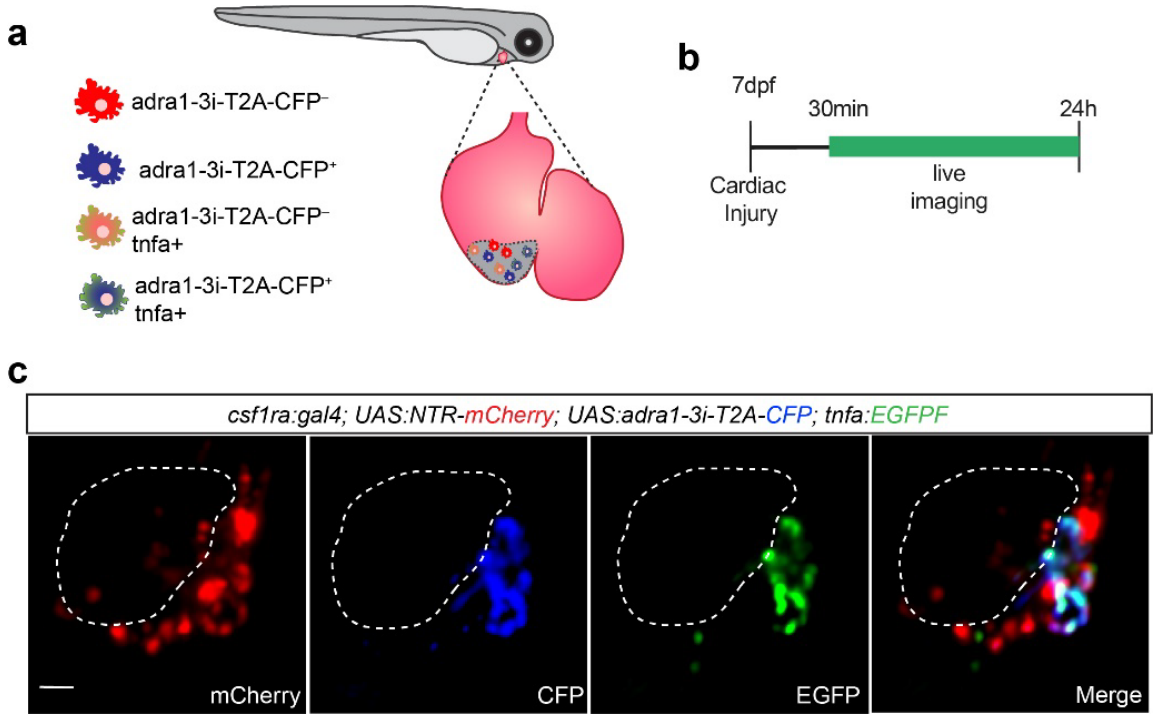

Figure 3.11 Heterogeneous macrophage pools in *csf1ra:Gal4; UAS:NTR-mCherry; UAS:adra1-3i-T2A-CFP; tnfa:EGFPF* larval heart after cardiac injury. (a) Scheme illustrating the diverse MP populations in a larval heart at 24hpi. (b) Scheme of experimental setup representing the timepoints of

2-photon laser-induced cardiac necrosis of 7dpf *csf1ra:Gal4; UAS:adra1-3i-T2A-CFP; UAS:NTR-mCherry; tnfa:EGFPF* larvae, and their time-lapse imaging from 30mpi to 24hpi. (c) Representative confocal images of 7dpf *csf1ra:Gal4; UAS:NTR-mCherry; UAS:adra1-3i-T2A-CFP; tnfa:EGFPF* larval heart showing total recruited MPs (mCherry+) in red, *adra1-3i+* (CFP+) MPs in blue, and *tnfa+* (EGFP+) ones in green at 24hpi. Dashed lines mark the injured area, scale bar is 20 μm.

Quantitative analysis revealed that the effect of Adra1 signaling on MP subtypes was not homogeneous **(Fig. 3.12)**. Specifically, the population of *adra1-3i+* anti-inflammatory (*tnfa-*) MPs' contribution to the total *tnfa-* MP pool was significantly lower in comparison to their *adra1-3i- tnfa-* counterparts **(Fig. 3.12b)**. Conversely, the pro-inflammatory (*tnfa+*) MP population displayed a higher proportion of *adra1-3i+ tnfa+* MPs relative to *adra1-3i- tnfa+* MPs **(Fig. 3.12a)**.

These observations clarified that the previously noted reduction in overall MP numbers **(Fig. 3.4)** was not attributable to a decrease in *tnfa+* MPs. This is substantiated by the considerable contribution of *adra1-3i+* MPs to the *tnfa+* population **(Fig. 3.12a)**. Moreover, the majority of *tnfa-* MPs were *adra1-3i-* **(Fig. 3.12b)**, indicating that Adra1 signaling may have a role in fostering the presence of anti-inflammatory MPs following MI.

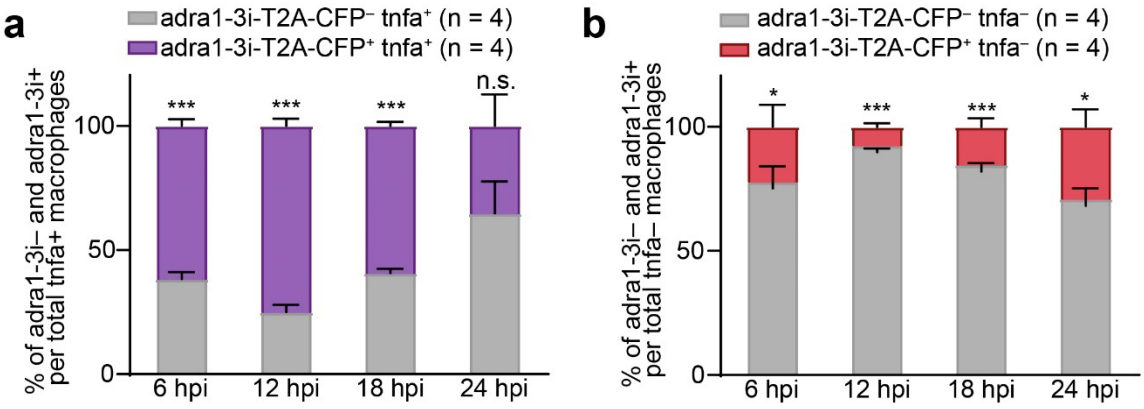

Figure 3.12 Macrophage cell-autonomous Adra1 signaling promotes the presence of anti-inflammatory macrophages. Segmented bar graphs depict the distribution of *adra1-3i–* and *adra1-3i+* MPs within the pro-inflammatory (*tnfa+*) (a) and anti-inflammatory (*tnfa–*) (b) MP populations in the same heart around the injured area at 6, 12, 18 and 24hpi as percentages. Experimental setup in **Fig. 3.11b** was used and the recruited populations in 2-photon laser applied *csf1ra:Gal4; UAS:NTR-mCherry; UAS:adra1-3i-T2A-CFP; tnfa:EGFPF* larval hearts were quantified. All data are presented as mean ± S.E.M, and n numbers denote the number of animals used in this experiment. * $p<0.05$, ** $p<0.01$, *** $p<0.001$, n.s. not significant, two-tailed t-test.

3.5 Adra1 signaling is required for cardiomyocyte and macrophage regenerative response in adult zebrafish model of myocardial infarction

Having delineated the crucial role of adra1 signaling in cardiac regeneration following laser-induced cardiac necrosis in larval zebrafish, I sought to extend these findings to fully developed adult zebrafish. Adult zebrafish offer a more comprehensive model to examine cellular events during cardiac regeneration post-MI. My first objective was to ascertain the impact of Adra1 signaling inhibition on cardiomyocyte and MP responses during adult cardiac regeneration, with the aim of corroborating my previous observations in the larval model **(Fig. 3.3d, Fig. 3.4e)**. For this purpose, I employed cryoinjury in adult *csf1ra:Gal4; UAS:NTR-mCherry* zebrafish and initiated treatment with either prazosin or vehicle control from 0dpi to 7dpi **(Fig. 3.13a)**. Tissue analysis was performed at 7dpi using immunofluorescence staining **(Fig. 3.13a)**. Cardiomyocyte mitotic activity was significantly elevated in control-treated hearts following cryoinjury when compared to sham-operated control-treated hearts, as assessed at 7 dpi **(Fig. 3.13b, c)**. Notably, pharmacological inhibition of Adra1 signaling with prazosin impaired the cardiomyocyte mitotic response at 7dpi, mirroring the phenotype observed in the larval model **(Fig. 3.13b, c; Fig. 3.3d)**.

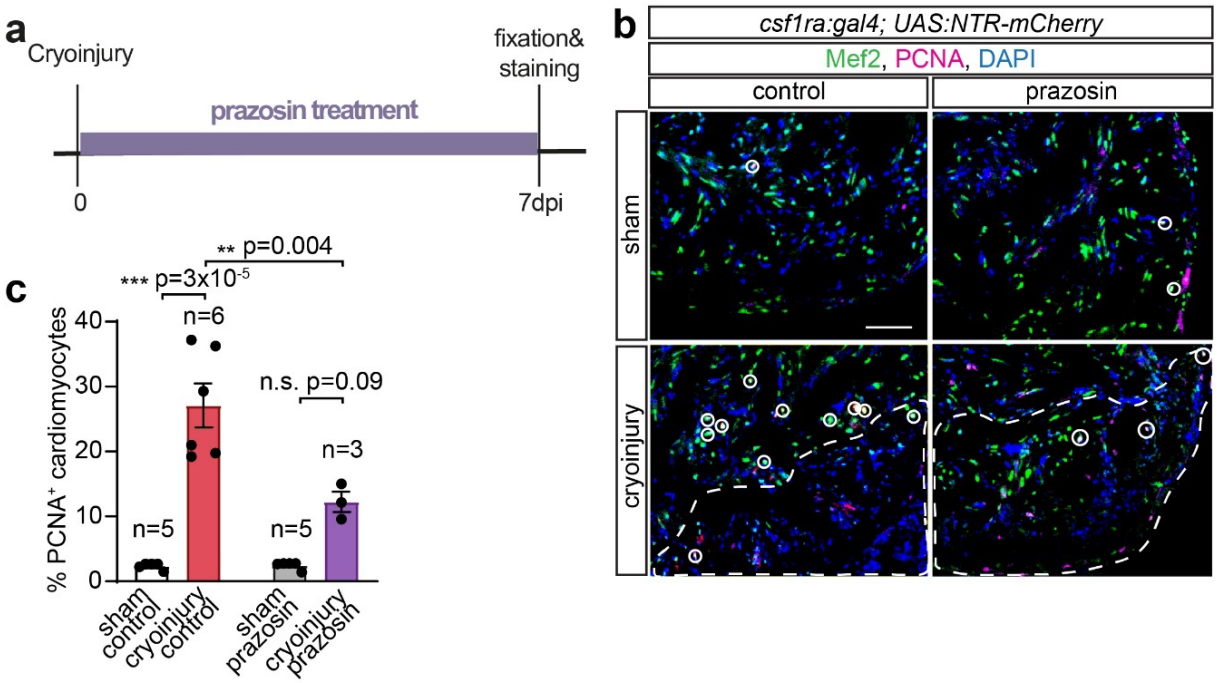

Figure 3.13 Alpha 1-adrenergic receptor regulates cardiomyocyte response to cryoinjury in adult zebrafish hearts. (a) Scheme of experimental setup representing the timepoints of cryoinjury on adult *csf1ra:Gal4*; *UAS:NTR-mCherry* hearts, their treatment with prazosin until 7dpi, their fixation and

staining. (b) Confocal images showing *csf1ra:Gal4; UAS:NTR-mCherry* heart cryosections treated with control (vehicle) or prazosin for 7 days after sham operation or cryoinjury. Sections are immunofluorescence stained for CMs with Mef2 shown in green, for proliferating cells with PCNA shown in magenta, and for cell nuclei with DAPI shown in blue. Dashed lines mark the injured area, white circles mark the colocalization of Mef2 and PCNA signals indicating proliferating CMs, scale bar is 50 µm. (c) Bar graph depicts the proliferating cardiomyocytes (Mef2+/PCNA+) inside and in the proximity of the injury zone, quantified as percentages of cardiomyocytes within the observed area. In sham-operated cryosections, similar sized areas are used for quantification. Data points indicate individual animals and n numbers denote the number of animals used for each group. All data are presented as mean ± S.E.M. * $p<0.05$, ** $p<0.01$, *** $p<0.001$, n.s. not significant, two-tailed t-test.

In the same experimental set, I also assessed the MP accumulation. Control-treated hearts displayed elevated MP presence post-cryoinjury compared to sham-operated hearts, while this accumulation was diminished in prazosin-treated hearts at 7dpi **(Fig. 3.14b, c)**. This phenotype closely paralleled observations from the larval model **(Fig. 3.4e)**.

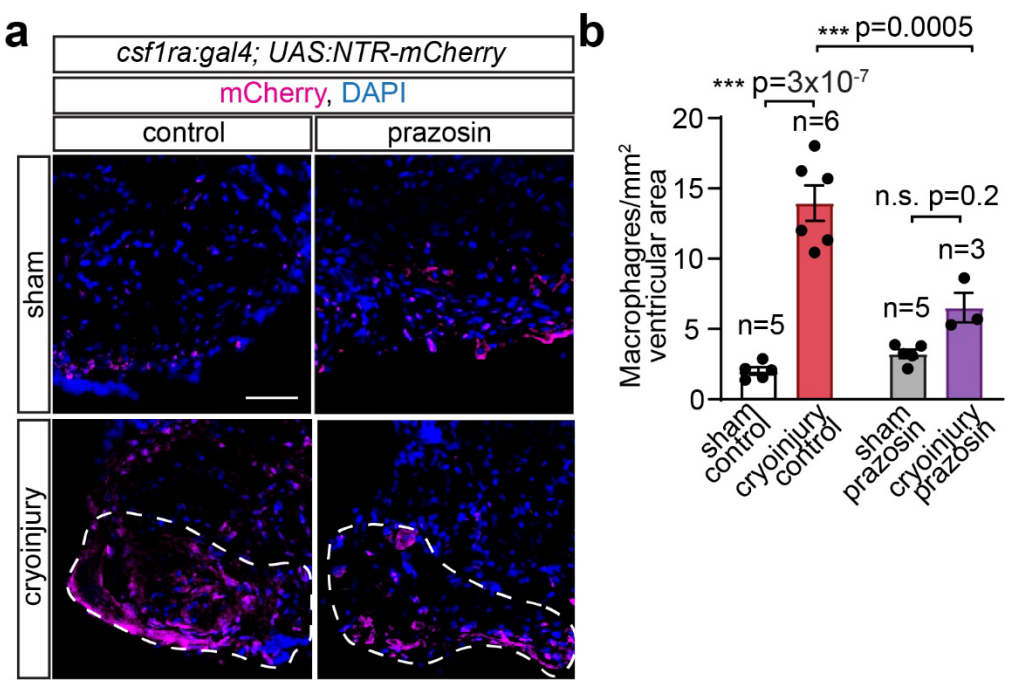

Figure 3.14 Alpha 1-adrenergic receptor regulates macrophage response to cryoinjury in adult zebrafish heart. Same experimental setup as in **Fig. 3.13a** (a) Confocal images showing *csf1ra:Gal4; UAS:NTR-mCherry* heart cryosections treated with control (vehicle) or prazosin for 7 days after sham operation or cryoinjury. Sections are immunofluorescence stained for MP with mCherry shown in magenta, and for cell nuclei with DAPI shown in blue. Dashed lines mark the injured area, scale bar is 50 µm. (b) Bar graph depicts number of MPs (mCherry+) inside and in the proximity of the injury zone, quantified as cell numbers per 1 mm2 ventricular area. In sham-operated cryosections, similar sized areas are used for quantification. Data points indicate individual

animals and n numbers denote the number of animals used for each group. All data are presented as mean ± S.E.M. * p<0.05, ** p<0.01, *** p<0.001, n.s. not significant, two-tailed t-test.

To dissect the underlying mechanisms of impaired MP accumulation, I examined MP mitotic activity **(Fig. 3.15)**. Intriguingly, MP proliferation remained unaltered following cryoinjury in the presence of Adra1 signaling blockage, as evidenced by comparable levels of PCNA+ MP percentages in both prazosin and control-treated hearts around the injury site **(Fig. 3.15)**. Thus, the observed reduction in MP accumulation in prazosin-treated hearts is not attributable to an inhibition of MP proliferation **(Fig. 3.15)**.

These data collectively underscore the pivotal role of Adra1 signaling in modulating the cardiac regenerative response in adult zebrafish. Specifically, inhibition of Adra1 signaling systemically led to similar impairments in both cardiomyocyte proliferation and MP accumulation, corroborating the observations made in the larval cardiac necrosis model.

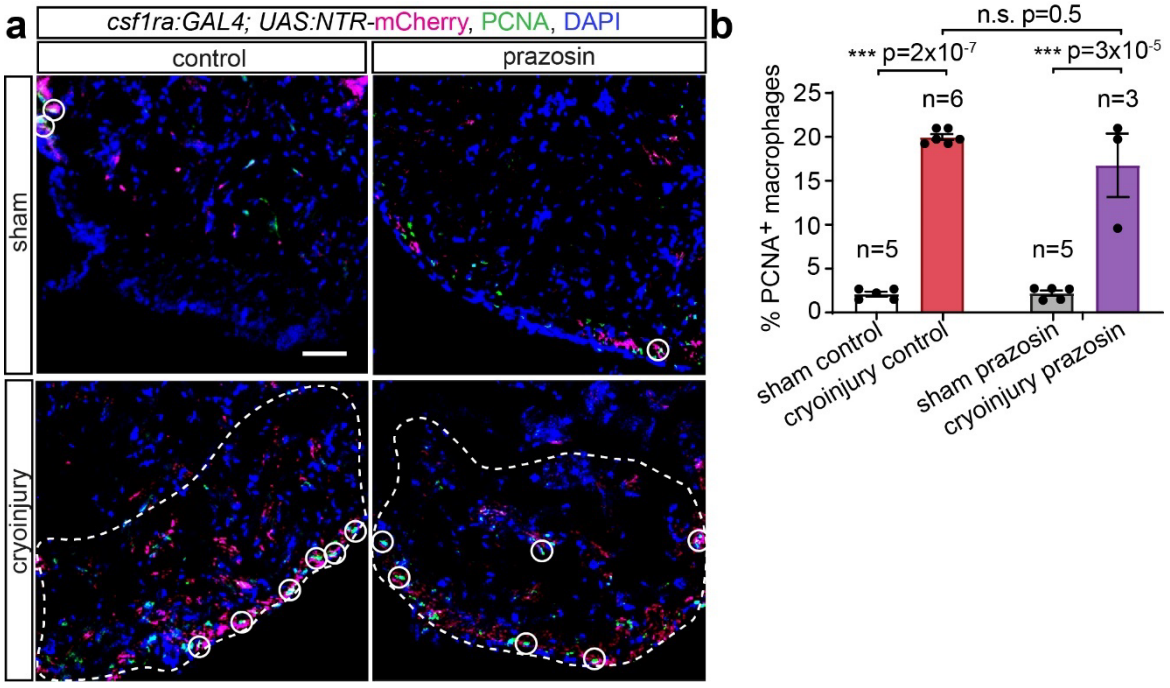

Figure 3.15 Macrophage proliferation is not affected by alpha 1-adrenergic receptor signaling inhibition after cryoinjury in adult zebrafish hearts. Same experimental setup as in **Fig. 3.13a** (a) Confocal images showing *csf1ra:Gal4; UAS:NTR-mCherry* heart cryosections treated with control (vehicle) or prazosin for 7 days after sham operation or cryoinjury. Sections are immunofluorescence stained for MP with mCherry shown in magenta, for proliferating cells with PCNA shown in green, and for cell nuclei with DAPI shown in blue. Dashed lines mark the injured area, white circles mark the colocalization of mCherry and PCNA signals indicating proliferating MPs, scale bar is 50 μm. (b) Bar graph depicts the proliferating MPs (mCherry+/PCNA+) inside and in the proximity of the injury zone,

quantified as percentages of MPs within the observed area. In sham-operated cryosections, similar sized areas are used for quantification. Data points indicate individual animals and n numbers denote the number of animals used for each group. All data are presented as mean ± S.E.M. * $p<0.05$, ** $p<0.01$, *** $p<0.001$, n.s. not significant, two-tailed t-test.

3.6 Macrophage cell-autonomous Adra1 signaling is required for cardiac regenerative response and macrophage polarization in adult zebrafish heart

Following the confirmation that Adra1 signaling plays an indispensable role in regulating cardiomyocyte and MP responses to cardiac injury in adult zebrafish via pharmacological inhibition, my next objective was to explore whether MP cell-autonomous Adra1 signaling serves as the principal mediator in shaping the regenerative response in adult hearts. To this end, I used transgenic adult zebrafish expressing *csf1ra:Gal4; UAS:adra1-3i-T2A-CFP; UAS:NTR-mCherry* and evaluated cardiomyocyte mitotic activity and MP accumulation at 7dpi, in comparison with control *csf1ra:Gal4; UAS:NTR-mCherry* adult zebrafish hearts **(Fig. 3.16)**. As anticipated, cardiomyocyte proliferation was enhanced in control hearts following cryoinjury when compared to sham-operated controls **(Fig. 3.16b, c)**. However, in *adra1-3i* hearts, cryoinjury led to a significant attenuation of cardiomyocyte proliferation, with activity levels comparable to those observed in sham-operated *adra1-3i* hearts at 7 dpi **(Fig. 3.16b, c)**. Concurrently, MP accumulation was found to be diminished in *adra1-3i* hearts relative to control hearts post-cryoinjury **(Fig. 3.17)**.

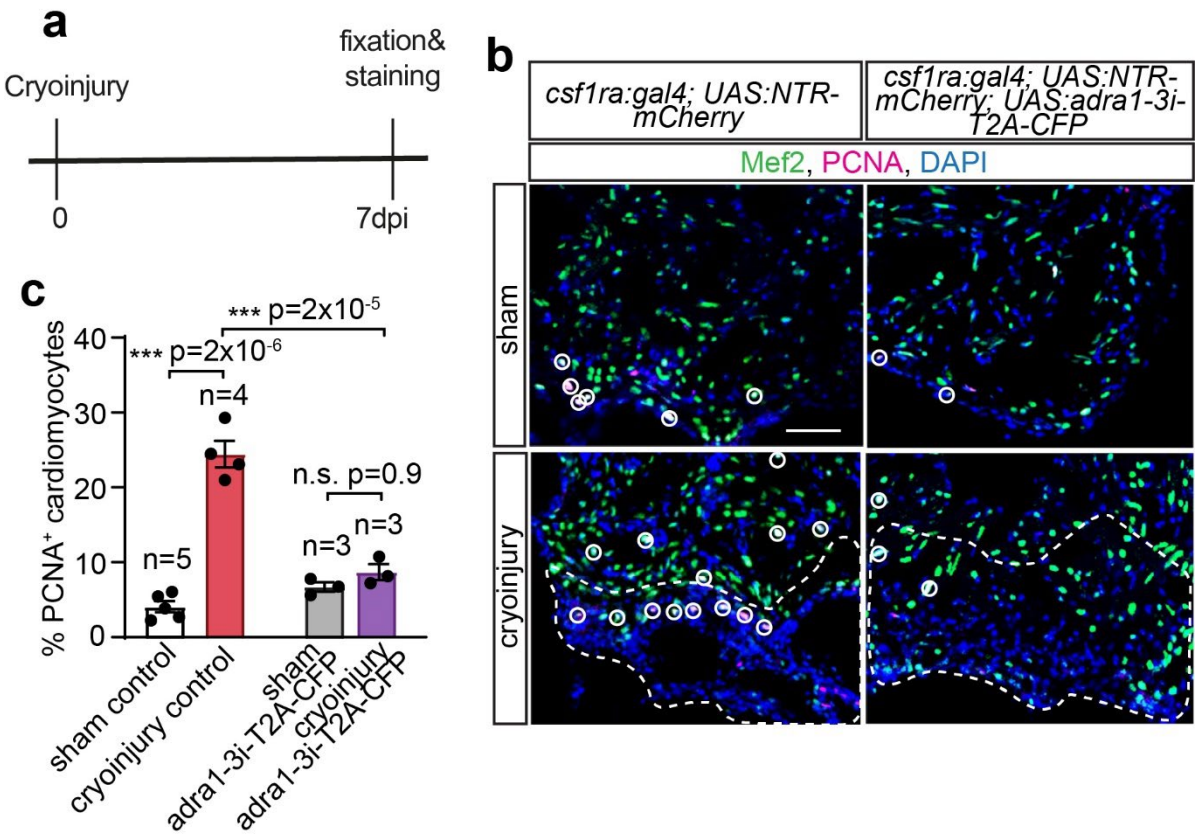

Figure 3.16 Macrophage cell-autonomous Adra1 signaling is critical for cardiomyocyte response to cryoinjury in adult zebrafish hearts. (a) Scheme of experimental setup representing the timepoints of cryoinjury on adult *csf1ra:Gal4*; *UAS:NTR-mCherry* (control) and *csf1ra:Gal4; UAS:adra1-3i-T2A-CFP; UAS:NTR-mCherry* hearts, and their fixation and staining at 7dpi. (b) Confocal images showing sham-operated or cryoinjured *csf1ra:Gal4; UAS:NTR-mCherry* (control) and *csf1ra:Gal4; UAS:adra1-3i-T2A-CFP; UAS:NTR-mCherry* heart cryosections at 7dpi. Sections are immunofluorescence stained for CMs with Mef2 shown in green, for proliferating cells with PCNA shown in magenta, and for cell nuclei with DAPI shown in blue. Dashed lines mark the injured area, white circles mark the colocalization of Mef2 and PCNA signals indicating proliferating CMs, scale bar is 50 μm. (c) Bar graph depicts the proliferating cardiomyocytes (Mef2+/PCNA+) inside and in the proximity of the injury zone, quantified as percentages of cardiomyocytes within the observed area. In sham-operated cryosections, similar sized areas are used for quantification. Data points indicate individual animals and n numbers denote the number of animals used for each group. All data are presented as mean ± S.E.M. * $p<0.05$, ** $p<0.01$, *** $p<0.001$, n.s. not significant, two-tailed t-test.

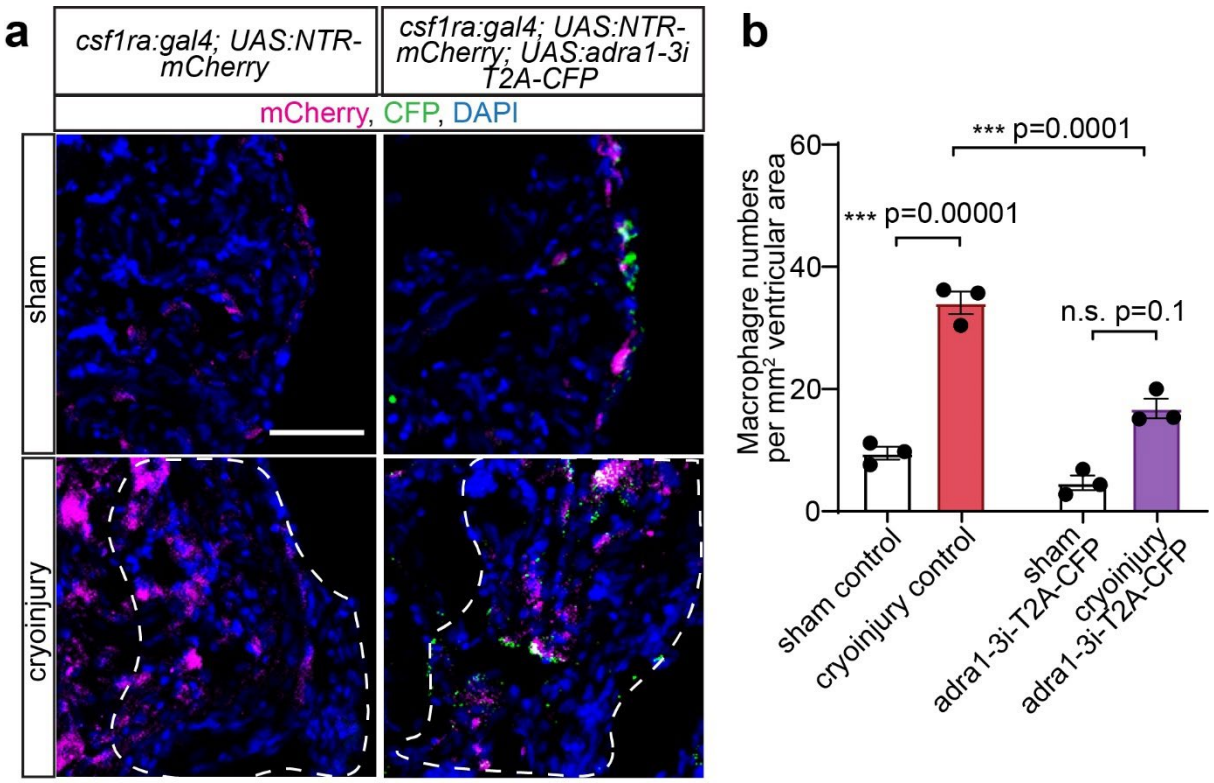

Figure 3.17 Macrophage cell-autonomous Adra1 signaling is critical for macrophage response to cryoinjury in adult zebrafish hearts. Same experimental setup as in **Fig. 3.16a** (a) Confocal images showing sham-operated or cryoinjured *csf1ra:Gal4; UAS:NTR-mCherry* (control) and *csf1ra:Gal4; UAS:adra1-3i-T2A-CFP; UAS:NTR-mCherry* heart cryosections at 7dpi. Sections are immunofluorescence stained for MPs with mCherry shown in magenta, for *adra1-3i-T2A*-CFP with CFP shown in green, and for cell nuclei with DAPI shown in blue. Dashed lines mark the injured area, scale bar is 50 μm. (b) Bar graph depicts number of MPs (mCherry+) inside and in the proximity of the injury zone, quantified as cell numbers per 1 mm2 ventricular area. In sham-operated cryosections, similar sized areas are used for quantification. Data points indicate individual animals and n numbers denote the number of animals used for each group. All data are presented as mean ± S.E.M. * $p<0.05$, ** $p<0.01$, *** $p<0.001$, n.s. not significant, two-tailed t-test.

Considering these observations regarding the role of MP Adra1 signaling in the cardiac regenerative response, I proceeded to examine its influence on various MP subtypes, mirroring my prior investigation in the larval model. To this end, I performed immunostaining for Tnfα on sections of *adra1-3i* hearts to evaluate shifts in pro- and anti-inflammatory MP populations **(Fig. 3.18)**. Remarkably, the contribution of *adra1-3i*+ MPs to the *tnfa*+ MP pool was elevated **(Fig. 3.18b)**, while their contribution to the *tnfa*- MP population was considerably reduced **(Fig. 3.18c)** compared to *adra1-3i*- contributions to both populations. Given that 7 dpi represents a critical juncture in cardiac regeneration - when *tnfa*+ pro-inflammatory MPs are

generally supplanted by *tnfa*- anti-inflammatory MPs - this disruption of equilibrium due to the inhibition of MP Adra1 signaling suggests a potential role for Adra1 signaling in transitioning MP phenotypes from pro- to anti-inflammatory.

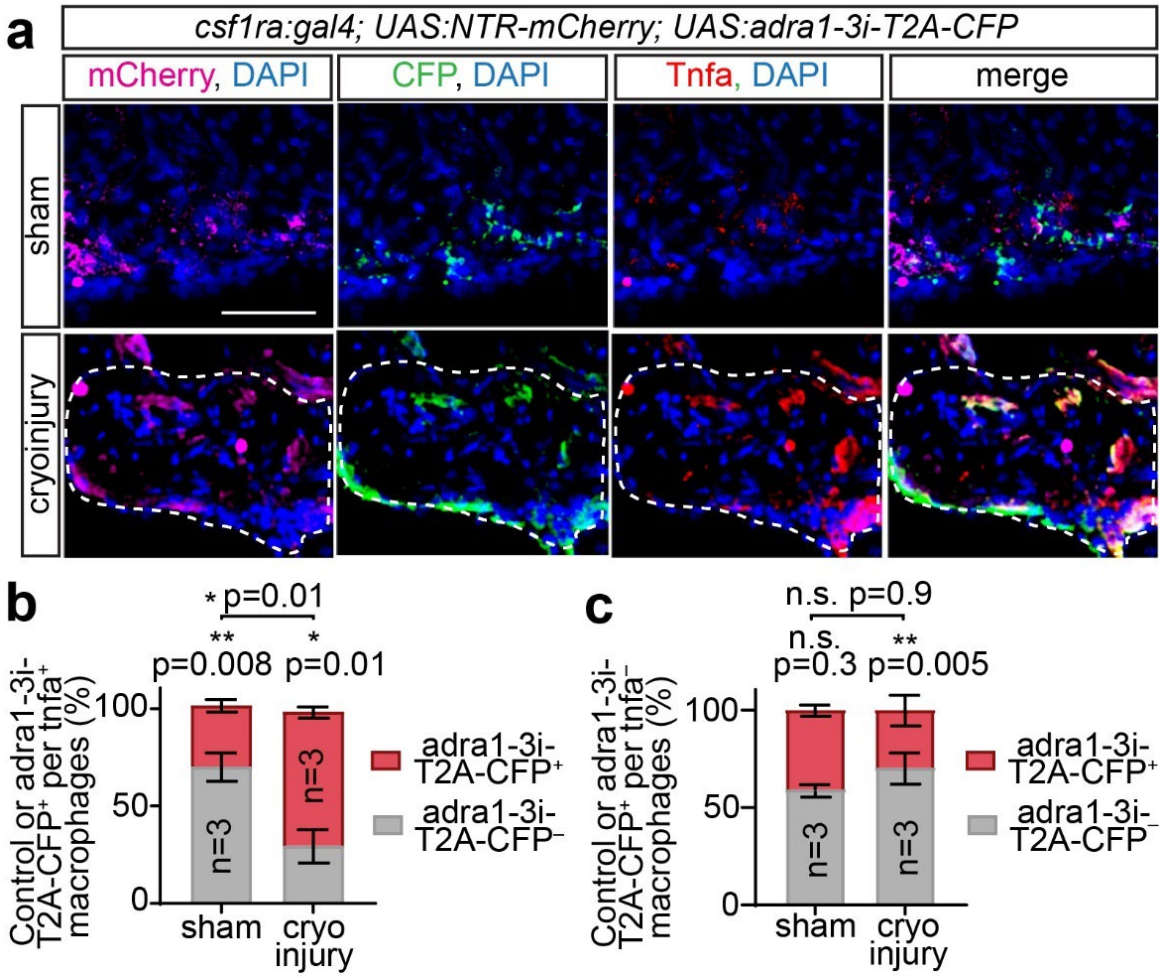

Figure 3.18 Macrophage cell-autonomous Adra1 signaling promotes the presence of anti-inflammatory macrophages in adult zebrafish hearts. (a) Confocal images showing sham-operated or cryoinjured *csf1ra:Gal4; UAS:adra1-3i-T2A-CFP; UAS:NTR-mCherry* heart cryosections at 7dpi. Sections are immunofluorescence stained for MPs with mCherry shown in magenta, for *adra1-3i-T2A-CFP* with CFP shown in green, with Tnfa shown in red, and for cell nuclei with DAPI shown in blue. Dashed lines mark the injured area, scale bar is 50 μm. Experimental setup in **Fig. 3.16a** was used. (b, c) Segmented bar graphs depict the distribution of *adra1-3i*– and *adra1-3i*+ MPs within the pro-inflammatory (*tnfa*+) (b) and anti-inflammatory (*tnfa*–) (c) MP populations in the same sham-operated or cryoinjured hearts at 7dpi as percentages. All data are presented as mean ± S.E.M, and n numbers denote the number of animals used for each group, sham-operated or cryoinjured. * $p<0.05$, ** $p<0.01$, *** $p<0.001$, n.s. not significant, two-tailed t-test.

In summary, these findings affirm that MP cell-autonomous Adra1 signaling is instrumental in modulating core regenerative processes such as cardiomyocyte proliferation and MP accumulation, as well as the phenotypic differentiation of MPs following cryoinjury in adult zebrafish hearts, consistent with observations made in the larval cardiac necrosis model.

3.7 Adra1 signaling promotes 'Extracellular matrix remodeling' expression profile in a macrophage subset after cryoinjury

After observing the pivotal role of Adra1 signaling in cardiac regeneration and its potential impact on MP phenotype, I aimed to dissect its effects on MP subsets to a greater extent. I conducted scRNAseq on cryoinjured *csf1ra:Gal4; UAS:adra1-3i-T2A-CFP; UAS:NTR-mCherry* hearts at 7dpi, sorting viable cells through FACS **(Fig. 3.19a)**. This transgenic line allowed the simultaneous analysis of adra1-3i+ and adra1-3i- MPs within the same heart post-cryoinjury, minimizing sample variability, due to the mosaic expression **(Fig. 3.19b)**. Through unbiased clustering, I identified the majority of expected cardiac resident cell types using established marker genes **(Fig. 3.19c)**. I was able to identify cardiomyocytes (*myl7, tnnt2a*), MPs (*mpeg1.1, lygl1*), monocytes (*lcp1, lyz*), neutrophils (*lect2l, mpx*), fibroblasts (*fn1b, tagln*) and more **(Fig. 3.19c)**. I then separated MP populations and further divided them based on *adra1-3i-CFP* expression into two subpopulations: *adra1-3i+* and *adra1-3i-* **(Fig. 3.19d)**. Four distinct clusters emerged within the *adra1-3i-* MP population, each identified by their top 70 most differentially expressed genes **(Fig. 3.20a, b)**. Cluster 1 was highly expressing genes related to antigen-presenting and T cell activation, such as *ctss2.1, ifi30, cd74a, cd74b, mhc2a, and mhc2dab*. Cluster 2 was expressing *atp5mc1, atp5pd, cox6b1, cox6b2, cox7a2a, and pdrx6* genes, which are related to anti-inflammation phenotype through oxidative stress protection and mitochondrial oxidative metabolism. Cluster 3 had genes such as *hp, timp4.2, timp2b, and csf3b* among its top 70 most differentially expressed genes list, which are related to wound repair processes such as hemolytic-related antioxidation, platelet recruitment, and neutrophil chemotaxis. Cluster 4 had an ECM remodeling and fibrosis related expression profile with higher expression of genes such as *mmp2, col1a1a, col1a2, col5a1, fn1b, sparc, mdka, and tagln.* Strikingly, the *adra1-3i+* MP population lacked cluster 4, suggesting a critical

role for adra1 signaling in modulating ECM remodeling transcriptional profile in MPs **(Fig. 3.19d)**.

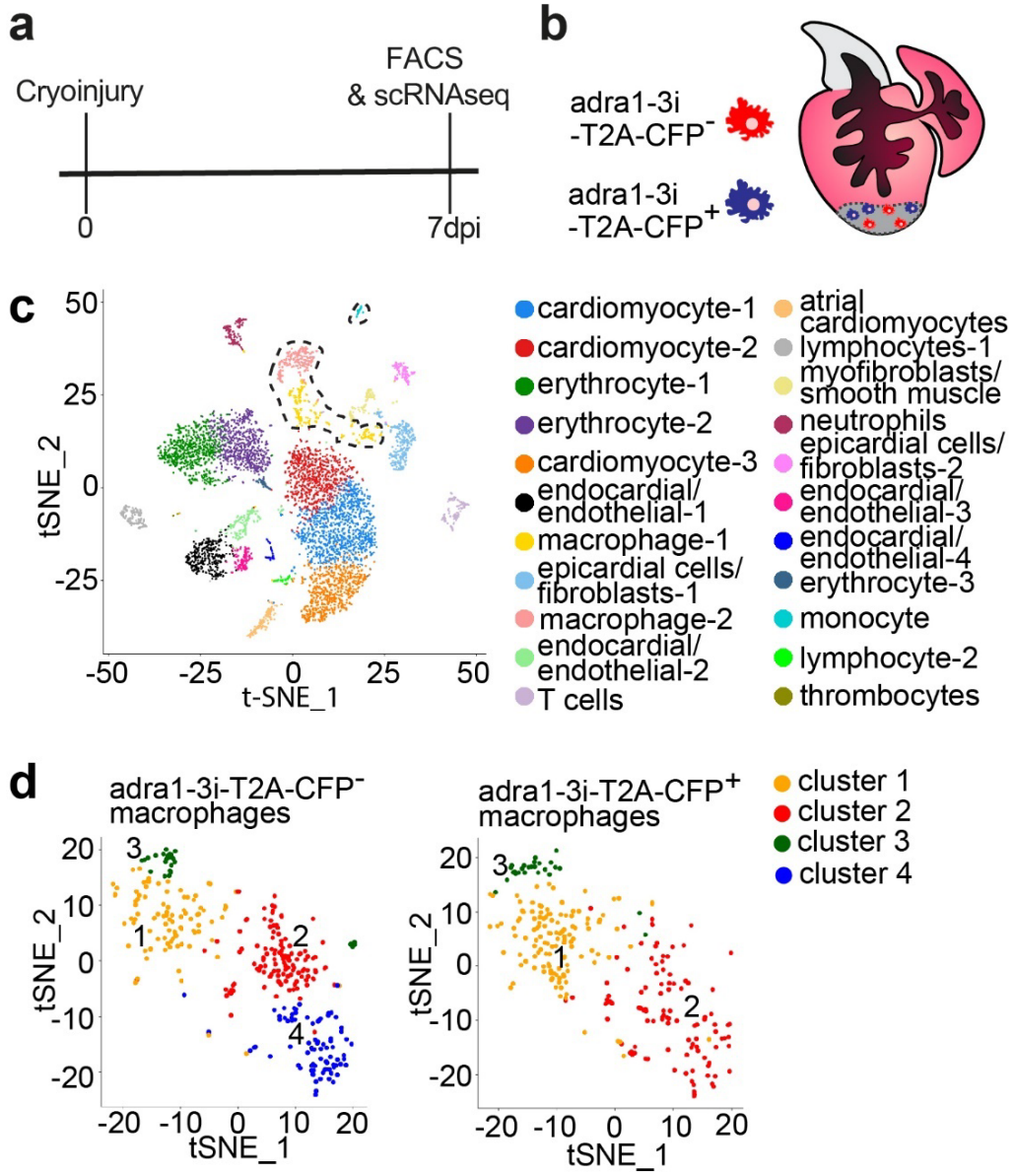

Figure 3.19 Adra1 signaling inhibition alters macrophage cluster content in the cryoinjured heart. (a) Scheme of experimental setup representing the timepoints of cryoinjury on adult *csf1ra:Gal4; UAS:adra1-3i-T2A-CFP; UAS:NTR-mCherry* hearts, and at 7dpi sorting of viable cells and using them for scRNAseq. A dissociated pool of 3 hearts was used for this experiment. (b) Scheme illustrating mixed MP populations consisting of control (*adra1-3i-*) and Adra1 signaling-deficient (*adra1-3i+*) MPs in the same cryoinjured heart. (c) Graph depicts clustering results of the whole heart with t-distributed stochastic neighbor embedding (t-SNE) representation. Dashed line outlines all the cells identified as MP/monocyte populations. (d) Graphs depict the clusters within *adra1-3i-* and *adra1-3i+* MP

populations with t-SNE representation, indicating 4 clusters in the *adra1-3i-* and 3 clusters in *adra1-3i+* populations.

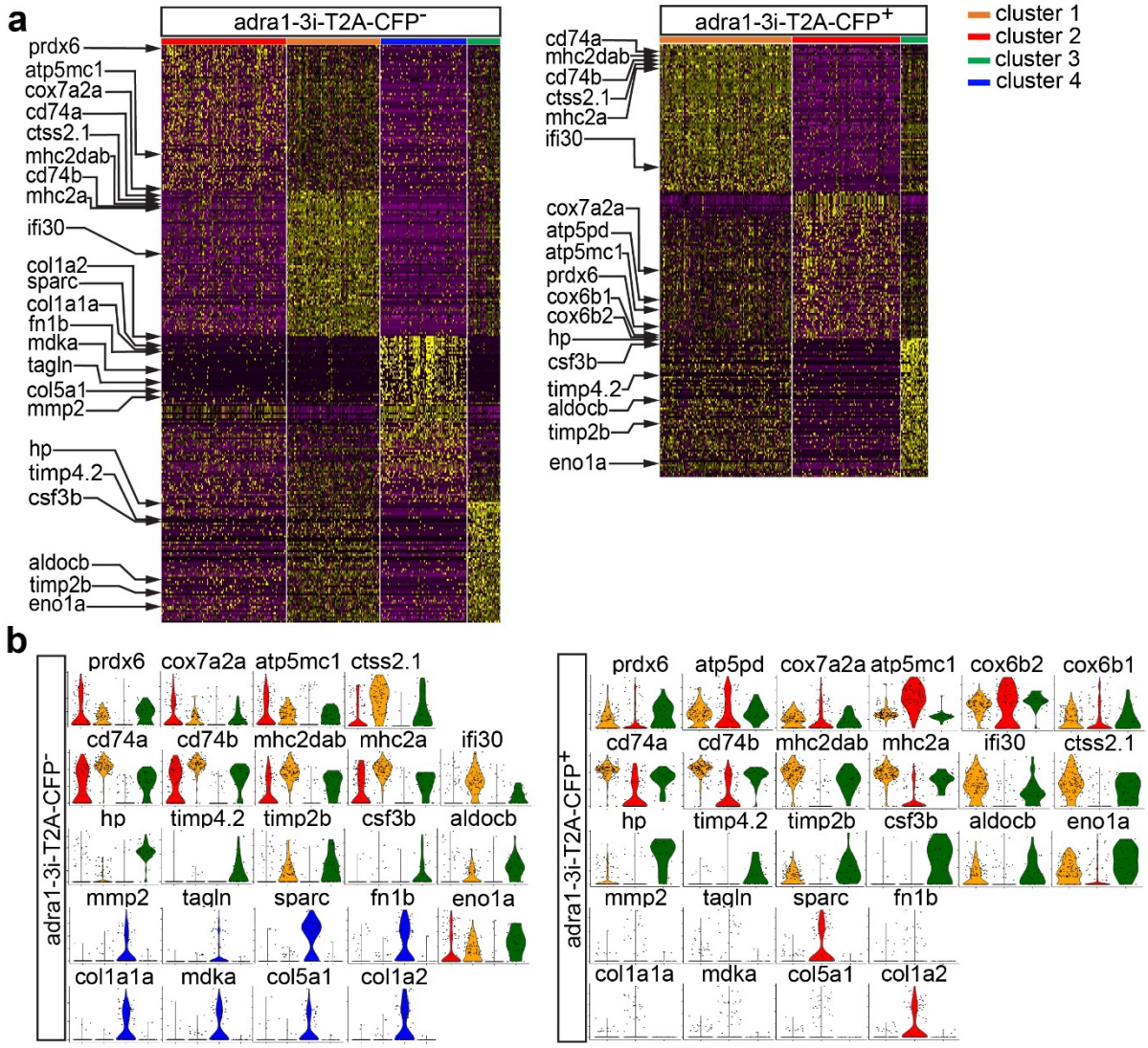

Figure 3.20 Differentially expressed genes of clusters in *adra1-3i-* and *adra1-3i+* macrophage populations. (a) Heatmaps of the 70 most differentially expressed genes in each cluster from **Fig. 3.19d**, which were used as identifier genes for each cluster to determine their phenotype/function. Clusters 1-3 in both *adra1-3i-* and *adra1-3i+* populations share similar expression profiles with common identifier genes. Cluster 4, present only in the *adra1-3i-* population, has identifier genes related to ECM remodeling. (b) Violin plots of cluster-defining genes depicted in (a).

To investigate the possibility of *UAS:adra1-3i-T2A-CFP* transgene causing alterations in MP expression profile, I wanted to validate the presence of MP subsets after cryoinjury in a control heart. I carried out scRNAseq of cryoinjured *csf1ra:Gal4*; *UAS:NTR-mCherry* hearts and did the same analysis I performed on *adra1-3i* hearts **(Fig. 3.21)**. Control hearts contain most cardiac resident cell types identified by same marker gene expressions after clustering in

parallel with a*dra1-3i* hearts such as cardiomyocytes (*myl7, tnnt2a*), MPs (*mpeg1.1, lygl1*), monocytes (*lcp1, lyz*), neutrophils (*lect2l, mpx*), fibroblasts (*fn1b, tagln*) **(Fig. 3.21b)**. After separating MPs from the rest of the clusters and performing re-clustering on them, I found the same four clusters among MPs with similar differentially expressed gene sets as in adra1-3i hearts **(Fig. 3.19, Fig. 3.20)**.

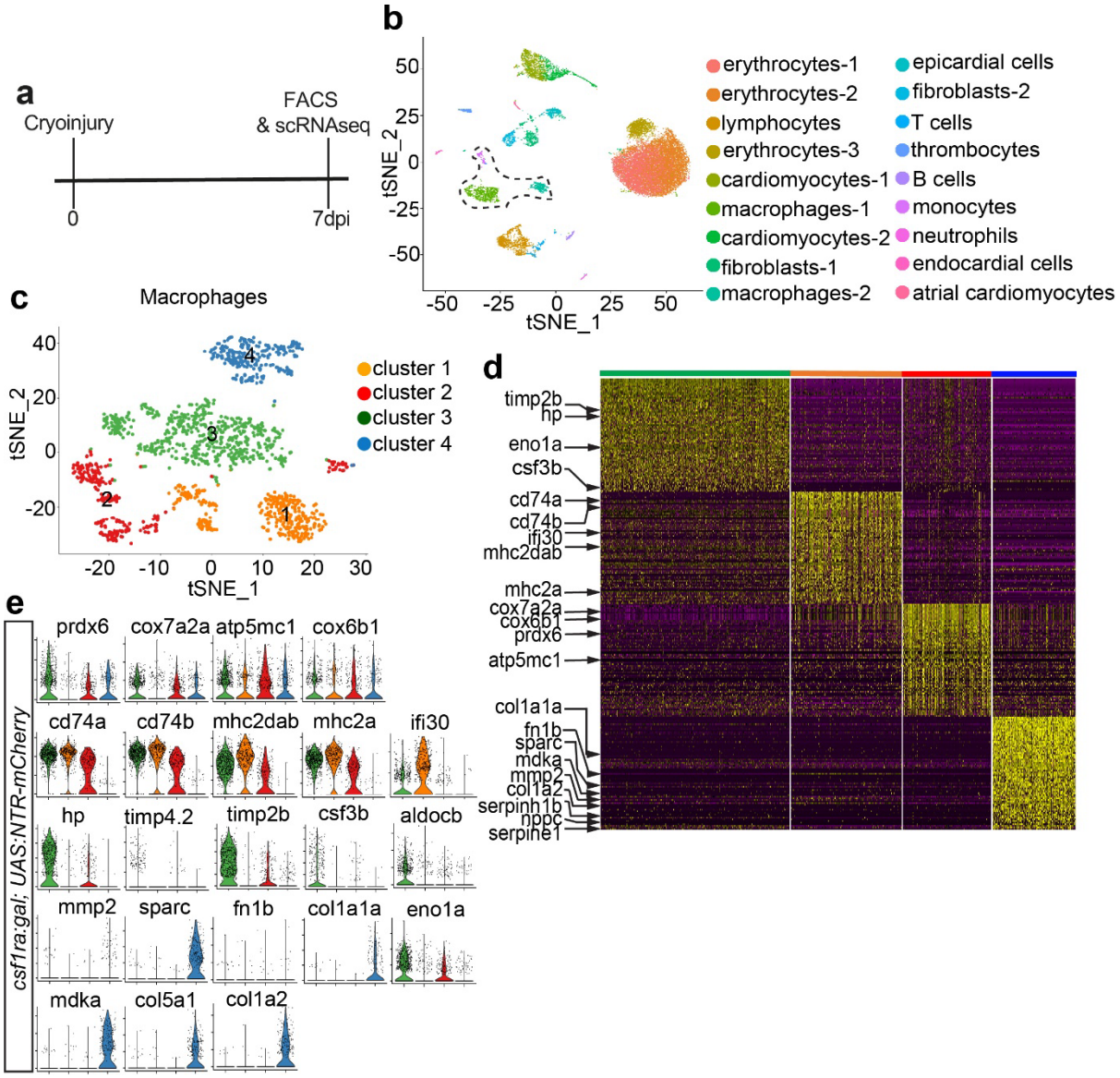

Figure 3.21 ***Adra1-3i-*** **macrophage cluster content and phenotype/function are conserved in** ***csf1r:Gal4; UAS:NTR-mCherry*** **(control) after cryoinjury.** (a) Scheme of experimental setup representing the timepoints of cryoinjury on adult *csf1ra:Gal4; UAS:NTR-mCherry* hearts, and at 7dpi sorting of viable cells and using them for scRNAseq. A dissociated pool of 3 hearts was used for this experiment. (b) Graph depicts clustering results of the whole heart with t-SNE representation. Dashed line outlines all the cells identified as MP/monocyte populations. (c) Graph depicts the clusters within

MP population with t-SNE representation, indicating 4 clusters. (d) Heatmap of the 70 most differentially expressed genes in each cluster from (c), used as identifier genes for clusters to determine their phenotype/function. All clusters share a similar expression profile and have common identifier genes with **Fig. 3.20a** *adra1-3i-* clusters. (e) Violin plots of cluster-defining genes depicted in (d).

To further establish that the profile of cluster 4, ECM remodeling transcription program, is influenced by Adra1 signaling, I also examined the expression of *adra1bb* and *adra1d* in MP populations **(Fig. 3.22)**. Analysis of *adra1-3i* heart scRNAseq data revealed that *adra1bb* was enriched in cluster 4 of *adra1-3i-* MPs, while *adra1d* expression was negligible **(Fig. 3.22)**. Immunostaining coupled with HCR-FISH validated the presence of marker genes for cluster 4, such as *col1a1a*, *fn1b*, and *tagln* **(Fig. 3.23)**. I found a reduction in the proportion of *fn1b+/col1a1a+* MPs in total (marked by *mCherry*) MPs as well as a reduction in their absolute numbers normalized to injury area in *adra1-3i* hearts compared to control hearts at 7dpi **(Fig. 3.23b, c)**. These observations, on top of validating the in-silico findings, provided further support for the specific role of Adra1 signaling in cluster 4, ECM remodeling, identity emergence among MPs.

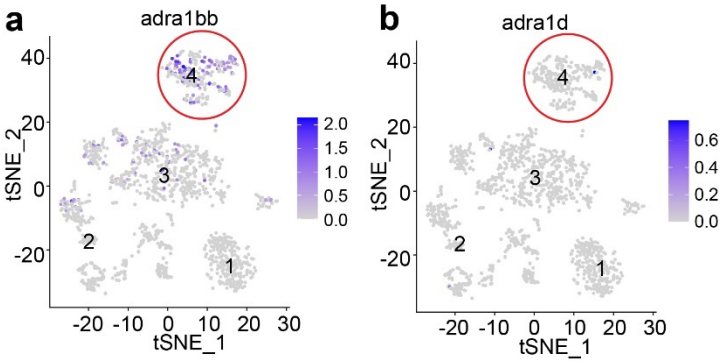

Figure 3.22 Expression of *adra1bb* and *adra1d* in macrophage clusters of 7dpi *csf1ra:Gal4; UAS:NTR-mCherry* hearts. (a, b) Feature plots depict the cells expressing adra1bb (a) and adra1d (b) in MPs from 7 dpi hearts with the same t-SNE representation as in **Fig. 3.21c** but marking the cells with color gradient according to the expression level of the gene depicted on the plot. Cells that fall under cluster 4, designated as the 'ECM remodeling' subset, are marked with a red circle in each plot. Gradient color bars indicate normalized expression values of the genes in each plot.

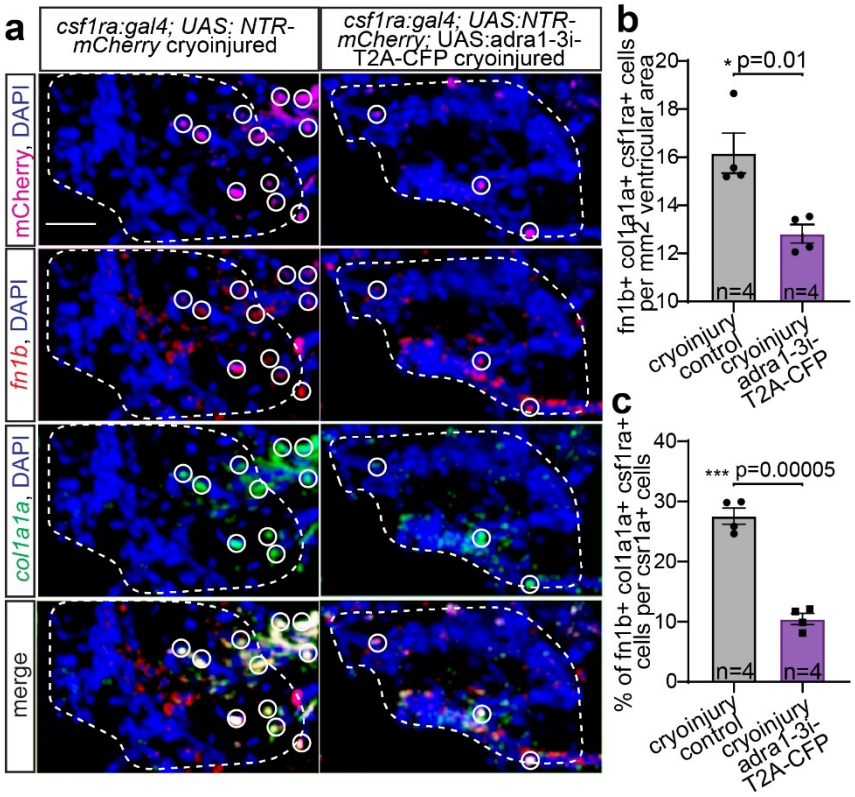

Figure 3.23 Verification of macrophage cluster 4 identifier gene expressions in cryoinjured hearts. (a) Confocal images showing cryoinjured *csf1ra:Gal4; UAS:NTR-mCherry* (control) and *csf1ra:Gal4; UAS:adra1-3i-T2A-CFP; UAS:NTR-mCherry* heart cryosections at 7dpi. Sections are immunofluorescence stained for MPs with mCherry shown in magenta and HCR-FISH stained for *col1a1a* shown in green, *fn1b* shown in red, and cell nuclei stained with DAPI shown in blue. Dashed lines mark the injured area, white circles mark *col1a1a+/fn1b+* MPs, scale bar is 20 µm. (b) Graph depicts the number of *col1a1a+/fn1b+* MPs inside and in the proximity of the injury zone, quantified as cell numbers per 1 mm2 ventricular area. (c) Bar graph depicts the *col1a1a+/fn1b+* MPs inside and in the proximity of the injury zone, quantified as percentages of MPs within the observed area. All data points indicate individual animals and n numbers denote the number of animals used for each group. All data are presented as mean ± S.E.M. * $p<0.05$, ** $p<0.01$, *** $p<0.001$, n.s. not significant, two-tailed t-test.

I also performed pathway analysis comparing *adra1-3i+* and *adra1-3i-* MPs and revealed the suppression of heart/muscle cell/circulatory system development-related pathways and activation of hydrogen peroxide/reactive oxygen species metabolism-related pathways when Adra1 signaling was inhibited **(Fig. 3.24)**.

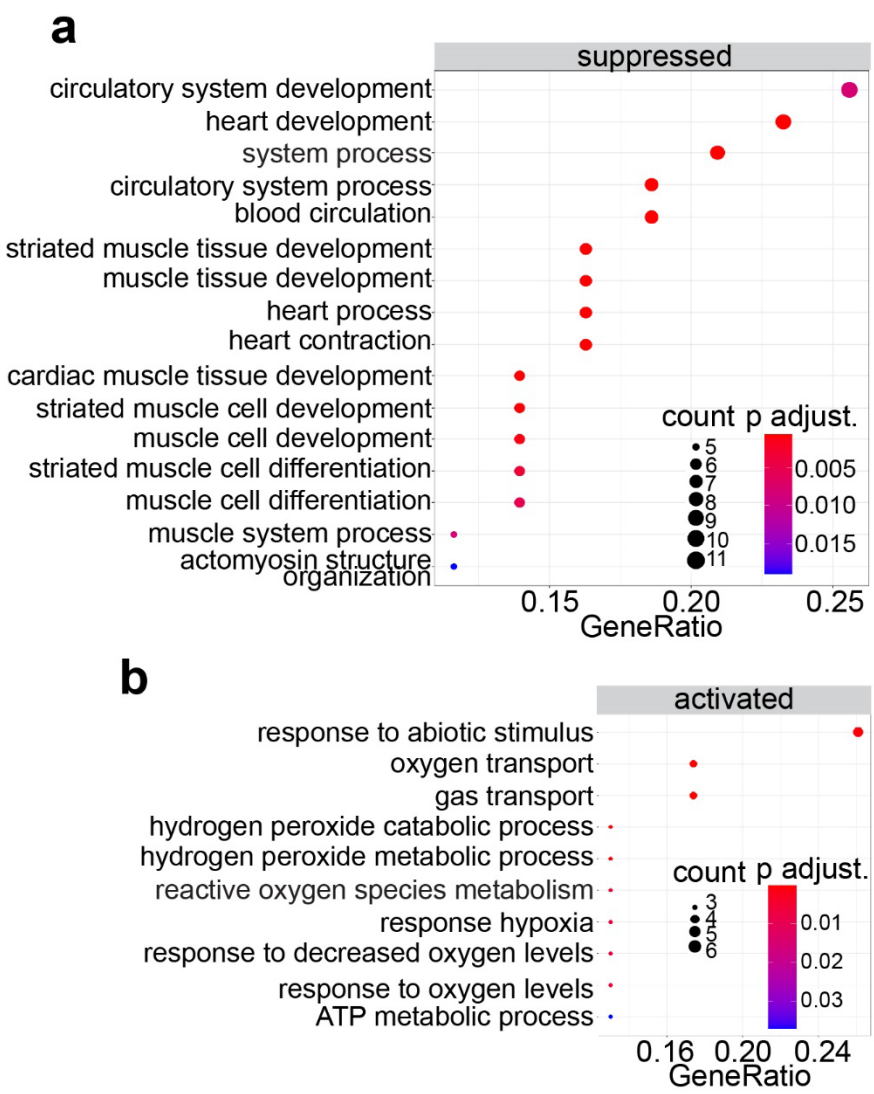

Figure 3.24 Adra1 signaling activates tissue regenerative pathways in macrophages. (a, b) GO enrichment analysis of differentially expressed genes in *adra1-3i+* MPs compared to *adra1-3i+* MPs and depiction of suppressed (a) and activated (b) pathways. Graphs depict the pathways with gene ratio (differentially expressed genes related to GO term / total number of differentially expressed genes). Dot size in the graph represents the count, which is the number of differentially expressed genes belonging to a GO term. The color gradient bar represents the Bonferroni-Holm adjusted p values, and dots are colored according to this scale.

In summary, these findings elucidate the instrumental role of Adra1 signaling in selectively activating distinct MP subtypes during the transition from the acute inflammatory to the fibrotic resolution phase within the cardiac regenerative cascade. The transcriptomic profiles of these MP populations point to their critical involvement in ECM modifications, essential for the regulation of fibrotic activity and subsequent myocardial regeneration.

3.8 Adra1-activated macrophages are critical for fibroblast activation, collagenous scar turnover, and blood and lymphatic neovascularization during cardiac regeneration

To elucidate the role of Adra1-activated MPs in cardiac regeneration, I compared the regenerative processes in *csf1ra:Gal4; UAS:adra1-3i-T2A-CFP; UAS:NTR-mCherry* cryoinjured hearts to those in control *csf1ra:Gal4; UAS:NTR-mCherry* cryoinjured hearts. I first evaluated scar formation dynamics at 7dpi using AFOG staining **(Fig. 3.25a)**. In *adra1-3i* hearts, deposition of fibrin- and collagen-rich ECM was significantly reduced compared to control hearts, although it was still increased relative to sham-operated hearts **(Fig. 3.25b, c)**.

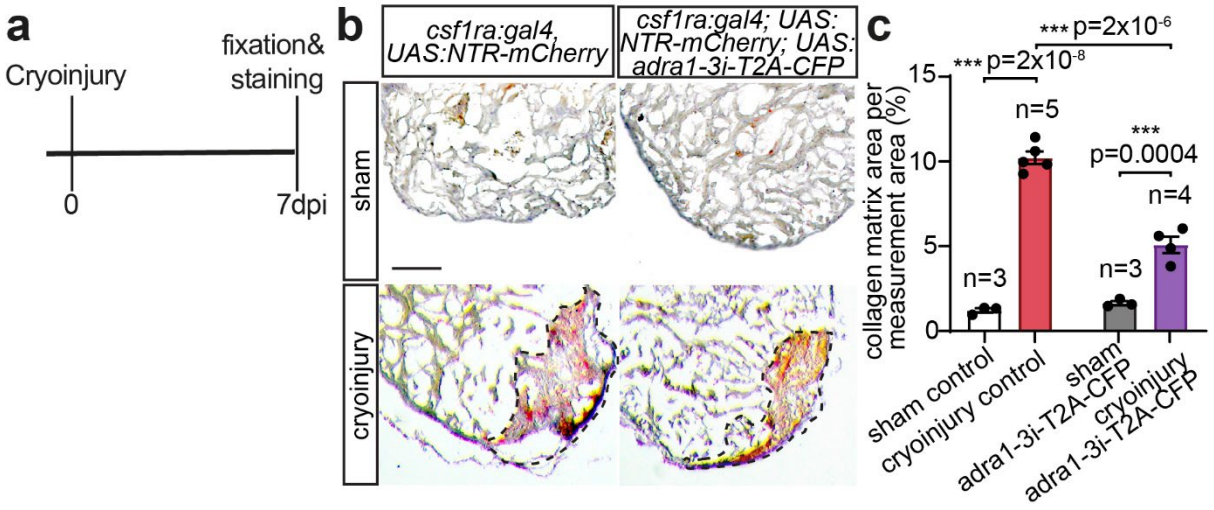

Figure 3.25 Extracellular matrix deposition is impaired after cryoinjury when macrophage Adra1-activation is inhibited. (a) Scheme of experimental setup representing the timepoints of cryoinjury on adult *csf1ra:Gal4*; *UAS:NTR-mCherry* (control) and *csf1ra:Gal4; UAS:adra1-3i-T2A-CFP; UAS:NTR-mCherry* hearts, and their fixation and staining at 7dpi. (b) Confocal images showing sham-operated or cryoinjured *csf1ra:Gal4; UAS:NTR-mCherry* (control) and *csf1ra:Gal4; UAS:adra1-3i-T2A-CFP; UAS:NTR-mCherry* heart cryosections at 7dpi. Sections are stained with AFOG for visualization of fibrin and collagen-rich scar tissue formation after cryoinjury. Healthy muscles are stained in brown, fibrin in red, and collagen in blue, black dashed lines mark the injury zone, scale bar is 0.1 mm. (c) Bar graph depicts the collagen content in the injury zone, quantified as percentage of collagen covered area within the measurement area. Data points indicate individual animals and n numbers denote the number of animals used for each group. All data are presented as mean ± S.E.M. * $p<0.05$, ** $p<0.01$, *** $p<0.001$, n.s. not significant, two-tailed t-test.

I performed further analysis on collagen I, the primary structural component of the ECM, with the same experimental setup. Immunostaining of collagen I and quantification of Col1+

area around the injury site revealed a marked decrease in collagen I content in *adra1-3i* hearts compared to control hearts **(Fig. 3.26a, b)**. Additionally, CHP staining showed impaired ECM turnover in *adra1-3i* hearts, as evidenced by decreased levels of degraded collagen **(Fig. 3.27)**. Collectively, these findings underscore the pivotal role of Adra1-activated MPs in ECM regulation, corroborating scRNAseq data that highlighted the importance of Adra1 signaling in MP subset associated with ECM remodeling.

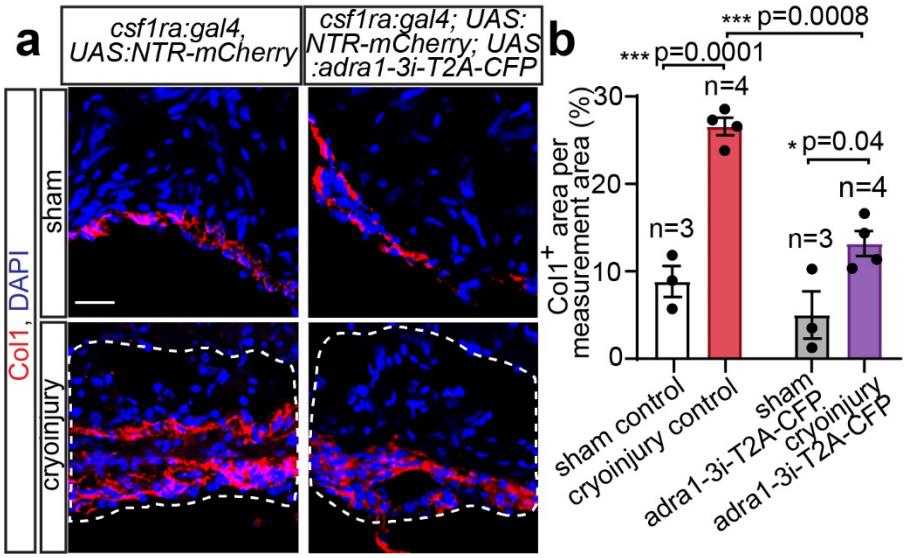

Figure 3.26 Collagen I deposition is impaired after cryoinjury when macrophage Adra1-activation is inhibited. Same experimental setup as in **Fig. 3.25a** (a) Confocal images showing sham-operated or cryoinjured *csf1ra:Gal4; UAS:NTR-mCherry* (control) and *csf1ra:Gal4; UAS:adra1-3i-T2A-CFP; UAS:NTR-mCherry* heart cryosections at 7dpi. Sections are immunofluorescence stained for Collagen I shown in red, and for cell nuclei with DAPI shown in blue. Dashed lines mark the injured area, scale bar is 20 µm. (b) Bar graph depicts the collagen I content in the injury zone, quantified as percentage of collagen I covered area within the measurement area. Data points indicate individual animals and n numbers denote the number of animals used for each group. All data are presented as mean ± S.E.M. * $p<0.05$, ** $p<0.01$, *** $p<0.001$, n.s. not significant, two-tailed t-test.

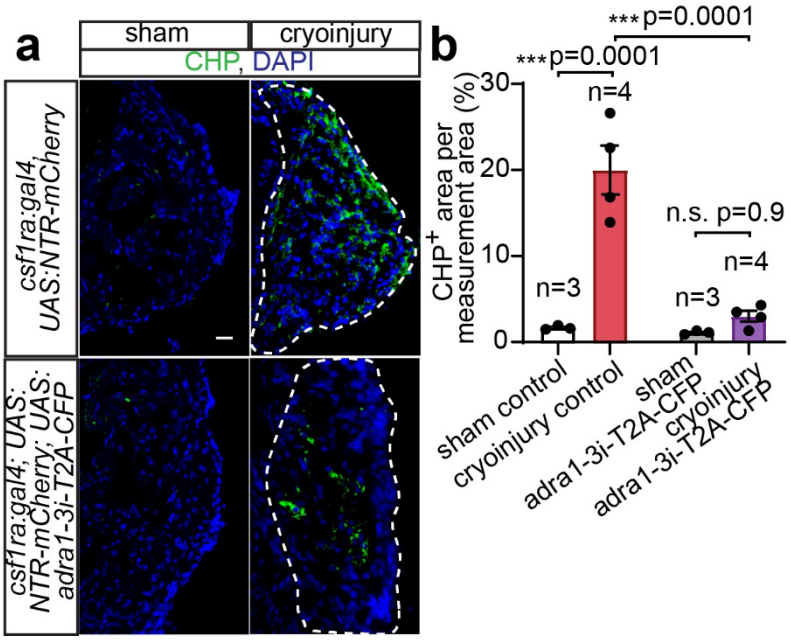

Figure 3.27 Collagen turnover in the cardiac injury zone requires Adra1-activated macrophages. Same experimental setup as in **Fig. 3.25a** (a) Confocal images showing sham-operated or cryoinjured *csf1ra:Gal4; UAS:NTR-mCherry* (control) and *csf1ra:Gal4; UAS:adra1-3i-T2A-CFP; UAS:NTR-mCherry* heart cryosections at 7dpi. Sections are immunofluorescence stained for degraded collagen content with CHP shown in green, and for cell nuclei with DAPI shown in blue. Dashed lines mark the injured area, scale bar is 20 μm. (b) Bar graph depicts the degraded collagen content in the injury zone, quantified as percentage of CHP covered area within the measurement area. Data points indicate individual animals and n numbers denote the number of animals used for each group. All data are presented as mean ± S.E.M. * $p<0.05$, ** $p<0.01$, *** $p<0.001$, n.s. not significant, two-tailed t-test.

To investigate the underlying mechanisms of altered ECM composition and dynamics, I focused on fibroblasts, the primary cell type responsible for ECM regulation. Particularly in zebrafish, activated fibroblasts are known to upregulate ECM components and remodeling proteins such as matrix metalloproteinases (MMPs) following cardiac injury. Immunofluorescence staining for markers of activated (*postnb*+) and differentiated (α-SMA+ and Col1+) fibroblasts was performed at 7dpi **(Fig. 3.28)**. While fibroblast activation was comparable between *adra1-3i* and control hearts **(Fig. 3.28a, b)**, differentiation into pro-fibrotic fibroblasts was reduced in *adra1-3i* hearts, indicated by reduced Col1+/α-SMA+ fibroblast content post-injury **(Fig. 3.28a, c)**. This suggests that Adra1-activated MPs influence fibroblast differentiation during cardiac regeneration.

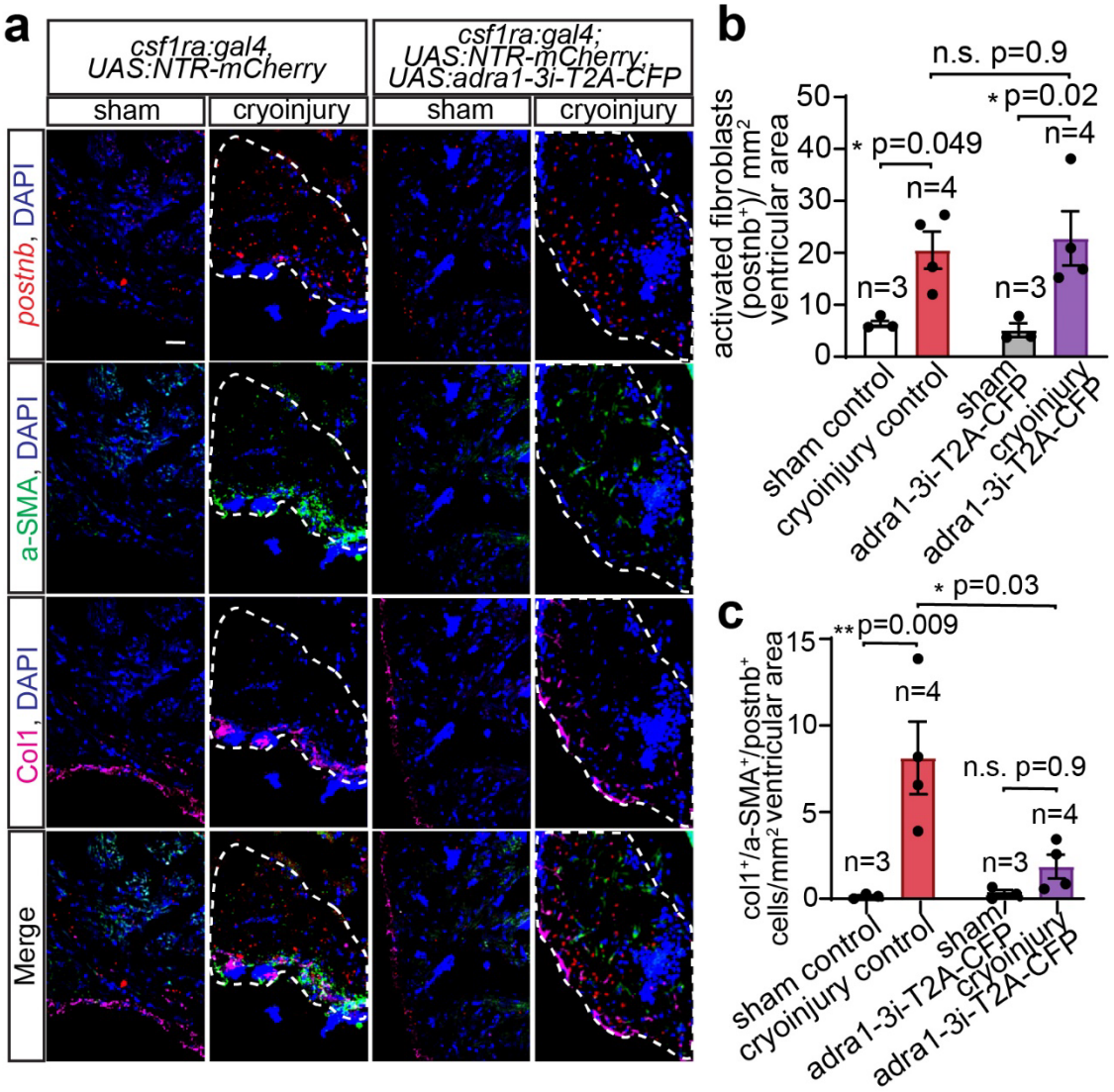

Figure 3.28 Adra1-activated macrophages are required for fibroblast differentiation to fibrotic fibroblasts. Same experimental setup as in **Fig. 3.25a** (a) Confocal images showing sham-operated or cryoinjured *csf1ra:Gal4; UAS:NTR-mCherry* (control) and *csf1ra:Gal4; UAS:adra1-3i-T2A-CFP; UAS:NTR-mCherry* heart cryosections at 7dpi. Sections are HCR-FISH stained for activated fibroblasts with *postnb* probe shown in red, immunofluorescence stained for pro-fibrotic fibroblasts with a-SMA and Collagen I shown in green and magenta respectively, and for cell nuclei with DAPI shown in blue. Dashed lines mark the injured area, scale bar is 20 µm. (b, c) Bar graphs depict the activated fibroblast (*postnb*+) numbers (b) and pro-fibrotic fibroblast (a-SMA+/Col1+/*postnb*+) numbers (c) in the injury zone, quantified as cell numbers per 1 mm2 ventricular area. Data points indicate individual animals and n numbers denote the number of animals used for each group. All data are presented as mean ± S.E.M. * p<0.05, ** p<0.01, *** p<0.001, n.s. not significant, two-tailed t-test.

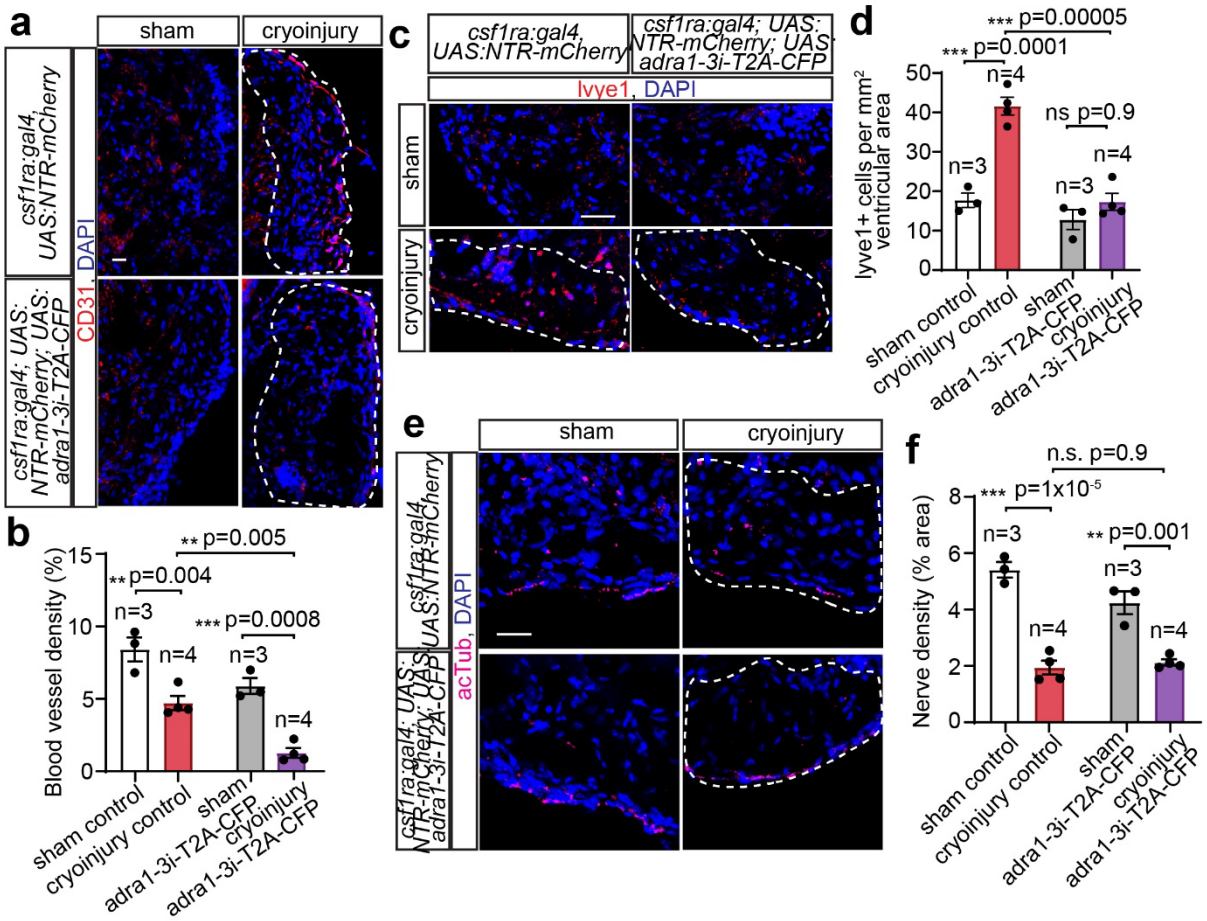

Figure 3.29 Adra1-activated macrophages are required for re-vascularization but not for re-innervation of the cardiac injury zone. Same experimental setup as in **Fig. 3.25a** (a, c, e) Confocal images showing sham-operated or cryoinjured *csf1ra:Gal4; UAS:NTR-mCherry* (control) and *csf1ra:Gal4; UAS:adra1-3i-T2A-CFP; UAS:NTR-mCherry* heart cryosections at 7dpi. Sections are immunofluorescence stained for blood vasculature with CD31 shown in red (a), HCR-FISH stained for lymphatic vasculature with *lyve1* probe shown in red (c), immunofluorescence stained for nerves with acTub shown in magenta (e), and for cell nuclei with DAPI shown in blue. Dashed lines mark the injured area, scale bars are 20 µm (a, c, e). (b, d, f) Bar graphs depict the blood vessel area (b), lymphatic endothelial cell numbers (d), nerve density (f) in the injury zone, quantified as percentage vessel area (CD31+) in the measurement area (b), cell numbers (*lyve1*+) per 1 mm2 ventricular area (d), and percentage of nerve covered area (acTub+) in the measurement area. All data points indicate individual animals and n numbers denote the number of animals used for each group. All data are presented as mean ± S.E.M. * p<0.05, ** p<0.01, *** p<0.001, n.s. not significant, two-tailed t-test.

In summary, these results indicate that Adra1-activated MPs play a crucial role in cardiac regeneration by modulating ECM composition and turnover. Their absence leads to impairments in critical regenerative pathways, such as angiogenesis and lymphangiogenesis,

in the context of altered ECM dynamics, emphasizing the central role of Adra1-activated MPs in cardiac tissue repair and regeneration.

3.9 Macrophage-derived paracrine signaling promotes activation of a pro-regenerative fibroblast subset

Cardiac regeneration in zebrafish entails a complex interplay among various cell types, each displaying different activation states crucial for myocardial renewal and scar resolution. Consistent with my earlier findings, Adra1-activated MPs significantly contribute to this process by stimulating pro-fibrotic fibroblasts. To better understand these interactions, I delved deeper into the heterogeneity of fibroblast subsets and their relationship with Adra1-activated MPs. Examining scRNAseq data from cryoinjured 7dpi *csf1ra:Gal4; UAS:adra1-3i-T2A-CFP; UAS:NTR-mCherry* and *csf1ra:Gal4; UAS:NTR-mCherry* hearts, I focused on fibroblasts, re-clustered them and identified seven distinct subsets based on differentially expressed genes **(Fig. 3.30)**. Particularly, cluster 1 fibroblasts exhibited elevated expression levels of ECM remodeling genes, such as collagen types (*col1a1a*, *col12a1a*, *col5a1*), MMPs, and pro-fibrotic markers (*postnb*, *sparc*, *rgcc*, and *edil3a*) **(Fig. 3.30c)**. This subset closely resembled a previously identified, transient pro-regenerative fibroblast population termed *col12a1a*+ fibroblasts, which were shown to be vital for cardiac regeneration.

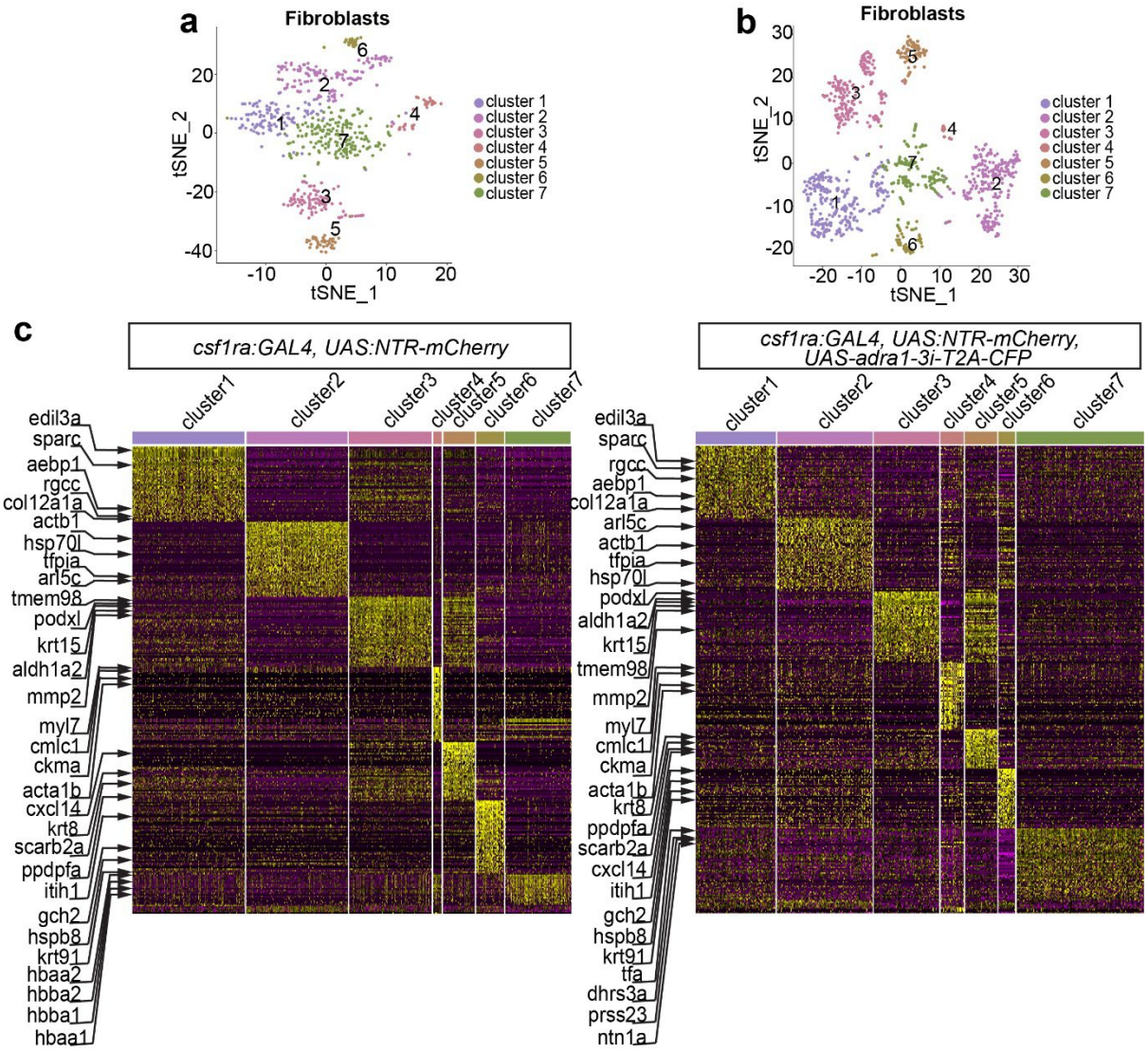

Figure 3.30 Identification of fibroblast sub-populations after cryoinjury in control and macrophage-specific Adra1-signaling deficient hearts. scRNAseq data from **Fig. 3.19** and **3.21**, populations identified as fibroblasts from *csf1ra:Gal4; UAS:NTR-mCherry* (control) and *csf1ra:Gal4; UAS:adra1-3i-T2A-CFP; UAS:NTR-mCherry* hearts are analyzed separately. (a, b) Graphs depict clustering results of the fibroblasts from cryoinjured 7dpi *csf1ra:Gal4; UAS:NTR-mCherry* (control) hearts (a) and *csf1ra:Gal4; UAS:adra1-3i-T2A-CFP; UAS:NTR-mCherry* hearts (b) with t-SNE representation, indicating 7 clusters in each group. (c) Heatmaps of the 50 most differentially expressed genes in each cluster from (a) and (b), respectively, were used as identifier genes for clusters to determine their phenotype/function. Fibroblast clusters in each group share a similar expression profile and have common identifier genes.

Similar expression profiles of the pro-regenerative *col12a1a*+ fibroblasts and the Adra1-activated MPs in regard to ECM remodeling related genes led me to consider the potential of Adra1-activated MP transdifferentiation into *col12a1a*+ fibroblasts. Utilizing RNA velocity

based trajectory inference analysis with partition-based graph abstraction (PAGA), I found no evidence of transdifferentiation events between MPs and fibroblasts **(Fig. 3.31b)**. Instead, I discovered that *col12a1a+* fibroblasts predominantly originated from cluster 7 fibroblasts, corroborated by a recent study **(Fig. 3.31b)**. Cluster 7 fibroblasts showed a distinct, less pro-fibrotic gene expression profile (*sparc, edil3a, postnb)* **(Fig. 3.30d)**. Cluster 7 fibroblasts had higher expression levels of genes (*hbba1*, *hbaa1*, *krt91*) in support of their more 'pre-activated' state, emphasizing their potential to be the source for cluster 1 **(Fig. 3.30d)**.

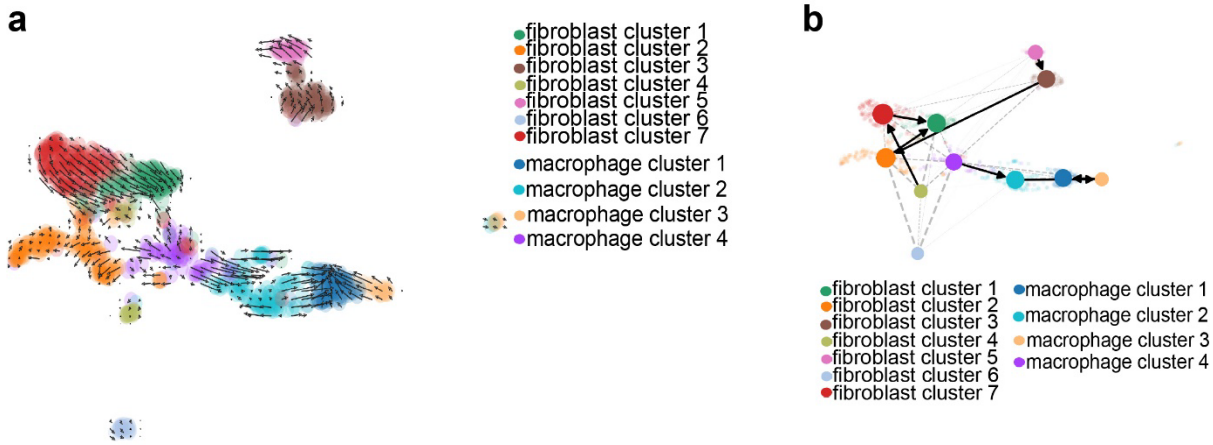

Figure 3.31 'ECM remodeling' macrophages do not transdifferentiate into fibroblasts. MP and fibroblast clusters from scRNAseq data of *csf1ra:Gal4; UAS:adra1-3i-T2A-CFP; UAS:NTR-mCherry* hearts depicted in **Fig. 3.19** and **Fig. 3.30** used for RNA velocity based analysis. (a) Graph depicts the UMAP representation of MP and fibroblast clusters of *csf1ra:Gal4; UAS:adra1-3i-T2A-CFP; UAS:NTR-mCherry* hearts, showing the RNA velocity vectors for each cell indicating no transitions from MPs to fibroblasts however, showing cluster 7 fibroblasts as a possible precursor of cluster 1 fibroblasts (*col12a1a+* subset). (b) Graph depicts the trajectory inference analysis with partition-based graph abstraction (PAGA) of MP and fibroblast clusters. Indicating no lineage relationship between MPs and fibroblasts, however, representing cluster 7 fibroblasts as a source for cluster 1 fibroblasts (*col12a1a+* subset).

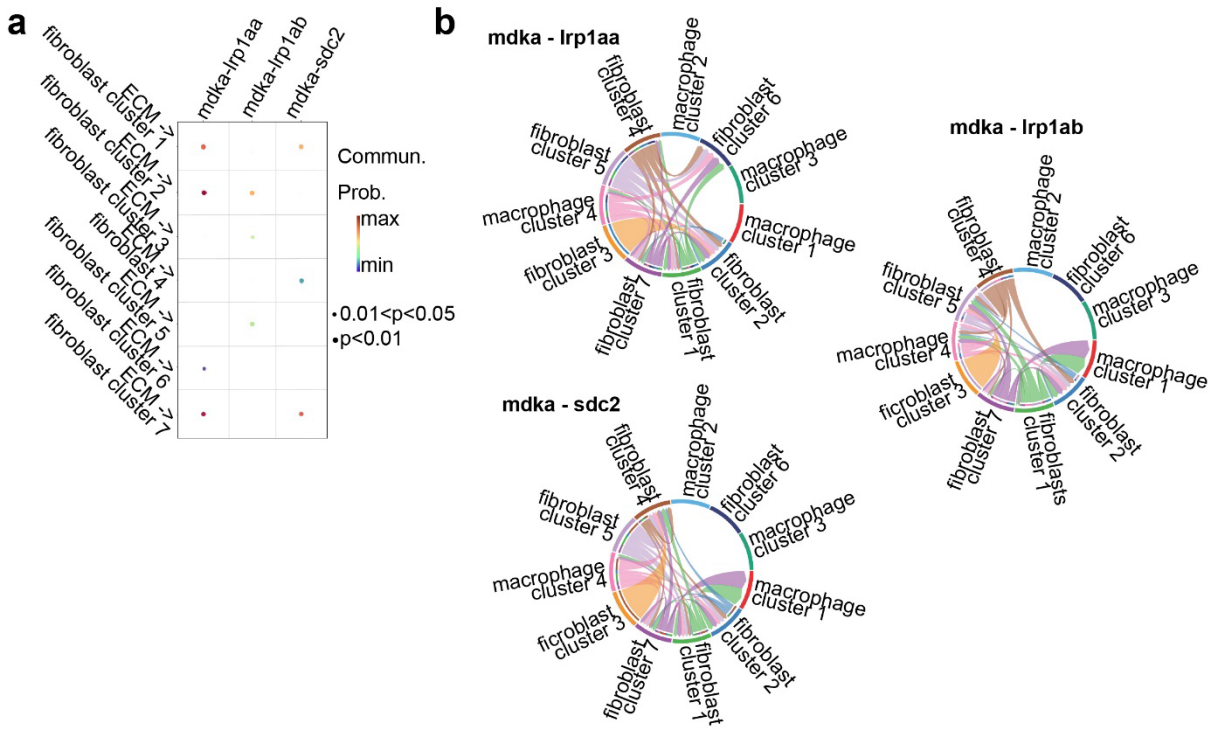

Figure 3.32 Paracrine crosstalk of Adra1-activated macrophages and pro-regenerative fibroblasts in cardiac regeneration. Communication probabilities of Adra1-activated MPs, depicted as ECM in (a) and as cluster 4 MPs in (b), with fibroblast clusters quantified with CellChat inference method using scRNAseq data of *csf1ra:Gal4; UAS:adra1-3i-T2A-CFP; UAS:NTR-mCherry* hearts (**Fig. 3.19**). (a) Plot depicts the communication probabilites of cluster 4 MPs with fibroblast clusters and also shows through which receptor-ligand pair with probabilities represented as dot color based on gradient scale and with p values represented as dot size. (b) Chord diagrams depict all communications between MP clusters and fibroblast clusters through Mdka-Lrp1aa, Mdka-Lrp1ab, and Mdka-Sdc2. Colored outer segments of the diagrams represent cluster identity, and the thickness of the colored lines between clusters in the inner segments of the diagrams represent the interaction strength of clusters through respective receptor-ligand pairs.

Next, I wanted to investigate other possible mechanisms for Adra1-activated MPs to influence pro-regenerative fibroblasts. For this purpose, I focused on paracrine interactions and employed CellChat, a quantitative inference method for cell-cell communications, analyzing scRNAseq data from *adra1-3i* hearts **(Fig. 3.32)**. I found various possible communications between different fibroblast clusters and Adra1-activated MPs **(Fig. 3.32)**. Interestingly, this analysis revealed a high probability of interaction between Cluster 7 fibroblasts and Adra1-activated MPs, mediated by the Mdka-Lrp1aa receptor-ligand pair **(Fig. 3.32a)**. This observation led me to focus on possible alterations in the expression profile of cluster 1 fibroblasts when Adra1 signaling was inhibited in MPs via comparison of *adra1-3i* hearts and

control hearts **(Fig. 3.30)**. Control heart cluster 1 fibroblasts were high in expression of ECM regulatory genes such as collagens and MMPs whereas cluster 1 in *adra1-3i* hearts were expressing the same genes at lower levels that are not considered differentially expressed anymore **(Fig. 3.33a)**. On the other hand, there was a higher level of expression for the same genes in cluster 7 of *adra1-3i* hearts compared to control, which indicates the possibility of an attempt at functional compensation for the impairment in cluster 1 **(Fig. 3.33a)**. To validate these computational findings, I performed HCR-FISH on 7dpi *adra1-3i* and control hearts. The expression of key ECM components, collagen I and V, were significantly reduced in *adra1-3i* hearts marked by probes for *col1a1a* and *col5a1* **(Fig. 3.33b, c, d)**. These results showed altered main fibrillar component of ECM, collagen I, and a minor fibrillar component, collagen V, which was shown to be critical for scar size limitation after injury, in the absence of Adra1-activated MPs.

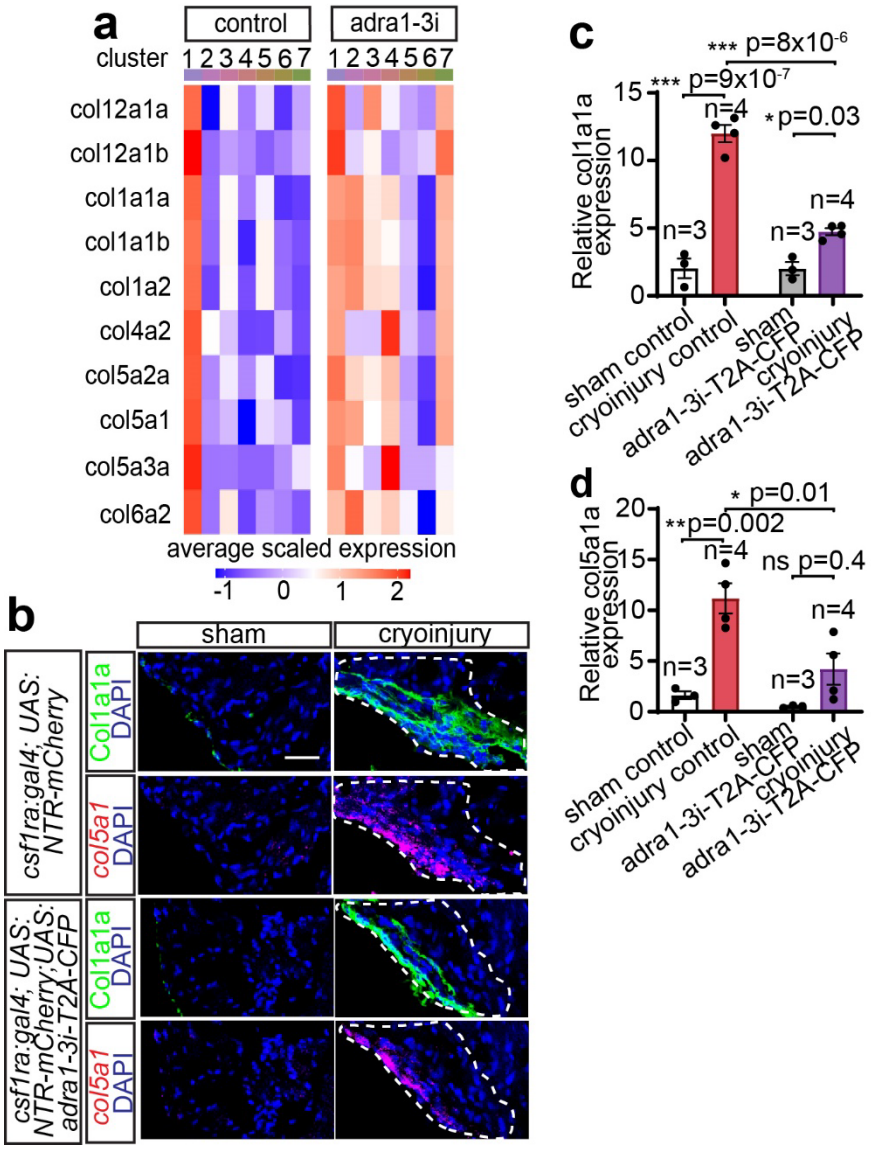

Figure 3.33 Adra1-activated macrophages alter the expression profile of specific fibroblast subsets. (a) Cluster-defining genes of fibroblast clusters identified in scRNAseq data of *csf1ra:Gal4; UAS:NTR-mCherry* (control) and *csf1ra:Gal4; UAS:adra1-3i-T2A-CFP; UAS:NTR-mCherry* hearts are represented. Heatmap depicts cluster-defining genes, represented with color gradient based on normalized average expression values in each cluster of each group. Selected ECM component genes are shown. (b) Confocal images showing sham-operated or cryoinjured *csf1ra:Gal4; UAS:NTR-mCherry* (control) and *csf1ra:Gal4; UAS:adra1-3i-T2A-CFP; UAS:NTR-mCherry* heart cryosections at 7dpi. Sections are HCR-FISH stained for *col5a1* shown in red, immunofluorescence stained for Col1a1a shown in green, and for cell nuclei with DAPI shown in blue. Dashed lines mark the injured area, scale bars are 20 μm. (c, d) Bar graphs depict the relative expression of *col1a1a* (c) and *col5a1* (d) in each group, quantified as the integrated density of the respective signal normalized by measurement area. All data points indicate individual animals and n numbers denote the number of

animals used for each group. All data are presented as mean ± S.E.M. * p<0.05, ** p<0.01, *** p<0.001, n.s. not significant, two-tailed t-test.

I also examined the expression of *col12a1a*, the main identifier of pro-regenerative cluster 1 fibroblasts, and *lrp1aa* with HCR-FISH on the same samples coupled with immunofluorescence staining of α-SMA to mark the fibroblast population in general at 7dpi **(Fig. 3.34)**. I observed increased *col12a1a* relative expression in adra1-3i hearts compared to control hearts at 7dpi in line with computational findings **(Fig. 3.34b, c)**. Also, I observed a decrease in *lrp1aa* expressing *col12a1a*+ fibroblasts in *adra1-3i* hearts compared to controls at 7dpi, verifying their presence and affirming the importance of Adra1-activated MPs for the activation of this fibroblast subset **(Fig. 3.34b, d)**.

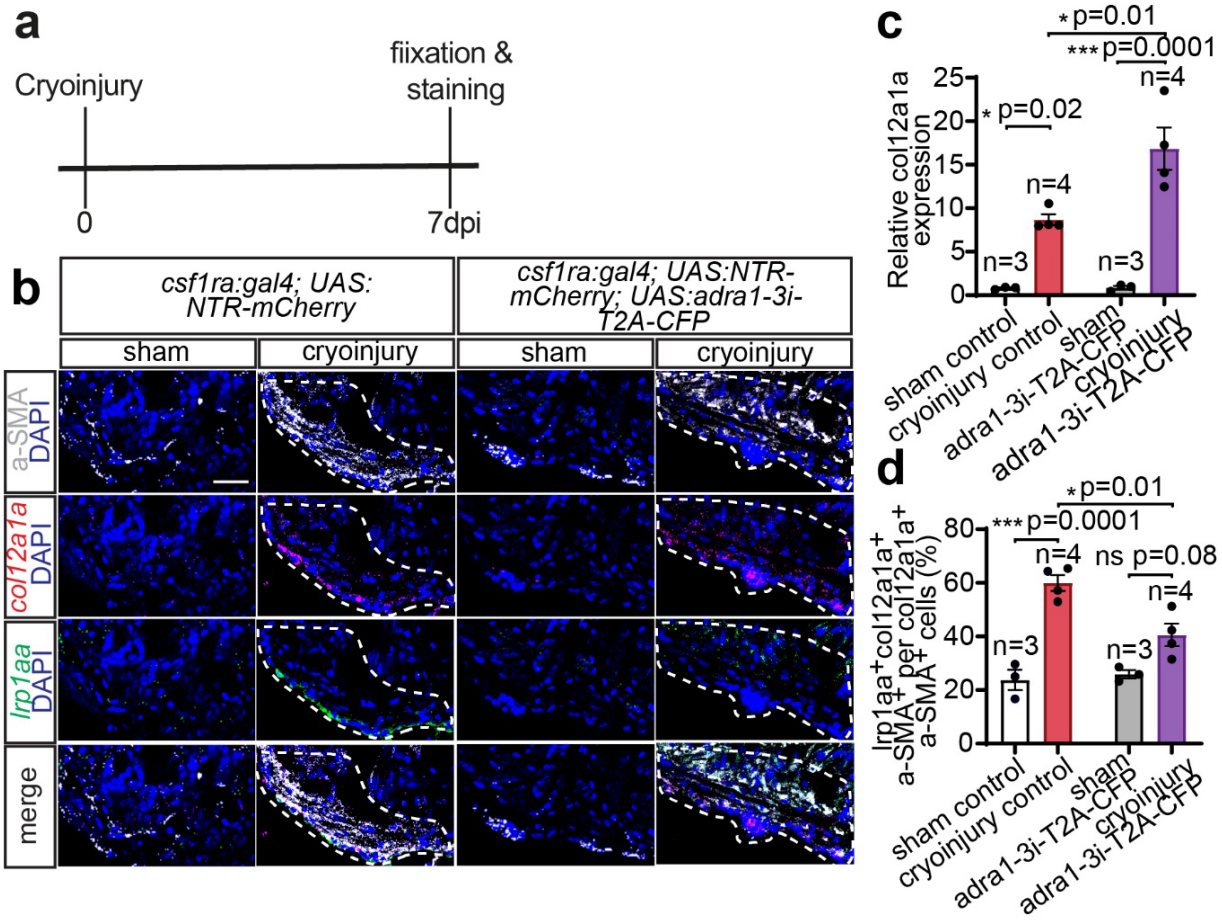

Figure 3.34 Pro-regenerative fibroblast subset activation requires Adra1-activated macrophage input. (a) Scheme of experimental setup representing the timepoints of cryoinjury on adult *csf1ra:Gal4; UAS:NTR-mCherry* (control) and *csf1ra:Gal4; UAS:adra1-3i-T2A-CFP; UAS:NTR-mCherry* hearts, and their fixation and staining at 7dpi. (b) Confocal images showing sham-operated or cryoinjured *csf1ra:Gal4; UAS:NTR-mCherry* (control) and *csf1ra:Gal4; UAS:adra1-3i-T2A-CFP; UAS:NTR-mCherry* heart cryosections at 7dpi. Sections are HCR-FISH stained for *lrp1aa* and *col12a1a* shown in

green and red, respectively, immunofluorescence stained for a-SMA shown in gray, and for cell nuclei with DAPI shown in blue. Dashed lines mark the injured area, scale bars are 20 µm. (c, d) Bar graphs depict the relative expression of *col12a1a* (c), quantified as quantified as the integrated density of the respective signal normalized by measurement area, and content of *lrp1aa+* fibroblasts among *col12a1a+* fibroblasts (d), quantified as percentage of *lrp1aa+/col12a1a+/a-SMA+* fibroblasts in total *col12a1a+/a-SMA+* fibroblasts within the observed area. All data points indicate individual animals and n numbers denote the number of animals used for each group. All data are presented as mean ± S.E.M. * p<0.05, ** p<0.01, *** p<0.001, n.s. not significant, two-tailed t-test.

In the same experimental setup **(Fig. 3.34a),** I performed HCR-FISH to examine *mdka* expression, coupled with immunofluorescence staining for mCherry to mark the MPs, therefore validating the expression of *mdka* in MPs and assess *mdka+* MPs when Adra1 signaling is inhibited **(Fig. 3.35)**. I observed impaired *mdka+* MP presence in *adra1-3i* hearts compared to control hearts at 7dpi **(Fig. 3.35)**.

All in all, I have discovered a previously unknown paracrine crosstalk between specific MP subset, activated through Adra1 signaling, and fibroblasts through Mdka-Lrp1aa receptor-ligand pair and resulting in activation of pro-regenerative fibroblast subset during cardiac regeneration.

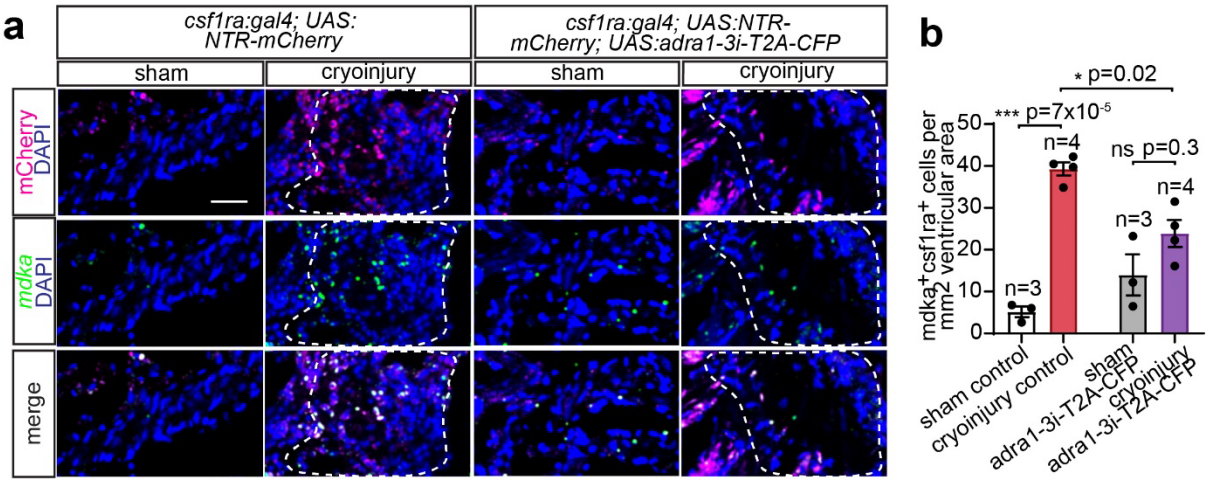

Figure 3.35 Adra1-signaling in macrophages alters *mdka* expression. (a) Confocal images showing sham-operated or cryoinjured *csf1ra:Gal4; UAS:NTR-mCherry* (control) and *csf1ra:Gal4; UAS:adra1-3i-T2A-CFP; UAS:NTR-mCherry* heart cryosections at 7dpi. Sections are immunofluorescence stained for MPs with mCherry shown in magenta, HCR-FISH stained for *mdka* shown in green, and for cell nuclei with DAPI shown in blue. Dashed lines mark the injured area, scale bar is 20 µm. (b) Bar graph depicts the number of *mdka* expressing MPs (mCherry+), quantified as cell numbers per 1 mm2 ventricular area. Data points indicate individual animals and n numbers denote the number of animals

used for each group. All data are presented as mean ± S.E.M. * p<0.05, ** p<0.01, *** p<0.001, n.s. not significant, two-tailed t-test.

3.10 Mdka-Lrp1aa signaling underlies macrophages-fibroblast crosstalk

To further elucidate the role of Adra1-activated MPs in the activation of pro-regenerative *col12a1a*+ fibroblasts, I focused on the impact of *mdka* signaling on cardiac regeneration. Initially, I generated a recombinant zebrafish protein, Lrpap1, a known antagonist of the LRP1 receptor, with the aim of inhibiting Mdka-Lrp1aa signaling in cryoinjured hearts for subsequent evaluations. Lrpap1 is an endoplasmic reticulum protein with high-affinity binding to the LRP1 receptor. I employed an explant culture approach, wherein zebrafish hearts were dissected, subjected to cryoinjury, and cultured in the presence of either vehicle control or Lrpap1 until 7dpi **(Fig. 3.36a)**. I first assessed collagen I deposition and ECM turnover in Lrpap1-treated hearts versus controls at 7dpi using immunofluorescence staining **(Fig. 3.36b-e)**. Consistent with my in vivo observations in *adra1-3i* hearts, I found diminished collagen I deposition indicated by Col1+ area around the injury site **(Fig. 3.36b, c)** and a significantly reduced ECM turnover indicated by CHP+ area **(Fig. 3.36d, e)** in Lrpap1-treated hearts.

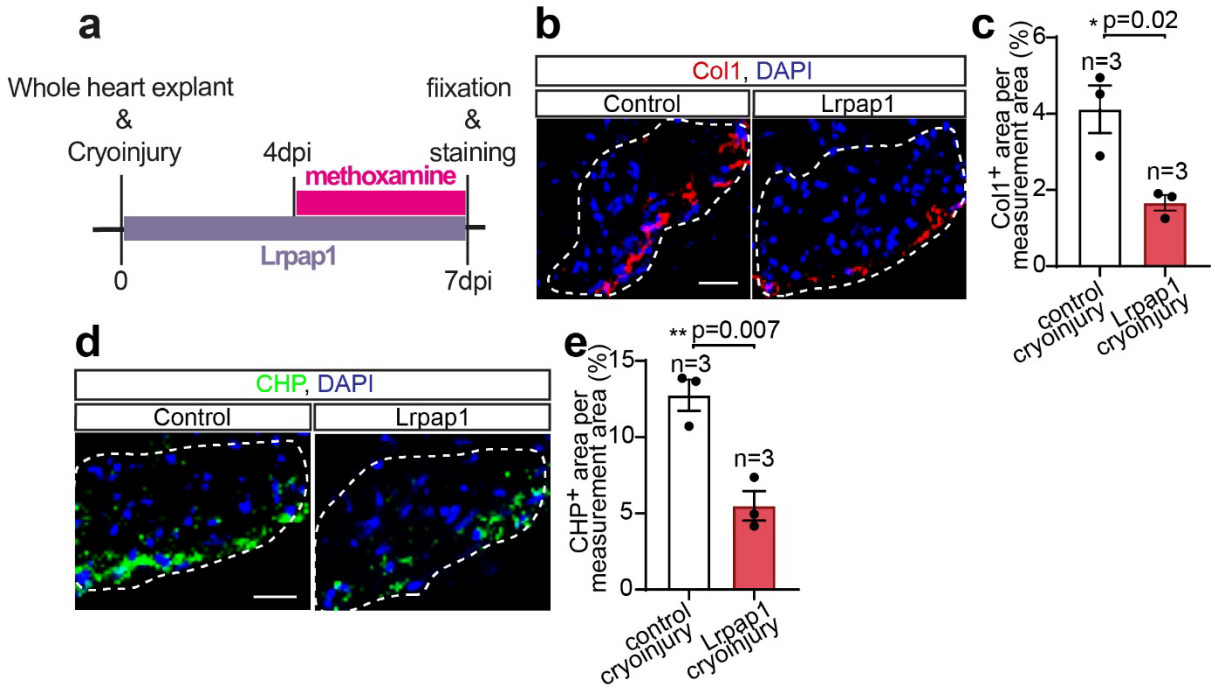

Figure 3.36 Cardiac fibrosis dynamics after cryoinjury are dependent on Mdka-Lrp1 signaling. (a) Scheme of experimental setup representing the timepoints of adult wild-type zebrafish heart

dissection, cryoinjury, and explant culture preparation, their treatment with recombinant zebrafish Lrpap1 protein until 7dpi, with Adra1 agonist methoxamine from 4dpi to 7dpi, and their fixation and staining at 7dpi. (b, d) Confocal images showing cryoinjured explant heart sections treated with control (vehicle) or Lrpap1 at 7dpi. Sections are immunofluorescence stained for Collagen I shown in red (b), degraded collagen content with CHP shown in green (d), and for cell nuclei with DAPI shown in blue. Dashed lines mark the injured area, scale bars are 20 μm. (c, e) Bar graphs depict the Collagen I deposition, quantified as percentage of Collagen I covered area within the measurement area (c), and degraded collagen content, quantified as percentage of CHP covered area within the measurement area (e), of cryoinjured explant hearts at 7dpi. All data points indicate individual animals and n numbers denote the number of animals used for each group. All data are presented as mean ± S.E.M. * $p<0.05$, ** $p<0.01$, *** $p<0.001$, n.s. not significant, two-tailed t-test. This data was generated by Altaikyzy A.

Subsequently, I evaluated other regenerative processes, such as cardiomyocyte proliferation, and blood and lymphatic vessel formation in Lrpap1-treated hearts **(Fig. 3.37)**. Blocking Mdka-Lrp1aa signaling led to a decline in cardiomyocyte proliferation, underlining its essential role in cardiomyocyte response to cardiac injury **(Fig. 3.37a, b)**. Additionally, Lrpap1-treated hearts displayed compromised blood **(Fig. 3.37c, d)** and lymphatic **(Fig. 3.37c, e)** vessel density at 7dpi, highlighting the detrimental effects of dysregulated fibrosis on regenerative processes and emphasizing the critical role of Mdka-Lrp1aa signaling in this context.

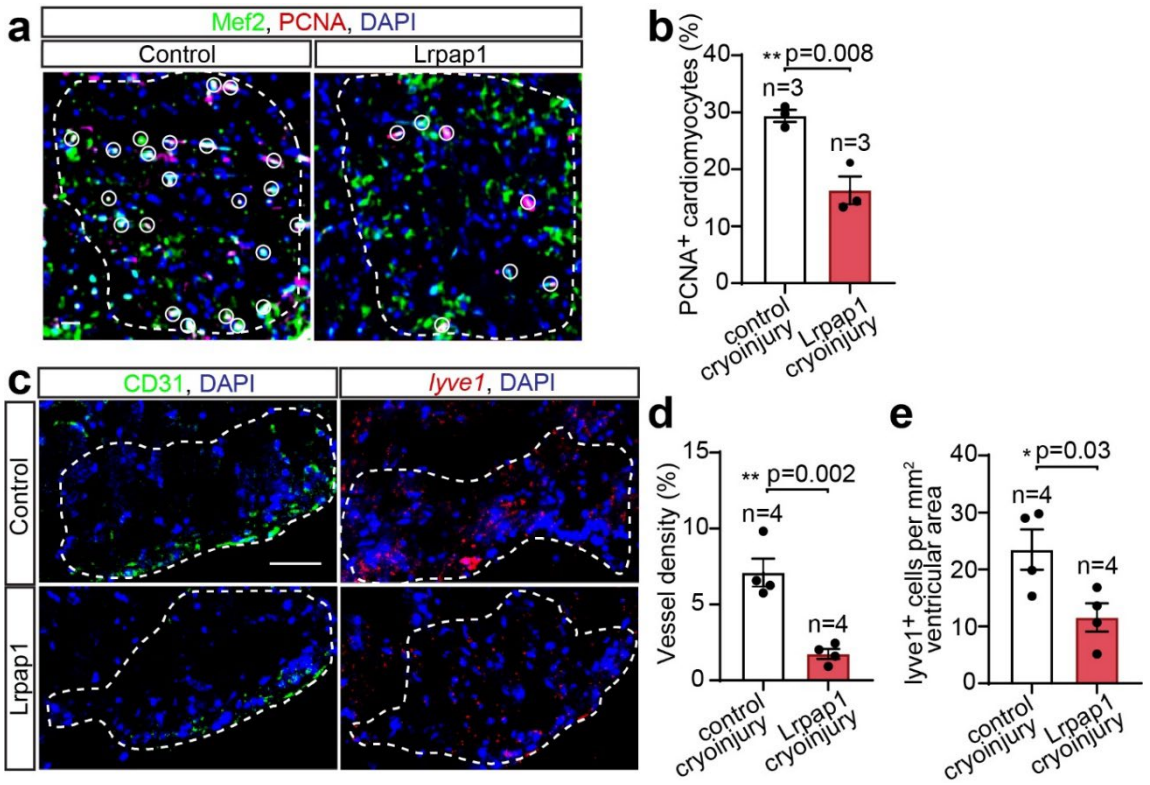

Figure 3.37 Cardiomyocyte proliferation, and blood and lymphatic vascularization require Mdka-Lrp1 signaling during cardiac regeneration. Same experimental setup as in **Fig. 3.36a**. (a, c) Confocal images showing cryoinjured explant heart sections treated with control (vehicle) or Lrpap1 at 7dpi. Sections are immunofluorescence stained for CMs with Mef2 shown in green (a), for proliferating cells with PCNA shown in red (a), white circles mark the colocalization of Mef2 and PCNA signals indicating proliferating CMs (a). Sections are immunofluorescence stained for blood vasculature with CD31 shown in green (c), HCR-FISH stained for lymphatic vasculature with *lyve1* probe shown in red (c). All sections are also stained for cell nuclei with DAPI shown in blue and all dashed lines mark the injured areas, scale bars are 20 µm. (b, d, e) Bar graphs depict the proliferating cardiomyocytes (PCNA+/Mef2+), quantified as percentages of total cardiomyocytes within the measurement area (b), the blood vessel area, quantified as percentage vessel area (CD31+) in the measurement area (d), and lymphatic endothelial cell numbers, cell numbers (*lyve1*+) per 1 mm2 ventricular area (e) in the injury zone at 7dpi. All data points indicate individual animals and n numbers denote the number of animals used for each group. All data are presented as mean ± S.E.M. * $p<0.05$, ** $p<0.01$, *** $p<0.001$, n.s. not significant, two-tailed t-test. The data in (a) and (b) was generated by Altaikyzy A.

Finally, I examined changes in pro-regenerative *col12a1a*+ fibroblasts when Mdka-Lrp1aa signaling was inhibited at 7dpi **(Fig. 3.38)**. A significant reduction in *lrp1aa+/col12a1a*+ fibroblasts among the total *col12a1a*+ fibroblasts was observed in Lrpap1-treated hearts at 7dpi **(Fig. 3.38a, b)**. This further supported the notion that Adra1-

activated MP-mediated Mdka-Lrp1aa signaling is crucial for activating a pro-regenerative subset of fibroblasts during cardiac regeneration.

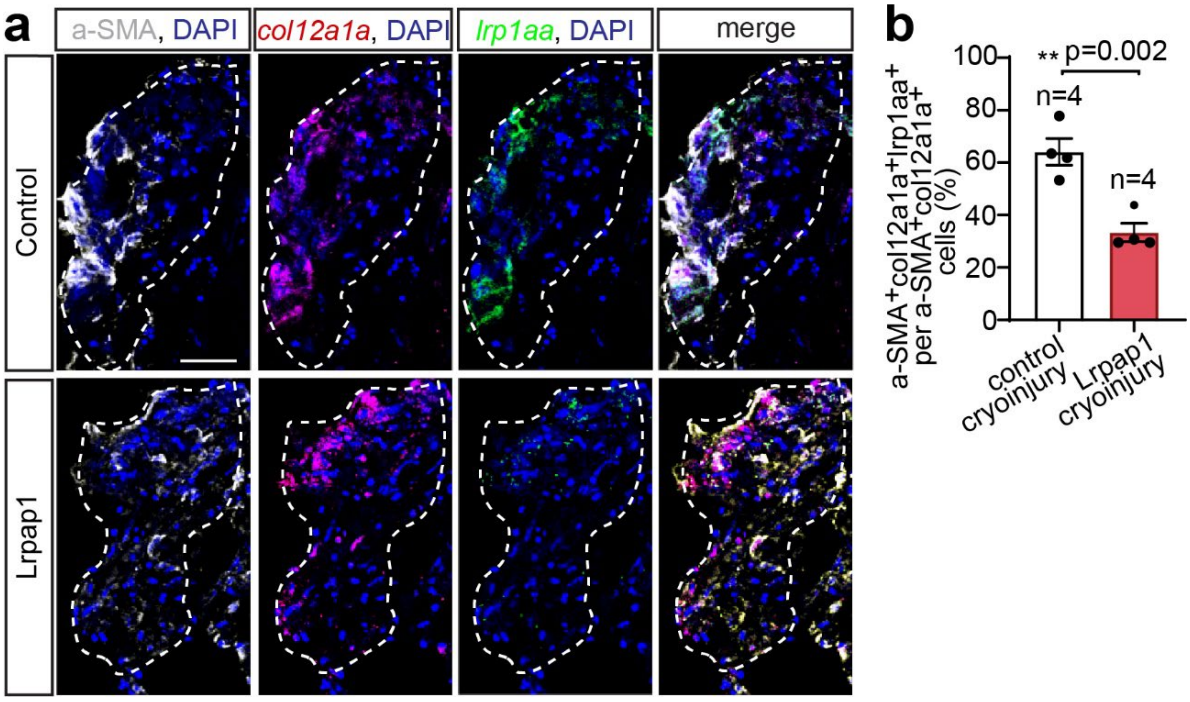

Figure 3.38 Mdka-Lrp1 signaling is critical for pro-regenerative fibroblast activation. Same experimental setup as in **Fig. 3.36a**. (a) Confocal images showing cryoinjured explant heart sections treated with control (vehicle) or Lrpap1 at 7dpi. Sections are HCR-FISH stained for *lrp1aa* and *col12a1a* shown in green and red, respectively, immunofluorescence stained for a-SMA shown in gray, and for cell nuclei with DAPI shown in blue. Dashed lines mark the injured area, scale bar is 20 µm. (b) Bar graph depicts the content of *lrp1aa*+ fibroblast among *col12a1a*+ fibroblasts, quantified as percentage of *lrp1aa+/col12a1a+/a-SMA+* fibroblasts in total *col12a1a+/a-SMA+* fibroblasts within the observed area. All data points indicate individual animals and n numbers denote the number of animals used for each group. All data are presented as mean ± S.E.M. * $p<0.05$, ** $p<0.01$, *** $p<0.001$, n.s. not significant, two-tailed t-test.

In summary, the data presented in this dissertation substantially elucidates the pivotal role of Adra1-activated MPs in fostering a cardiac microenvironment conducive to effective regeneration. This specialized MP subset influences scar tissue composition and degradation kinetics, thereby facilitating subsequent phases of myocardial repair. This is partially achieved through paracrine signaling mechanisms that activate a specific pro-regenerative fibroblast subset. By modulating the regenerative microenvironment, Adra1-activated MPs also affect myocardial lesion revascularization, thus underscoring their multifaceted contributions to the overall cardiac regenerative program.

4 Discussion

Ischemic heart disease remains a predominant global health concern, often leading to significant mortality and morbidity [198,199]. At its core lies the irrevocable loss of cardiomyocytes, cells which, once lost, prove challenging to replace due to the limited self-renewal capacity inherent to the human heart [4,133,200]. As these cells perish, fibrotic scars take their place, culminating in compromised cardiac function and heart failure[4,10,133,142,200]. While a myriad of clinical interventions has been tried, primarily focused on cellular replacements via stem and progenitor cells, their effectiveness remains minimal [2,3,201,202]. However, in neonatal mammals and several other vertebrates, such as zebrafish, hearts show a remarkable ability to regenerate post-injury [19,20,31,90,133,203]. This points towards a necessity for therapies that not only target cell replacement but also manage fibrotic responses to ensure scar regression underpinned by the post-injury cardiac microenvironment.

The heterogeneity seen among MPs, with diverse activation states and functions, implies their central role in the intricate relationship of repair and scar formation [42,65,71,101–103]. Historically perceived as solely inflammatory agents causing more harm than good post-cardiac injury, our understanding of these cells has evolved [37,38,44,58,67,75]. In fact, these versatile immune cells play dual roles: they can instigate inflammation while also aiding in regeneration [15,33,37,38,67]. The challenge now lies in understanding the mechanisms guiding these diverse MP functions and determining the elements that direct their activation.

Intriguingly, the nervous system, essential for maintaining immune balance and resolving inflammation, appears to have a pivotal role in this scenario [27,31,156]. Sensory neurons constantly communicate with our immune system and, under conditions like tissue injury, initiate responses to mitigate excessive inflammation [31,149,155,156,168,200,204,205]. The efficiency of this neural control system, particularly over MPs, is evident in its direct and swift action compared to other pathways. Findings up to date hint at the importance of the nervous system in heart regeneration, emphasizing the entwined nature of neuro-immune interactions [152,159,161,163].

Due to the complex nature of the cardiac niche during regeneration and the intricate relationship of the residing cells and other components, even though a plethora of studies revealed several critical aspects either as individual roles of the niche residents or with respect to other components, a complete picture of the network of interactions is still missing

[9,15,34,200,206]. The findings in this dissertation provide a comprehensive examination of the nuanced relationship between the nervous and immune systems. I specifically investigated the indispensable role of neuro-immune crosstalk in determining the phenotypic reprogramming of MPs, which in turn could allow new perspectives for potential therapeutic strategies in cardiac regenerative medicine.

4.1 Sympathetic regulation of macrophage phenotypes and its impact on cardiac regeneration

Nervous regulation of the immune system is a widely studied topic [152,163,164,204,207]. The ANS is known to take a role in both inflammation resolution and its induction [152,159,161,205,207–209]. For instance, one of the primary cases that leads to altered nervous signaling is stress [210–213]. It has long been linked to systemic inflammation by studies that show chronic stress induction of pro-inflammatory phenotypes in MP through toll-like receptor (TLR) pathways [214–217]. Catecholamines secreted by peripheral neurons were shown to drive MP phenotype towards pro-inflammatory by the same pathways [204,218–220]. Studies showed that sympathetic input from the nervous system through adrenergic receptor beta 3 (ADRB3) can suppress mobilization of myeloid-derived suppressor cells to increase activation of HSCs [221]. This was shown to selectively increase MP/monocyte accumulation, thus pro-inflammatory phenotype [221]. On another note, TLRs and receptors of IL1 are present in afferent neurons that can take up local cues and activate systemic nervous response to regulate inflammatory response [222–224]. These peripheral afferent neurons transmit these signals to the brain and can activate the vagus nerve, which can inhibit the inflammatory phenotype of MPs in specific locations [171,218,222,223,225]. In fact, it was shown that MPs can be shifted towards an anti-inflammatory phenotype through muscarinic 2 and CHRNA7 activity in the gut [226–228]. These responses were attributed to reflex control of immunity with the purpose of alerting the CNS to threats before they are severe [218,225,229]. Although inputs such as stress, leading to excessive inflammation, or inputs leading to alterations in cholinergic regulation of immunity, seem to be detrimental to the homeostasis of an organism, acute sympathetic response was shown to be required for an adaptive reparative response to injury [27,145,149,156]. However, various receptors involved in nervous signaling and differences between systemic and site-specific effects of these in inflammation regulation still require further research. Research on elucidating the mechanisms

underlying the regulation of inflammation and the importance of acute sympathetic response for regeneration showed that accumulation of DAMPs or other molecules from the damaged cells, for instance, leads to pro-inflammatory response from the responding immune cells [104,159,161,172,207–209,219,222]. These, in turn, can also activate TLRs and interleukin receptors of sensory neurons, leading to similar inflammation regulation response mechanisms with stress [222,223]. The exact mechanisms of how nerves regulate such sterile inflammation cases like injury are not fully understood. For instance, in adult mice, when sympathetic signaling is inhibited, increased cardiomyocyte proliferation with more mononucleated cardiomyocyte presence was seen [230], thereby suggesting a detrimental effect for sympathetic signaling in non-regenerative models. However, when sympathetic innervation of the heart is disrupted in neonatal mice hearts, their normally existing regenerative capability was significantly impaired [30]. On top of that, in zebrafish, when adrenergic signaling is blocked, regeneration was impaired, as seen by reduced cardiomyocyte proliferation and increased scar size following MI [27]. These reports clearly suggest a critical role for sympathetic input in regeneration in terms of immune modulation.

In line with previous findings indicating the critical role of sympathetic signaling in regeneration [27,30], data in this dissertation showed impaired regenerative response upon adrenergic signaling blocking through adrenergic alpha and beta receptors. Utilizing MP-specific Adra1-loss-of-function, I detected reduced cardiomyocyte proliferation and selective reduction in the anti-inflammatory subset of MPs around the injury site. Results of Adra1 inhibited MP contribution to the *tnfa*+ MP pool mostly, and very little contribution to the *tnfa*- MP pool also suggests a phenotypic regulation of MPs. These results indicate a novel role of Adra1 signaling in MP phenotypic determination during regeneration.

By delving into MP phenotypic differences using scRNAseq, I showed activation of an 'ECM remodeling' transcription program in a subset of MPs. This is noted by the increased expression of ECM remodeling genes translated into collagen types such as I, II, and V or proteases such as Mmp2 and Mmp9. To elucidate the functional consequences of this activation, I assessed subsequent regenerative processes. The data showed impaired blood and lymphatic vascularization, altered ECM composition, impaired turnover, and reduced pro-regenerative fibroblast population after injury when Adra1 activation is inhibited in MPs. These results provide new insights into the role of sympathetic input in immune modulation functional diversification of MPs during regeneration, expanding the previous findings mechanistically.

However, the exact location of this neuro-immune interaction is still not clear. I detected a normal proliferative rate for MPs even though their numbers were reduced when Adra1 signaling was blocked. This shows the possibility of sympathetic regulation of MPs outside of the heart. However, further studies using optogenetic tools such as light-activatable chimeric Adra1 receptors will be needed to express them in an MP-specific way that can help us selectively activate this signaling in various locations to assess the subsequent effect on regeneration.

4.2 Mechanistic insights into functional diversity of macrophage subsets in cardiac regeneration

MPs are critical in cardiac regeneration with various functions [65,101–103]. A Plethora of studies showed their functions during regeneration, such as activation of fibroblasts through TGF-β signaling, thus providing ECM regulatory elements to the environment, such as proteinases like MMPs, contributing to the collagen deposition themselves, clearing debris and contributing to the inflammatory phenotype shift of the microenvironment, acting as chaperons for vascular sprouting through VEGF signaling, providing inflammatory cytokines to mount up the initial inflammatory response through IL1β, TNFα, contribute to sending signals to CNS through activation of TLRs on the peripheral neurons [20,57,65,68,73,75,101,103,115,117,131,142]. However, it is important to note that these functions are not uniformly exhibited by all MPs, given their significant heterogeneity in terms of origin, activation mechanisms, final localization, and interaction partners. Understanding this diversity is essential for a more comprehensive view of MP roles in cardiac regeneration [65,71,103,183].

Studies in zebrafish showed that in the absence of MPs, regeneration is impaired [75,231]. Similarly, the presence of MPs is required for neonatal mice to mount a proper regenerative response [44]. Further studies to elucidate the role of specific MP subsets showed distinctions between cardiac resident and circulating MPs [70–72,232]. For instance, depleting resident MPs by chlodronate liposome (CL) injection in zebrafish 8 days prior to MI resulted in impaired regenerative processes such as vascularization defect, indicating that the circulating MP population is not enough to compensate critical MP functions [71]. Further elucidating distinct roles of MPs, a zebrafish study showed different maintenance dynamics of MP subsets following injury [72]. For instance, *timd4* expressing resident MP population, noted by lacking

ccr2 expression, was shown to self-renew with negligible circulating monocyte contribution [72]. Furthermore, the injury was shown to reduce both the *timd4+* and *timd4-* resident MP populations, but when all resident MPs were ablated, regeneration was impaired [72]. Resident MPs were also found to be enriched in ECM regulatory genes such as collagen types and MMPs compared to circulating ones [68,70,71,74]. These reports provide evidence about the resident MP function being distinct and not redundant in regeneration. Other studies revealed the distinction of activation mechanisms among MP subsets [41,63,71,231,233,234]. For instance, when mice with *Adrb3* knockout were analyzed for MP population expansion following MI, it was shown that MP and neutrophil levels were not increased [235]. This shows an impairment in the initial inflammatory response necessary for mounting a proper regenerative response [235]. Another study showed that *Adrb2* was important for CCR2 activity regulation in MPs, affecting their proper recruitment to the injury site [236,237]. Altogether, it is now known that distinct MP subsets have specific functions and modes of activation. However, a complete picture of MP functional and phenotypical diversification with spatial and temporal regulation and subsequent modulation of the regenerative response is still required for targeted and effective regenerative therapies.

In this dissertation, I found that a specific MP subset was activated through Adra1 signaling after MI. scRNAseq results showed that this population is enriched in ECM remodeling genes such as *col1a1a* and *mmp2* and genes suggestive of their interaction with fibroblasts such as *mdka*, *sparc*, and *fn1b*. Findings here also show that when Adra1 signaling was impaired in MPs, it led to altered ECM regulation, such as reduced collagen I and collagen V content indicated by antibody and *in-situ* staining, respectively, and reduced turnover indicated by lower CHP levels. A pro-regenerative fibroblast population activation was compromised, providing a mechanistic link as to how these Adra1-activated MPs influence ECM organization. To further elucidate the mechanism underlying this influence, I showed via in silico analysis the interaction between Adra1-activated MPs and fibroblast subsets. I also provided experimental verifications. I found that the Mdka-Lrp1aa receptor-ligand pair was, with high probability, responsible for the activation of the pro-regenerative fibroblast subset by Adra1-activated MPs. Firstly, I showed that in-silico, *mdka* was enriched in this MP subset. Also, there was a reduction in *mdka* expressing MPs when Adra1 in them was inhibited. Furthermore, I revealed a reduction in *lrp1aa+col12a1a+* fibroblasts (pro-regenerative) when Adra1 signaling in MPs was inhibited. Together with my results showing impairment in the

subsequent regenerative processes such as cardiomyocyte proliferation, lymphatic and blood vessel formation, I expand the understanding of the neuronal influence on regeneration through novel mechanistic insight such as MP functional and phenotypical diversification.

Although my findings show a specific function and a novel activation and regulation mechanism of the particular MP subset here, the heterogeneity in terms of origin or location is still debatable. Therefore, further research with localized tools to elucidate this MP subset's niche and location of nervous interaction is required. Optogenetic tools enabling localized activation of MPs through specific pathways might come in handy in this endeavor. Alongside possible site-specific delivery methods to inquire about the effects of possible cues coming from such MPs on other residents of the injury niche, it would provide valuable insight into the intricate tapestry of cardiac regeneration for future therapeutic strategies.

4.3 Extracellular matrix provides not only structural support but also actively influences cardiac regeneration

The ECM is an intricate network of proteins, glycoproteins, and proteoglycans that not only provide structural support to cells but also play a pivotal role in cellular functions such as adhesion, migration, differentiation, and proliferation [131,134,142]. In the context of the heart, the ECM is especially critical, given its role in transmitting mechanical signals, maintaining structural integrity, and mediating cellular interactions through mechanisms such as the release of growth factors and cytokines that promote the repair of damaged tissue [88,131,142,238].

During cardiac regeneration, the ECM provides a niche for cardiac cells, including cardiomyocytes, fibroblasts, endothelial cells, and MPs [88,142]. Specific components of the ECM, such as collagen, fibronectin, laminin, and proteoglycans, are known to affect the cardiac niche, steering cellular behaviors fundamental for regeneration. For instance, fibronectin was identified as a vital component in zebrafish heart regeneration, mediating the activation of epicardial cells after injury [239]. Similarly, laminins, particularly laminin-511, have been shown to enhance cardiomyocyte adhesion and promote their maturation [240]. Proteoglycans can bind growth factors and cytokines and help to deliver these signals to cells [241].

ECM is not just a passive structural entity but actively influences cardiac regeneration, adding another layer of complexity in the pursuit of effective cardiac repair strategies [88,131,142,238]. Harnessing the ECM's potential could pave the way for novel therapeutic

approaches to treat heart diseases and injuries. Findings in this study provide novel insights into the regulation of ECM properties that were reported to be critical for subsequent regenerative processes from myocardium renewal to revascularization while revealing novel mechanistic underpinnings.

4.3.1 Neuro-Immune modulation of extracellular matrix dynamics and its implications for cardiac regeneration

Following cardiac insult and subsequent cardiomyocyte death, the ECM undergoes significant temporal changes that can be broadly summarized as the inflammatory phase, the proliferative phase, and the maturation phase [88,142,242,243]. Triggered by the death of cardiomyocytes, an influx of inflammatory mediators fosters increased vascular permeability, leading to an accumulation of plasma proteins like fibrin and fibrinogen and intensifying MMP activity, thus resulting in the degradation of the existing interstitial matrix, paving the way for the formation of the provisional ECM, a unique matrix saturated with growth factors (such as VEGF) and cytokines [142,243,244]. The provisional ECM allows infiltration of inflammatory cells and facilitates fibroblast adhesion [142,244]. This allows further activation and expansion of fibroblasts by differentiating into myofibroblasts and proliferation [142,244]. Clearance of debris through phagocytosis leads to a shift in the environment towards anti-inflammatory through pathways such as TGF-β/smad3 supporting the activation of fibroblasts and ECM regulation [142,244]. The provisional matrix at this proliferative phase exhibits more of a secretory purpose rather than structural support. The inputs from the provisional matrix, with the shift in the environment, lead to the degradation of the provisional matrix and subsequent deposition of ECM components, primarily collagen I [142]. Later, the maturation phase starts to initiate as collagen content becomes enriched, and collagen cross-linking occurs, thus forming a rigid scar [142,245,246]. The shift from the proliferative phase to the maturation phase, where the complete scar is formed, was thought to be marked by myofibroblast [142,243,247]. Although the importance of ECM properties for regeneration was partially revealed, a complete understanding of ECM dynamics is still missing for efficient regulation of fibrotic response for regenerative therapies.

Studies trying to elucidate the dynamics of fibrotic response in cardiac regeneration revealed differences between regenerative organisms such as zebrafish and non-regenerative

organisms, most mammals [131,133,244]. A recent study showed that myofibroblasts, rather than being completely removed or completely undergoing apoptosis, are being inactivated [134]. Other studies showed periostin and collagen I in the injury border zone are critical for inducing CM cell cycle re-entry and guiding the rapid vascular sprouting occurring in the zebrafish after injury, respectively [142,248,249]. Paracrine interaction with endothelial cells and ECM was also shown to be important for vascularization through Vegfc signaling, inducing Emilin2a ECM protein secretion and subsequently resulting in c*xcl8a* expression in epicardial cells, resulting in vascularization and myocardium renewal[115]. Thus, the availability of the input from ECM seems to be an important factor in its role in inducing proper regenerative response.

Fibrosis was once believed to be detrimental to cardiac repair. However, the importance of fibrosis for proper repair or regeneration is beginning to draw more attention [94,129,130,142]. For example, a lineage tracing study showed that epicardial Tcf21-derived cells give rise to *Postn* expressing activated fibroblasts after MI in mice, and ablation of *Postn*+ cells decreased survival after MI [127]. Another study showed that increased MMP activity is a common process in both zebrafish and newts, which are regeneration-capable [133]. MMP inhibition in neonatal mice was also shown to be detrimental to its regenerative ability [250]. In zebrafish, it was shown that collagenous ECM deposition precedes cardiomyocyte renewal, and collagen deposition is dynamic, reducing around 7dpi and up to 21dpi [143]. Taken together, it is evident that the availability of a tightly regulated fibrotic response is not at all mutually exclusive with regeneration and required. However, the presence of innate systems that modulate matricellular signals to shield the myocardium from ongoing fibrosis in a fully developed ECM setting and the dynamics of this setting are yet to be thoroughly investigated.

The results presented here revealed that when neuro-immune interaction is inhibited by both pharmacological treatments and genetic manipulation, ECM regulation during the regeneration process is impaired. I showed impairment in the collagen I deposition and ECM turnover, indicated by a reduction in CHP amount. The data indicating impairment in subsequent regenerative processes, such as cardiomyocyte proliferation and revascularization, provides a link between proper ECM dynamics and regeneration. I showed that Adra1-activated MP activity is critical for this regulation, thereby providing mechanical insight into ECM regulation. Furthermore, these findings revealed anti-inflammatory MPs, being the primarily affected population, support the requirement of an anti-inflammatory shift in the microenvironment for proper fibrotic response. This was also evident by the reduced collagen

I expressing fibroblast presence, which reportedly requires also preceding proper immune response. All in all, this work supports the necessity of timely ECM regulation for regenerative response and provides novel mechanistic insights into how neuro-immune interaction is involved.

4.3.2 Differential roles of collagen types in extracellular matrix regulation: insights from neuro-immune modulation

Strict regulation of fibrotic response is critical for proper regeneration of the heart [142,143]. Studies investigating ECM's role in cardiac regeneration showed the critical role of its composition for a proper regenerative response on top of its precise regulation dynamics [131,142,238,244,250].

One of the major components of the ECM, collagen I, is a prominent member of the fibrillar collagen family, stands as a pillar of structural and functional integrity within the cardiac ECM [68,142,243,251–254]. Its robust fibrillar network serves as a scaffold, conferring the myocardium its requisite tensile strength and elasticity [142,252–254]. In the acute phase post-MI, collagen III to collagen I ratio is higher in the ECM. However, collagen III is lysed and replaced rapidly by collagen I, which provides tensile strength to the injured area to temporarily compensate for the cardiac function [142,254,255]. In fact, elevated levels of collagen I were observed in infarcted hearts, leading to fibrosis and scar formation [142,255]. A study showed that collagen I promotes differentiation and proliferation of myofibroblasts through modulation of α2β1 integrin expression [256]. Whereas another study showed that MMP2 and MMP9 mediated degradation of type I collagen reduced the scar formation and induced angiogenesis [257]. It was also shown that the presence of collagen I is important for the guidance of vascular sprouting following injury [258]. Even though the reports about collagen I are seemingly conflicting, the requirement of its presence and strict regulation for proper regenerative response remains.

Another component of the ECM, collagen V, was reported to be critical for scar size regulation after MI [116]. Mice lacking collagen V were shown to be exhibiting significantly increased scar size after MI[116]. It was shown that collagen V is usually highly expressed before the other components of ECM and later becomes buried under them, thus being critical for ECM organization initiation, supporting its role in scar size modulation [116,138]. It was shown that it is critical for remodeling in usual interstitial pneumonia in human biopsy samples [259].

Varying levels of fibrosis were shown to be correlated with collagen V density in these samples [259]. On top of its role in the organization of ECM components, collagen V was shown to affect the mechanical properties of the ECM [116]. It was shown that it can modulate mechanosensitive feedback provided by the integrin-related inputs in the ECM [116]. Based on these reports, collagen V seems to be one of the critical components of the ECM, necessary for proper regenerative response.

ECM contains several collagen types with largely unknown functions related to regeneration [88,142,251]. Another one is collagen XII. This is a non-fibrillar collagen and largely non-existent in homeostasis conditions and transiently upregulated following cardiac injury [87]. It was shown to have critical functions related to regeneration [111–113]. Epicardial cells were shown to be guided by collagen XII to the heart surface and to the adjacent pericardial region, thus providing a bridge for epicardial connective tissue [260]. It is largely associated with fibrillar collagens such as collagen I and was shown to have a role in ECM organization by providing connective support for its components [260–262]. It forms bridges in the ECM and promotes cell-to-cell communications, which are critical during regeneration [111,113,260]. Furthermore, when collagen XII-expressing cells were ablated, regeneration of the heart was impaired [87]. Although its exact role in the regenerative processes is not fully understood, it was shown that collagen XII, around 7dpi in zebrafish hearts, localizes to the edge of the wound area between healthy CMs and injury zone [87]. Based on its connective role, it might be regulating the accessibility of the wound area for the influx of cells following injury. Its regulation was reported to be correlated with TGF-β activity in the environment, linking it to the shift in the microenvironment during the regeneration process and even MPs [260]. In fact, its relationship with MPs was further supported by findings in collagen XII overexpressing mice, where inflammatory MPs were increased [111]. These findings suggest a requirement for strict regulation of collagen XII content in ECM for proper regenerative response.

Although ECM content, in general, seems to be important for regeneration, the exact role of this content, its regulation mechanisms during regeneration, and subsequent effects on complete myocardial renewal are not fully understood. My findings showed reduced collagen I deposition and impaired collagen turnover indicated by reduced CHP. I also showed reduced relative expression of *col5a1* and increased relative expression of *col12a1a*. On top of reporting alterations in ECM content, I also showed reduced vascularization and cardiomyocyte proliferation. This provides a link between these collagen types and regenerative processes.

Furthermore, alterations in the ECM after Adra1 signaling inhibition in MPs show novel mechanistic insights into immune modulation of ECM dynamics. My findings are in line with previous findings of collagen I's role in vascularization [258], ECM organizational change with varying collagen V and XII levels, and resulting failure to induce cardiomyocyte proliferation, impairment in the necessary fibroblast activation and expansion [111,113,116,260]. However, findings in this dissertation, resulting from neuro-immune interactions and comprehensive assessments of subsequent events, provide a novel sequential insight into the regulation of ECM composition and its effect on regeneration.

4.4 Neuro-immune interaction and functional diversity of fibroblast subsets: implications for cardiac regeneration

The role of fibroblasts in cardiac tissue has been a subject of intricate research, with growing evidence supporting their multifaceted contributions to cardiac regeneration and repair [87,129–131]. Previous studies have noted the importance of fibroblasts in cardiac tissue, but these have often been generalized as a uniform population [129–131]. Recent studies started to indicate the functional, ontogenic, and spatial heterogeneity of fibroblasts in cardiac regeneration[17,87,126,131,263]. For instance, studies showed that activated fibroblasts with *α-SMA* expression emerged in the proliferative stage after MI [127,142,251]. These are often called myofibroblasts and are responsible for collagen I deposition, organizing the microenvironment for initial rapid wound closure, and providing necessary signaling inputs for upcoming events leading to maturation phase [127,251]. They were shown to express *Postn* and mostly *Tcf21,* indicating that they are of epicardial origin[127,264]. Periostin provided by the fibroblasts near the injury border zone was shown to induce cardiomyocyte cell cycle re-entry [248]. Another study showed that *α-SMA, Postn, and Tcf21* expressing myofibroblasts are high in content around 3-7dpi , for instance, indicating their dynamic activation [127]. Furthermore, it was shown that both in the early stages after injury and around 10dpi, there are other myofibroblasts that can be distinguished by their expression profile [265]. Furthermore, improving scRNAseq technologies showed that there are actually transient states of fibroblasts following injury that are not present in homeostatic conditions [87]. A collagen XII expressing fibroblast population was transiently increased after MI [87]. When collagen XII-expressing cells were ablated, regeneration was impaired in zebrafish, showing their importance for regenerative function [87]. A mesh network

of fibroblast and collagen XII was shown to be localized to junctions of healthy/injured tissue in the heart, and this was shown to be critical for the mechanical organization of ECM [260].

Mechanical properties of the ECM are critical for regenerative response as they can facilitate cell-to-cell interactions and signaling input for other residents of the cardiac microenvironment [94,142,251,253,254]. Fibroblast functions to deposit different types of collagens, such as type I, III, IV, V, XII, and MMPs, are the main factors regulating these mechanical properties of the ECM [131,142,243,244,254]. This helps the shift towards repair/regeneration phase [142]. For instance, collagen V was shown to affect mechanosensitive myofibroblasts. The absence of collagen V leads to augmented activation of these cells [116]. These mechanical properties can also alter the inflammatory input to the other residents of the regenerative microenvironment [142,251]. Such an occurrence was exemplified by showing the differential effect of tense or relaxed ECM's effect on the inflammatory profile of MPs, for instance [116,142,266]. Collagen V was also shown to be involved in the initiation of collagen fibril formation, and lack of collagen V in mice was shown to lead to severe lack of fibril formation[138]. ECM's critical role in regenerative response and its varying regulation by fibroblast populations of distinct origin and phenotype shows that understanding fibroblast heterogeneity is critical to developing therapeutic strategies involving fibrotic response modulation.

Although recent studies provided insights into specific functions of distinct fibroblast subsets, exact mechanisms governing such functions and the activation of such subsets still require extensive work. Findings in this dissertation showed that Adra1-activated MPs are responsible for the activation of a pro-regenerative fibroblast population through the Mdka-Lrp1aa pathway. I show a novel activation mechanism of such transient and critical fibroblast subsets through neuro-immune interactions. Furthermore, I showed that collagen V and collagen I, together with ECM turnover, were impaired when this activation mechanism was disrupted. Collagen XII expression was increased, but the population of fibroblasts expressing *lrp1aa* and collagen XII was reduced. Together with the findings showing impaired regenerative processes such as vascularization and cardiomyocyte proliferation, I unveil a complex interaction network involving specific fibroblast subset activation, which leads to proper regulation of the ECM and subsequent regenerative response.

Although this work expands the understanding of fibroblast functional heterogeneity by providing specific mechanistic insight and showing their involvement in the neural influence

on the regenerating heart, the ontogeny analysis I performed is mostly in silico. Also, ex vivo findings where I blocked Lrp1 with its antagonist, Lrpap1 recombinant protein, show similar impaired regenerative processes as Adra1 inhibition in MPs. Even though these parallel results provide a link between MP and fibroblast during regeneration, fibroblast-specific loss-of-function or gain-of-function studies would shed more light on the underlying mechanisms behind this interaction.

4.5 Neuro-immune interaction influence on functional diversity of fibroblast subsets in cardiac regeneration

Timely activation/inactivation of fibroblasts was shown to be critical for strict regulation of ECM remodeling and microenvironment switch from one phase of repair to another after cardiac injury [134,142]. Recent studies showed distinct fibroblast roles in regeneration; however, to have a complete picture of multi-system interaction in regeneration, elucidating the specific mechanisms leading to activation of critical and often transient fibroblast subsets is indispensable [87,127]. One of the major ways of fibroblast activation, namely differentiation to myofibroblast, was shown to be TGF-β/smad3 pathway upregulation in the microenvironment following the debris cleaning phase after MI [267]. It was shown that MPs are primary contributors to this event [67,94,128,142,267]. Following phagocytosis, TGF-β release from MPs supports such change in the environment [20,36,67,94,142]. This helps switch to a more anti-inflammatory microenvironment and MP phenotype [36,67,94,142]. Factors such as IL4 and IL6 secreted from anti-inflammatory MPs lead to fibrosis [67,94,135,244,267]. However, excessive presence of inflammatory MPs was also shown to lead to fibrosis through factors such as TNF [36,67,94,142]. One study showed that even though there are conflicting reports about which type of MPs lead to fibrosis, regulation of inflammatory to anti-inflammatory phenotypic switch of MPs can alter the ECM modulation [36,67,94]. Therefore, it is critical to have a balanced immune response for proper ECM modulation.

It is known that MPs can alter ECM modulation by either directly providing MMPs and depositing several collagen types, such as collagen I and IV or through activating fibroblasts [68]. Supporting this, a study showed reduced myofibroblast when MPs were ablated during cardiac regeneration [20]. Furthermore, ECM composition and rigidity were also shown to be affected by the impaired MP fibroblast interaction [57,88,94,142,251]. Prolonged inflammatory MP

presence was shown to increase collagen I content in the ECM [15,57]. However, the exact mechanisms behind MP fibroblast interaction and resulting ECM changes are still not clear.

One possible interaction mechanism is through LRP1 receptor activity on fibroblasts [121,268–270]. A study on rat kidneys showed that LRP1 is required for TGF-β mediated fibrotic response [268]. It can induce collagen I expressing fibroblasts[121,271]. Also, LRP1 was shown to mediate fibroblast survival through downstream ERK1 pathway [269–271]. Thus, previous reports showed that LRP1 is critical for fibroblast activation and survival. On top of this, LRP1 activity was indicated in adjusting the availability of several molecules in the microenvironment critical for ECM remodeling [119,120,268,272]. Studies showed that LRP1 in fibroblasts can mediate internalization of the MMP2/TIMP2 complex and MMP9/TIMP1 complex, which are critical for ECM remodeling [108,272,273]. Thus, reports show that LRP1 activity is important for regulating ECM through balancing matrix proteinase activity [123,268,270,272]. Its expression in the cardiac tissue following injury was shown to shift, also suggesting a link with the presence of transient fibroblast subsets [121,274]. For instance, a study in mice showed that LRP1 expression was significantly higher around 10 days and 21 days after MI and with differing levels based on location, focused on peri-infarct areas, thus suggesting a timely regulation requirement for LRP1 function [270]. Studies focusing on its role in cardiac regeneration showed that LRP1 agonist treatment provided prolonged cardioprotective effects in mice and patients [121,270,274,275]. A Plethora of research indicates the critical role of LRP1 receptor activity in fibroblast for proper cardiac repair/regeneration; however, due to its several distinct ligands and crosstalk with various downstream intracellular pathways, it is difficult to pinpoint its exact role.

One interesting ligand for LRP1 is MDK [140]. It was shown to increase in several tissues, such as the heart, fin, and retina, during regeneration [140,141,276–280]. Furthermore, it was indicated as a cardioprotective agent in studies with *Mdk* knockout mice, where following cardiac injury, these animals showed increased scar size and impaired heart function [279,281]. MDK is also involved in processes critical for proper cardiac repair, such as ECM remodeling and vascularization [276,282–284]. For instance, a study with rat hearts showed that prolonged exposure of injured hearts to mdk increased collagen deposition, leading to maladaptive fibrosis [285]. Other studies showed its role in angiogenesis, where injured rat hearts showed increased vasculature following MDK treatment [285,286]. These reports also showed *Mdk* transient upregulation following injury, thus once again indicating the importance of temporal regulation during regeneration [140,276,285]. Studies in zebrafish showed that *mdka* was critical for

regenerative response [276]. For instance, the absence of *mdka* led to impaired retinal regeneration, and fin regeneration was delayed [276,280,287]. Its role was linked to cell proliferation regulation and altering ECM content [140,276,288]. TGF-β signaling was also shown to be impaired in the absence of mdk, linking it to the required shift in the environment for activation of pro-regenerative fibroblast subsets [276,283]. Further studies supporting this link showed that MDK absence led to the upregulation of fibrotic genes in fibroblasts in line with mice studies leading to excessive collagen deposition, thus supporting MDK's role in proper ECM modulation [276,279,281,285,287]. However, the source of this molecule in the context of heart regeneration is unclear. Some studies showed that its expression in fibroblasts is high after injury [276,283]. One interesting source was shown to be MPs [289,290]. In humans following stent implantation, for instance, infiltrating MPs were shown to be expressing MDK in high levels [289]. Also, MDK produced by MPs was shown to be critical for triggering proliferation in endothelial cells in humans [291]. Altogether, MDK is a possible ligand for critical LRP1 receptor function in fibroblasts; however, the exact nature of this receptor-ligand pair's role and host cell types expressing these require further research.

I show that after MI, Adra1-activated MPs are upregulating their *mdka* expression. Furthermore, *mdka* expressing MP numbers were reduced when Adra1 signaling was inhibited after injury. I also show that *lrp1+col12a1a+* fibroblast numbers were reduced. Furthermore, my results showed that Lrp1 inhibition in ex vivo conditions leads to a similar phenotype with the Adra1 blockage, such as alterations in ECM and subsequent regenerative processes supporting the interaction of MP with the fibroblast subset. I also delved into the ECM composition, such as collagen I decrease, turnover decrease, and collagen V decrease.

Even though I provide new mechanical insight into the neuro-immune interaction role in activating distinct fibroblast subsets, a direct link between these MP-fibroblast subsets requires further research. Reports linking the Lrp1 function to the availability of ECM remodeling proteinases and the activation and expansion of fibroblasts make it possible that Lrp1-activated fibroblasts are regulating the ECM remodeling by balancing the availability of proteases. Fibroblast-specific loss-of-function or gain-of-function tools would come in handy with such research.

Overall, this dissertation provided novel insights for understanding the whole regeneration tapestry. I showed at the heart of the neuro-immune interaction mechanism; there is the MP cell autonomous Adra1 signaling. Once activated, it kickstarts an 'ECM remodeling'

transcriptional program. This is characterized by the expression of diverse structural and matricellular components associated with cardiac ECM and proteolytic enzymes that target ECM proteins for degradation. Delving deeper, I discovered that Adra1-activated MPs employ the intercellular Mdka-Lrp1 signaling to govern the differentiation of a distinct pro-regenerative fibroblast subset. This subset plays a significant role in modulating the balance of fibrillar and non-fibrillar collagens at the lesion site. This intricate interplay between MPs and fibroblasts offers fresh insights into the regulation of fibrosis and its timely resolution. Such interactions are paramount for promoting blood and lymphatic neovascularization and triggering the cardiomyocyte cell cycle re-entry, thereby renewing the myocardium.

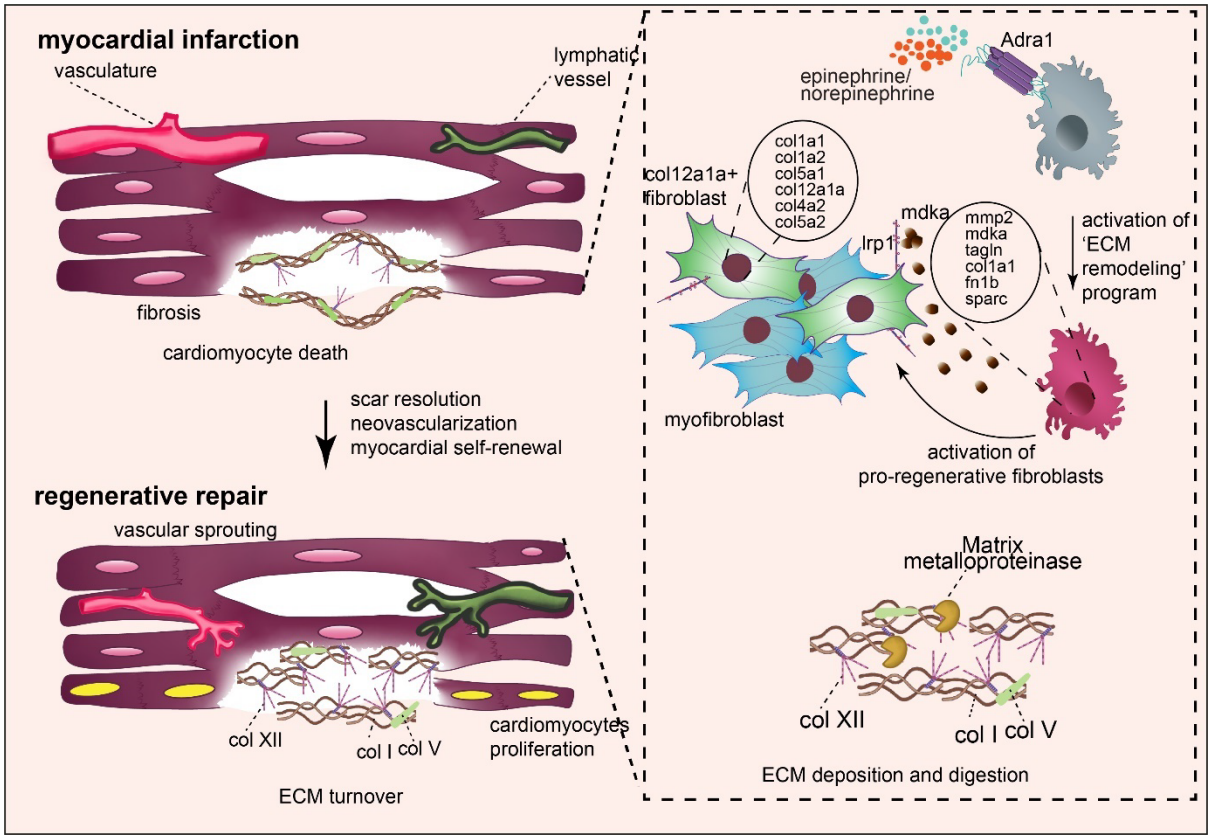

5 Bibliography

1. Tajabadi, M., Goran Orimi, H., Ramzgouyan, M.R., Nemati, A., Deravi, N., Beheshtizadeh, N., and Azami, M. (2022). Regenerative strategies for the consequences of myocardial infarction: Chronological indication and upcoming visions. Biomedicine and Pharmacotherapy *146*, 112584. 10.1016/j.biopha.2021.112584.
2. Cahill, T.J., Choudhury, R.P., and Riley, P.R. (2017). Heart regeneration and repair after myocardial infarction: Translational opportunities for novel therapeutics. Nat Rev Drug Discov *16*, 699–717. 10.1038/nrd.2017.106.
3. Frantz, S., Hundertmark, M.J., Schulz-Menger, J., Bengel, F.M., and Bauersachs, J. (2022). Left ventricular remodelling post-myocardial infarction: pathophysiology, imaging, and novel therapies. Eur Heart J *00*, 1–16. 10.1093/eurheartj/ehac223.
4. Sayers, J.R., and Riley, P.R. (2021). Heart regeneration: Beyond new muscle and vessels. Cardiovasc Res *117*, 727–742. 10.1093/cvr/cvaa320.
5. Roth, G.A., Mensah, G.A., Johnson, C.O., Addolorato, G., Ammirati, E., Baddour, L.M., Barengo, N.C., Beaton, A., Benjamin, E.J., Benziger, C.P., et al. (2020). Global Burden of Cardiovascular Diseases and Risk Factors, 1990-2019: Update From the GBD 2019 Study. J Am Coll Cardiol *76*, 2982–3021. 10.1016/J.JACC.2020.11.010/SUPPL_FILE/MMC3.DOCX.
6. Katz, A.M. (2008). The "modern" view of heart failure: how did we get here? Circ Heart Fail *1*, 63–71. 10.1161/CIRCHEARTFAILURE.108.772756.
7. Jhund, P.S., and McMurray, J.J.V. (2016). The neprilysin pathway in heart failure: A review and guide on the use of sacubitril/valsartan. Heart *102*, 1342–1347. 10.1136/heartjnl-2014-306775.
8. Ogle, M.E., Segar, C.E., Sridhar, S., and Botchwey, E.A. (2016). Monocytes and macrophages in tissue repair: Implications for immunoregenerative biomaterial design. Exp Biol Med *241*, 1084–1097. 10.1177/1535370216650293.
9. Handley, E.L., and Callanan, A. (2022). Modulation of Tissue Microenvironment Following Myocardial Infarction. Adv Nanobiomed Res, 2200005. 10.1002/anbr.202200005.
10. Kikuchi, K., and Poss, K.D. (2012). Cardiac regenerative capacity and mechanisms. Annu Rev Cell Dev Biol *28*, 719–741. 10.1146/annurev-cellbio-101011-155739.
11. Chablais, F., Veit, J., Rainer, G., and Jawiska, A. (2011). The zebrafish heart regenerates after cryoinjury-induced myocardial infarction. BMC Dev Biol *11*. 10.1186/1471-213X-11-21.
12. Schwinger, R.H.G. (2021). Pathophysiology of heart failure. Cardiovasc Diagn Ther *11*. 10.21037/CDT-20-302.
13. Femia, G., French, J.K., Juergens, C., Leung, D., and Lo, S. (2021). Right ventricular myocardial infarction: pathophysiology, clinical implications and management. Rev Cardiovasc Med *22*, 1229–1240. 10.31083/j.rcm2204131.

14. Klaourakis, K., Vieira, J.M., and Riley, P.R. (2021). The evolving cardiac lymphatic vasculature in development, repair and regeneration. Nat Rev Cardiol *18*, 368–379. 10.1038/s41569-020-00489-x.

15. Sun, K., Li, Y. yuan, and Jin, J. (2021). A double-edged sword of immuno-microenvironment in cardiac homeostasis and injury repair. Signal Transduct Target Ther *6*. 10.1038/s41392-020-00455-6.

16. Halade, G. V., and Lee, D.H. (2022). Inflammation and resolution signaling in cardiac repair and heart failure. EBioMedicine *79*, 103992. 10.1016/j.ebiom.2022.103992.

17. Han, M., and Zhou, B. (2022). Role of Cardiac Fibroblasts in Cardiac Injury and Repair. Curr Cardiol Rep *24*, 295–304. 10.1007/s11886-022-01647-y.

18. González-Rosa, J.M., Sharpe, M., Field, D., Soonpaa, M.H., Field, L.J., Burns, C.E., and Burns, C.G. (2018). Myocardial Polyploidization Creates a Barrier to Heart Regeneration in Zebrafish. Dev Cell *44*, 433-446.e7. 10.1016/j.devcel.2018.01.021.

19. Ross Stewart, K.M., Walker, S.L., Baker, A.H., Riley, P.R., and Brittan, M. (2022). Hooked on heart regeneration: the zebrafish guide to recovery. Cardiovasc Res *118*, 1667–1679. 10.1093/cvr/cvab214.

20. Godwin, J.W., Debuque, R., Salimova, E., and Rosenthal, N.A. (2017). Heart regeneration in the salamander relies on macrophage-mediated control of fibroblast activation and the extracellular landscape. NPJ Regen Med *2*, 1–11. 10.1038/s41536-017-0027-y.

21. Porrello, E.R., Mahmoud, A.I., Simpson, E., Hill, J.A., Richardson, J.A., Olson, E.N., and Sadek, H.A. (2011). Transient regenerative potential of the neonatal mouse heart. Science (1979) *331*, 1078–1080. 10.1126/science.1200708.

22. Shi, W.Y., and Smith, J.A. (2018). Role of Coronary Artery Bypass Surgery in Acute Myocardial Infarction. Primary Angioplasty, 211–221. 10.1007/978-981-13-1114-7_16.

23. Dicks, S., Jürgensen, L., Leuschner, F., Hassel, D., Andrieux, G., and Boerries, M. (2020). Cardiac Regeneration and Tumor Growth—What Do They Have in Common? Front Genet *11*, 586658. 10.3389/FGENE.2020.586658/BIBTEX.

24. Sorbini, M., Arab, S., Soni, T., Frisiras, A., and Mehta, S. (2023). How can the adult zebrafish and neonatal mice teach us about stimulating cardiac regeneration in the human heart? Regenerative Med *18*, 85–99. 10.2217/RME-2022-0161/ASSET/IMAGES/LARGE/FIGURE2.JPEG.

25. Simões, F.C., Cahill, T.J., Kenyon, A., Gavriouchkina, D., Vieira, J.M., Sun, X., Pezzolla, D., Ravaud, C., Masmanian, E., Weinberger, M., et al. (2020). Macrophages directly contribute collagen to scar formation during zebrafish heart regeneration and mouse heart repair. Nat Commun *11*, 600. 10.1038/s41467-019-14263-2.

26. Quijada, P., Trembley, M.A., and Small, E.M. (2020). The Role of the Epicardium during Heart Development and Repair. Circ Res, 377–394. 10.1161/CIRCRESAHA.119.315857.

27. Mahmoud, A.I., O'Meara, C.C., Gemberling, M., Zhao, L., Bryant, D.M., Zheng, R., Gannon, J.B., Cai, L., Choi, W.Y., Egnaczyk, G.F., et al. (2015). Nerves Regulate

Cardiomyocyte Proliferation and Heart Regeneration. Dev Cell *34*, 387–399. 10.1016/j.devcel.2015.06.017.

28. Grande, M.T., and López-Novoa, J.M. (2009). Fibroblast activation and myofibroblast generation in obstructive nephropathy. Nat Rev Nephrol *5*, 319–328. 10.1038/nrneph.2009.74.

29. Zhang, Q., Wang, L., Wang, S., Cheng, H., Xu, L., Pei, G., Wang, Y., Fu, C., Jiang, Y., He, C., et al. (2022). Signaling pathways and targeted therapy for myocardial infarction. Signal Transduct Target Ther *7*, 1–38. 10.1038/s41392-022-00925-z.

30. White, I.A., Gordon, J., Balkan, W., and Hare, J.M. (2015). Sympathetic reinnervation is required for mammalian cardiac regeneration. Circ Res *117*, 990–994. 10.1161/CIRCRESAHA.115.307465.

31. Brandt, E.B., Bashar, S.J., and Mahmoud, A.I. (2019). Stimulating ideas for heart regeneration: the future of nerve-directed heart therapy. Bioelectron Med *5*, 1–8. 10.1186/s42234-019-0024-0.

32. Tan, C.M.J., and Lewandowski, A.J. (2020). The Transitional Heart: From Early Embryonic and Fetal Development to Neonatal Life. Fetal Diagn Ther *47*, 373–386. 10.1159/000501906.

33. Simões, F.C., and Riley, P.R. (2022). Immune cells in cardiac repair and regeneration. Development *149*. 10.1242/DEV.199906.

34. Filosa, A., and Sawamiphak, S. (2021). Heart development and regeneration—a multi-organ effort. FEBS Journal. 10.1111/FEBS.16319.

35. Peiseler, M., and Kubes, P. (2019). More friend than foe: the emerging role of neutrophils in tissue repair. J Clin Invest *129*, 2629. 10.1172/JCI124616.

36. Lafuse, W.P., Wozniak, D.J., and Rajaram, M.V.S. (2021). Role of cardiac macrophages on cardiac inflammation, fibrosis and tissue repair. Cells *10*, 1–27. 10.3390/cells10010051.

37. Alvarez-Argote, S., and O'meara, C.C. (2021). The evolving roles of cardiac macrophages in homeostasis, regeneration, and repair. Int J Mol Sci *22*. 10.3390/ijms22157923.

38. Gao, Y., Qian, N., Xu, J., and Wang, Y. (2021). The Roles of Macrophages in Heart Regeneration and Repair After Injury. Front Cardiovasc Med *8*, 1–10. 10.3389/fcvm.2021.744615.

39. McGrath, K.E., Frame, J.M., and Palis, J. (2015). Early hematopoiesis and macrophage development. Semin Immunol *27*, 379. 10.1016/J.SMIM.2016.03.013.

40. Wynn, T.A., Chawla, A., and Pollard, J.W. (2013). Origins and Hallmarks of Macrophages: Development, Homeostasis, and Disease. Nature *496*, 445. 10.1038/NATURE12034.

41. Bajpai, G., Schneider, C., Wong, N., Bredemeyer, A., Hulsmans, M., Nahrendorf, M., Epelman, S., Kreisel, D., Liu, Y., Itoh, A., et al. (2018). The human heart contains distinct macrophage subsets with divergent origins and functions. Nat Med *24*, 1234–1245. 10.1038/s41591-018-0059-x.

42. Hettinger, J., Richards, D.M., Hansson, J., Barra, M.M., Joschko, A.C., Krijgsveld, J., and Feuerer, M. (2013). Origin of monocytes and macrophages in a committed progenitor. Nature Immunology 2013 14:8 *14*, 821–830. 10.1038/ni.2638.

43. Hoeffel, G., Wang, Y., Greter, M., See, P., Teo, P., Malleret, B., Leboeuf, M., Low, D., Oller, G., Almeida, F., et al. (2012). Adult Langerhans cells derive predominantly from embryonic fetal liver monocytes with a minor contribution of yolk sac–derived macrophages. J Exp Med *209*, 1167. 10.1084/JEM.20120340.

44. Aurora, A.B., Porrello, E.R., Tan, W., Mahmoud, A.I., Hill, J.A., Bassel-Duby, R., Sadek, H.A., and Olson, E.N. (2014). Macrophages are required for neonatal heart regeneration. Journal of Clinical Investigation *124*, 1382–1392. 10.1172/JCI72181.

45. Epelman, S., Lavine, K.J., Beaudin, A.E., Sojka, D.K., Carrero, J.A., Calderon, B., Brija, T., Gautier, E.L., Ivanov, S., Satpathy, A.T., et al. (2014). Embryonic and adult-derived resident cardiac macrophages are maintained through distinct mechanisms at steady state and during inflammation. Immunity *40*, 91–104. 10.1016/j.immuni.2013.11.019.

46. Lavine, K.J., Epelman, S., Uchida, K., Weber, K.J., Nichols, C.G., Schilling, J.D., Ornitz, D.M., Randolph, G.J., and Mann, D.L. (2014). Distinct macrophage lineages contribute to disparate patterns of cardiac recovery and remodeling in the neonatal and adult heart. Proc Natl Acad Sci U S A *111*, 16029–16034. 10.1073/pnas.1406508111.

47. Molawi, K., Wolf, Y., Kandalla, P.K., Favret, J., Hagemeyer, N., Frenzel, K., Pinto, A.R., Klapproth, K., Henri, S., Malissen, B., et al. (2014). Progressive replacement of embryo-derived cardiac macrophages with age. J Exp Med *211*, 2151–2158. 10.1084/JEM.20140639.

48. Traver, D., Paw, B.H., Poss, K.D., Penberthy, W.T., Lin, S., and Zon, L.I. (2003). Transplantation and in vivo imaging of multilineage engraftment in zebrafish bloodless mutants. Nature Immunology 2003 4:12 *4*, 1238–1246. 10.1038/ni1007.

49. Yu, T., Guo, W., Tian, Y., Xu, J., Chen, J., Li, L., and Wen, Z. (2017). Distinct regulatory networks control the development of macrophages of different origins in zebrafish. Blood *129*, 509–519. 10.1182/BLOOD-2016-07-727651.

50. Shiau, C.E., Kaufman, Z., Meireles, A.M., and Talbot, W.S. (2015). Differential Requirement for irf8 in Formation of Embryonic and Adult Macrophages in Zebrafish. PLoS One *10*, e0117513. 10.1371/JOURNAL.PONE.0117513.

51. Lin, X., Wen, Z., and Xu, J. (2019). Tissue-resident macrophages: from zebrafish to mouse. Blood Science *1*, 57. 10.1097/BS9.0000000000000013.

52. Graney, P.L., Ben-Shaul, S., Landau, S., Bajpai, A., Singh, B., Eager, J., Cohen, A., Levenberg, S., and Spiller, K.L. (2020). Macrophages of diverse phenotypes drive vascularization of engineered tissues. Sci Adv *6*. 10.1126/sciadv.aay6391.

53. Krzyszczyk, P., Schloss, R., Palmer, A., and Berthiaume, F. (2018). The role of macrophages in acute and chronic wound healing and interventions to promote pro-wound healing phenotypes. Front Physiol *9*, 419. 10.3389/fphys.2018.00419.

54. Lucas, T., Waisman, A., Ranjan, R., Roes, J., Krieg, T., Müller, W., Roers, A., and Eming, S.A. (2010). Differential Roles of Macrophages in Diverse Phases of Skin Repair. The Journal of Immunology *184*, 3964–3977. 10.4049/jimmunol.0903356.

55. Jimenez, J., and Lavine, K.J. (2022). The Dynamic Role of Cardiac Macrophages in Aging and Disease. Curr Cardiol Rep, 1–9. 10.1007/s11886-022-01714-4.

56. Bohaud, C., Johansen, M.D., Jorgensen, C., Kremer, L., Ipseiz, N., and Djouad, F. (2021). The Role of Macrophages During Mammalian Tissue Remodeling and Regeneration Under Infectious and Non-Infectious Conditions. Front Immunol *12*, 2704. 10.3389/FIMMU.2021.707856/BIBTEX.

57. O'Rourke, S.A., Dunne, A., and Monaghan, M.G. (2019). The Role of Macrophages in the Infarcted Myocardium: Orchestrators of ECM Remodeling. Front Cardiovasc Med *6*, 1–12. 10.3389/fcvm.2019.00101.

58. Morales, R.A., and Allende, M.L. (2019). Peripheral macrophages promote tissue regeneration in zebrafish by fine-tuning the inflammatory response. Front Immunol *10*, 253. 10.3389/FIMMU.2019.00253/FULL.

59. Harwani, S.C. (2018). Macrophages Under Pressure: The Role of Macrophage Polarization in Hypertension. Transl Res *191*, 45. 10.1016/J.TRSL.2017.10.011.

60. Ley, K. (2017). M1 Means Kill; M2 Means Heal. The Journal of Immunology *199*, 2191–2193. 10.4049/jimmunol.1701135.

61. Jetten, N., Verbruggen, S., Gijbels, M.J., Post, M.J., De Winther, M.P.J., and Donners, M.M.P.C. (2014). Anti-inflammatory M2, but not pro-inflammatory M1 macrophages promote angiogenesis in vivo. Angiogenesis *17*, 109–118. 10.1007/s10456-013-9381-6.

62. Lang, R.A., and Bishop, J.M. (1993). Macrophages are required for cell death and tissue remodeling in the developing mouse eye. Cell *74*, 453–462. 10.1016/0092-8674(93)80047-I.

63. DM, M., JP, E., Mosser, D.M., Edwards, J.P., DM, M., and JP, E. (2008). Exploring the full spectrum of macrophage activation. Nat Rev Immunol *8*, 958–969. 10.1038/nri2448.

64. Lamkin, D.M., Ho, H.Y., Ong, T.H., Kawanishi, C.K., Stoffers, V.L., Ahlawat, N., Ma, J.C.Y.Y., Arevalo, J.M.G.G., Cole, S.W., and Sloan, E.K. (2016). $β$-Adrenergic-stimulated macrophages: Comprehensive localization in the M1-M2 spectrum. Brain Behav Immun *57*, 338–346. 10.1016/j.bbi.2016.07.162.

65. Gordon, S., and Plüddemann, A. (2017). Tissue macrophages: Heterogeneity and functions. BMC Biol *15*, 53. 10.1186/s12915-017-0392-4.

66. Gordon, S., Crocker, P.R., Morris, L., Lee, S.H., Perry, V.H., and Hume, D.A. (1986). Localization and function of tissue macrophages. Ciba Found Symp *118*, 54–67. 10.1002/9780470720998.CH5.

67. Wynn, T.A., and Vannella, K.M. (2016). Macrophages in tissue repair, regeneration, and fibrosis. Immunity *44*, 450. 10.1016/J.IMMUNI.2016.02.015.

68. Simões, F.C., Cahill, T.J., Kenyon, A., Gavriouchkina, D., Vieira, J.M., Sun, X., Pezzolla, D., Ravaud, C., Masmanian, E., Weinberger, M., et al. (2020). Macrophages directly contribute collagen to scar formation during zebrafish heart regeneration and mouse heart repair. Nat Commun *11*. 10.1038/S41467-019-14263-2.

69. Bevan, L., Lim, Z.W., Venkatesh, B., Riley, P.R., Martin, P., and Richardson, R.J. (2020). Specific macrophage populations promote both cardiac scar deposition and

subsequent resolution in adult zebrafish. Cardiovasc Res *116*, 1357–1371. 10.1093/CVR/CVZ221.

70. Bajpai, G., Bredemeyer, A., Li, W., Zaitsev, K., Koenig, A.L., Lokshina, I., Mohan, J., Ivey, B., Hsiao, H.M., Weinheimer, C., et al. (2019). Tissue Resident CCR2- and CCR2+ Cardiac Macrophages Differentially Orchestrate Monocyte Recruitment and Fate Specification Following Myocardial Injury. Circ Res *124*, 263–278. 10.1161/CIRCRESAHA.118.314028.

71. Wei, K.-H., Lin, I.-T., Chowdhury, K., Lim, K.L., Liu, K.-T., Ko, T.-M., Chang, Y.-M., Yang, K.-C., and Lai, S.-L. (Ben) (2023). Comparative single-cell profiling reveals distinct cardiac resident macrophages essential for zebrafish heart regeneration. Elife *12*. 10.7554/ELIFE.84679.

72. Dick, S.A., Macklin, J.A., Nejat, S., Momen, A., Clemente-Casares, X., Althagafi, M.G., Chen, J., Kantores, C., Hosseinzadeh, S., Aronoff, L., et al. (2019). Self-renewing resident cardiac macrophages limit adverse remodeling following myocardial infarction. Nat Immunol *20*, 29–39. 10.1038/s41590-018-0272-2.

73. Burgess, M., Wicks, K., Gardasevic, M., and Mace, K.A. (2019). Cx3CR1 Expression Identifies Distinct Macrophage Populations That Contribute Differentially to Inflammation and Repair. Immunohorizons *3*, 262–273. 10.4049/IMMUNOHORIZONS.1900038.

74. Willenborg, S., Lucas, T., Van Loo, G., Knipper, J.A., Krieg, T., Haase, I., Brachvogel, B., Hammerschmidt, M., Nagy, A., Ferrara, N., et al. (2012). CCR2 recruits an inflammatory macrophage subpopulation critical for angiogenesis in tissue repair. Blood *120*, 613–625. 10.1182/blood-2012-01-403386.

75. Bruton, F.A., Kaveh, A., Ross-Stewart, K.M., Matrone, G., Oremek, M.E.M., Solomonidis, E.G., Tucker, C.S., Mullins, J.J., Lucas, C.D., Brittan, M., et al. (2022). Macrophages trigger cardiomyocyte proliferation by increasing epicardial vegfaa expression during larval zebrafish heart regeneration. Dev Cell *57*, 1512-1528.e5. 10.1016/J.DEVCEL.2022.05.014.

76. Van Amerongen, M.J., Harmsen, M.C., Van Rooijen, N., Petersen, A.H., and Van Luyn, M.J.A. (2007). Macrophage Depletion Impairs Wound Healing and Increases Left Ventricular Remodeling after Myocardial Injury in Mice. Am J Pathol *170*, 818. 10.2353/AJPATH.2007.060547.

77. Ong, S.B., Hernández-Reséndiz, S., Crespo-Avilan, G.E., Mukhametshina, R.T., Kwek, X.Y., Cabrera-Fuentes, H.A., and Hausenloy, D.J. (2018). Inflammation following acute myocardial infarction: Multiple players, dynamic roles, and novel therapeutic opportunities. Pharmacol Ther *186*, 73. 10.1016/J.PHARMTHERA.2018.01.001.

78. Yan, X., Anzai, A., Katsumata, Y., Matsuhashi, T., Ito, K., Endo, J., Yamamoto, T., Takeshima, A., Shinmura, K., Shen, W., et al. (2013). Temporal dynamics of cardiac immune cell accumulation following acute myocardial infarction. J Mol Cell Cardiol *62*, 24–35. 10.1016/j.yjmcc.2013.04.023.

79. Ma, Y., Mouton, A.J., and Lindsey, M.L. (2018). Cardiac macrophage biology in the steady-state heart, the aging heart, and following myocardial infarction. Translational Research *191*, 15–28. 10.1016/J.TRSL.2017.10.001.

80. Hilgendorf, I., Gerhardt, L.M.S., Tan, T.C., Winter, C., Holderried, T.A.W., Chousterman, B.G., Iwamoto, Y., Liao, R., Zirlik, A., Scherer-Crosbie, M., et al. (2014). Ly-6 chigh monocytes depend on nr4a1 to balance both inflammatory and reparative phases in the infarcted myocardium. Circ Res *114*, 1611–1622. 10.1161/CIRCRESAHA.114.303204.

81. Peet, C., Ivetic, A., Bromage, D.I., and Shah, A.M. (2020). Cardiac monocytes and macrophages after myocardial infarction. Cardiovasc Res *116*, 1101–1112. 10.1093/CVR/CVZ336.

82. Mentkowski, K.I., Euscher, L.M., Patel, A., Alevriadou, B.R., and Lang, J.K. (2020). Monocyte recruitment and fate specification after myocardial infarction. Am J Physiol Cell Physiol *319*, C797–C806. 10.1152/AJPCELL.00330.2020.

83. Bartekova, M., Radosinska, J., Jelemensky, M., and Dhalla, N.S. (2018). Role of cytokines and inflammation in heart function during health and disease 10.1007/s10741-018-9716-x.

84. Prabhu, S.D. (2021). Healing and repair after myocardial infarction: the forgotten but resurgent basophil. J Clin Invest *131*. 10.1172/JCI150555.

85. Prabhu, S.D., and Frangogiannis, N.G. (2016). The biological basis for cardiac repair after myocardial infarction. Circ Res *119*, 91–112. 10.1161/CIRCRESAHA.116.303577.

86. Haider, N., Boscá, L., Zandbergen, H.R., Kovacic, J.C., Narula, N., González-Ramos, S., Fernandez-Velasco, M., Agrawal, S., Paz-García, M., Gupta, S., et al. (2019). Transition of Macrophages to Fibroblast-Like Cells in Healing Myocardial Infarction. J Am Coll Cardiol *74*, 3124–3135. 10.1016/j.jacc.2019.10.036.

87. Hu, B., Lelek, S., Spanjaard, B., El-Sammak, H., Simões, M.G., Mintcheva, J., Aliee, H., Schäfer, R., Meyer, A.M., Theis, F., et al. (2022). Origin and function of activated fibroblast states during zebrafish heart regeneration. Nat Genet *54*, 1227–1237. 10.1038/S41588-022-01129-5.

88. Derrick, C.J., and Noël, E.S. (2021). The ECM as a driver of heart development and repair. Development *148*. 10.1242/dev.191320.

89. González-Rosa, J.M., Burns, C.E., and Burns, C.G. (2017). Zebrafish heart regeneration: 15 years of discoveries. Regeneration *4*, 105–123. 10.1002/reg2.83.

90. Poss, K.D., Wilson, L.G., and Keating, M.T. (2002). Heart regeneration in zebrafish. Science (1979) *298*, 2188–2190. 10.1126/science.1077857.

91. Wu, C.C., and Weidinger, G. (2014). Zebrafish as a Model for Studying Cardiac Regeneration. Curr Pathobiol Rep *2*, 93–100. 10.1007/s40139-014-0042-2.

92. Beffagna, G. (2019). Zebrafish as a Smart Model to Understand Regeneration After Heart Injury: How Fish Could Help Humans. Front Cardiovasc Med *6*, 1–8. 10.3389/fcvm.2019.00107.

93. Howe, K., Clark, M.D., Torroja, C.F., Torrance, J., Berthelot, C., Muffato, M., Collins, J.E., Humphray, S., McLaren, K., Matthews, L., et al. (2013). The zebrafish reference genome sequence and its relationship to the human genome. Nature *496*, 498–503. 10.1038/nature12111.

94. Pakshir, P., and Hinz, B. (2018). The big five in fibrosis: Macrophages, myofibroblasts, matrix, mechanics, and miscommunication. Matrix Biology *68–69*, 81–93. 10.1016/j.matbio.2018.01.019.

95. Moore, J.P., Vinh, A., Tuck, K.L., Sakkal, S., Krishnan, S.M., Chan, C.T., Lieu, M., Samuel, C.S., Diep, H., Kemp-Harper, B.K., et al. (2015). M2 macrophage accumulation in the aortic wall during angiotensin ii infusion in mice is associated with fibrosis, elastin loss, and elevated blood pressure. Am J Physiol Heart Circ Physiol *309*, H906–H917. 10.1152/ajpheart.00821.2014.

96. Nguyen-Chi, M., Laplace-Builhé, B., Travnickova, J., Luz-Crawford, P., Tejedor, G., Lutfalla, G., Kissa, K., Jorgensen, C., and Djouad, F. (2017). TNF signaling and macrophages govern fin regeneration in zebrafish larvae. Cell Death Dis *8*, e2979. 10.1038/cddis.2017.374.

97. Nguyen-Chi, M., Laplace-Builhe, B., Travnickova, J., Luz-Crawford, P., Tejedor, G., Phan, Q.T., Duroux-Richard, I., Levraud, J.P., Kissa, K., Lutfalla, G., et al. (2015). Identification of polarized macrophage subsets in zebrafish. Elife *4*, 1–14. 10.7554/eLife.07288.

98. Teplyi, V., and Grebchenko, K. (2019). Evaluation of the scars' vascularization using computer processing of the digital images. Skin Res Technol *25*, 194–199. 10.1111/srt.12634.

99. Vannella, K.M., and Wynn, T.A. (2017). Mechanisms of Organ Injury and Repair by Macrophages. Annu Rev Physiol *79*, 593–617. 10.1146/ANNUREV-PHYSIOL-022516-034356.

100. Glinton, K.E., Ma, W., Lantz, C., Grigoryeva, L.S., DeBerge, M., Liu, X., Febbraio, M., Kahn, M., Oliver, G., and Thorp, E.B. (2022). Macrophage-produced VEGFC is induced by efferocytosis to ameliorate cardiac injury and inflammation. J Clin Invest *132*. 10.1172/JCI140685.

101. Gordon, S., and Taylor, P.R. (2005). Monocyte and macrophage heterogeneity. Nature Reviews Immunology 2005 5:12 *5*, 953–964. 10.1038/nri1733.

102. Klotz, L., Norman, S., Vieira, J.M., Masters, M., Rohling, M., Dubé, K.N., Bollini, S., Matsuzaki, F., Carr, C.A., and Riley, P.R. (2015). Cardiac lymphatics are heterogeneous in origin and respond to injury. Nature *522*, 62–67. 10.1038/NATURE14483.

103. Zaman, R., Hamidzada, H., and Epelman, S. (2021). Exploring cardiac macrophage heterogeneity in the healthy and diseased myocardium. Curr Opin Immunol *68*, 54–63. 10.1016/j.coi.2020.09.005.

104. Fleshner, M., and Crane, C.R. (2017). Exosomes, DAMPs and miRNA: Features of Stress Physiology and Immune Homeostasis. Trends Immunol *38*, 768–776. 10.1016/J.IT.2017.08.002.

105. Flink, I.L. (2002). Cell cycle reentry of ventricular and atrial cardiomyocytes and cells within the epicardium following amputation of the ventricular apex in the axolotl, Amblystoma mexicanum: Confocal microscopic immunofluorescent image analysis of bromodeoxyuridine-label. Anat Embryol (Berl) *205*, 235–244. 10.1007/s00429-002-0249-6.

106. Weitkamp, B., Cullen, P., Plenz, G., Robenek, H., and Rauterberg, J. (1999). Human macrophages synthesize type VIII collagen in vitro and in the atherosclerotic plaque. The FASEB Journal *13*, 1445–1457. 10.1096/FASEBJ.13.11.1445.

107. Yamamoto, K., Okano, H., Miyagawa, W., Visse, R., Shitomi, Y., Santamaria, S., Dudhia, J., Troeberg, L., Strickland, D.K., Hirohata, S., et al. (2016). MMP-13 is constitutively produced in human chondrocytes and co-endocytosed with ADAMTS-5 and TIMP-3 by the endocytic receptor LRP1. Matrix Biology *56*, 57–73. https://doi.org/10.1016/j.matbio.2016.03.007.

108. Revuelta-López, E., Soler-Botija, C., Nasarre, L., Benitez-Amaro, A., de Gonzalo-Calvo, D., Bayes-Genis, A., and Llorente-Cortés, V. (2017). Relationship among LRP1 expression, Pyk2 phosphorylation and MMP-9 activation in left ventricular remodelling after myocardial infarction. J Cell Mol Med *21*, 1915–1928. 10.1111/JCMM.13113.

109. Zajac, E., Schweighofer, B., Kupriyanova, T.A., Juncker-Jensen, A., Minder, P., Quigley, J.P., and Deryugina, E.I. (2013). Angiogenic capacity of M1- and M2-polarized macrophages is determined by the levels of TIMP-1 complexed with their secreted proMMP-9. Blood *122*, 4054–4067. 10.1182/BLOOD-2013-05-501494.

110. Whitehead, A.J., and Engler, A.J. (2021). Deconstructing Organs: Single-Cell Analyses, Decellularized Organs, Organoids, and Organ-on-a-Chip Models: Regenerative cross talk between cardiac cells and macrophages. Am J Physiol Heart Circ Physiol *320*, H2211. 10.1152/AJPHEART.00056.2021.

111. Schönborn, K., Willenborg, S., Schulz, J.-N., Imhof, T., Eming, S.A., Quondamatteo, F., Brinckmann, J., Niehoff, A., Paulsson, M., Koch, M., et al. (2020). Role of collagen XII in skin homeostasis and repair. Matrix Biol *94*, 57–76. 10.1016/j.matbio.2020.08.002.

112. Izu, Y., Adams, S.M., Connizzo, B.K., Beason, D.P., Soslowsky, L.J., Koch, M., and Birk, D.E. (2021). Collagen XII mediated cellular and extracellular mechanisms regulate establishment of tendon structure and function. Matrix Biol *95*, 52–67. 10.1016/J.MATBIO.2020.10.004.

113. Wehner, D., Tsarouchas, T.M., Michael, A., Haase, C., Weidinger, G., Reimer, M.M., Becker, T., and Becker, C.G. (2017). Wnt signaling controls pro-regenerative Collagen XII in functional spinal cord regeneration in zebrafish. Nat Commun *8*, 126. 10.1038/s41467-017-00143-0.

114. Alonso-Herranz, L., Sahún-Español, Á., Paredes, A., Gonzalo, P., Gkontra, P., Núñez, V., Clemente, C., Cedenilla, M., Villalba-Orero, M., Inserte, J., et al. (2020). Macrophages promote endothelial-to-mesenchymal transition via MT1-MMP/ TGFβ1 after myocardial infarction. Elife *9*, 1–30. 10.7554/ELIFE.57920.

115. El-Sammak, H., Yang, B., Guenther, S., Chen, W., Marín-Juez, R., and Stainier, D.Y.R. (2022). A Vegfc-Emilin2a-Cxcl8a Signaling Axis Required for Zebrafish Cardiac Regeneration. Circ Res *130*, 1014–1029. 10.1161/CIRCRESAHA.121.319929.

116. Yokota, T., McCourt, J., Ma, F., Ren, S., Li, S., Kim, T.-H., Kurmangaliyev, Y.Z., Nasiri, R., Ahadian, S., Nguyen, T., et al. (2020). Type V Collagen in Scar Tissue Regulates the Size of Scar after Heart Injury. Cell *182*, 545-562.e23. 10.1016/j.cell.2020.06.030.

117. Fantin, A., Vieira, J.M., Gestri, G., Denti, L., Schwarz, Q., Prykhozhij, S., Peri, F., Wilson, S.W., and Ruhrberg, C. (2010). Tissue macrophages act as cellular chaperones for vascular anastomosis downstream of VEGF-mediated endothelial tip cell induction. Blood *116*, 829. 10.1182/BLOOD-2009-12-257832.

118. Yokota, T., McCourt, J., Ma, F., Ren, S., Li, S., Kim, T.H., Kurmangaliyev, Y.Z., Nasiri, R., Ahadian, S., Nguyen, T., et al. (2020). Type V collagen in scar tissue regulates the size of scar after heart injury. Cell *182*, 545. 10.1016/J.CELL.2020.06.030.

119. Lillis, A.P., Van Duyn, L.B., Murphy-Ullrich, J.E., and Strickland, D.K. (2008). LDL receptor-related protein 1: unique tissue-specific functions revealed by selective gene knockout studies. Physiol Rev *88*, 887–918. 10.1152/physrev.00033.2007.

120. Gonias, S.L., and Campana, W.M. (2014). LDL receptor-related protein-1: a regulator of inflammation in atherosclerosis, cancer, and injury to the nervous system. Am J Pathol *184*, 18–27. 10.1016/j.ajpath.2013.08.029.

121. Potere, N., Del Buono, M.G., Mauro, A.G., Abbate, A., and Toldo, S. (2019). Low Density Lipoprotein Receptor-Related Protein-1 in Cardiac Inflammation and Infarct Healing. Front Cardiovasc Med *6*, 51. 10.3389/FCVM.2019.00051.

122. May, P., Bock, H.H., and Nofer, J.R. (2013). Low density receptor-related protein 1 (LRP1) promotes anti-inflammatory phenotype in murine macrophages. Cell Tissue Res *354*, 887–889. 10.1007/S00441-013-1699-2/FIGURES/1.

123. Cabello-Verrugio, C., and Brandan, E. (2007). A novel modulatory mechanism of transforming growth factor-β signaling through decorin and LRP-1. Journal of Biological Chemistry *282*, 18842–18850. 10.1074/jbc.M700243200.

124. Cabello-Verrugio, C., Santander, C., Cofré, C., Acuña, M.J., Melo, F., and Brandan, E. (2012). The Internal Region Leucine-rich Repeat 6 of Decorin Interacts with Low Density Lipoprotein Receptor-related Protein-1, Modulates Transforming Growth Factor (TGF)-β-dependent Signaling, and Inhibits TGF-β-dependent Fibrotic Response in Skeletal Muscles. J Biol Chem *287*, 6773. 10.1074/JBC.M111.312488.

125. Sugimoto, H., Mundel, T.M., Kieran, M.W., and Kalluri, R. (2006). Identification of fibroblast heterogeneity in the tumor microenvironment. Cancer Biol Ther *5*, 1640–1646. 10.4161/cbt.5.12.3354.

126. Driskell, R.R., and Watt, F.M. (2015). Understanding fibroblast heterogeneity in the skin. Trends Cell Biol *25*, 92–99. 10.1016/j.tcb.2014.10.001.

127. Kanisicak, O., Khalil, H., Ivey, M.J., Karch, J., Maliken, B.D., Correll, R.N., Brody, M.J., Lin, S.C.J., Aronow, B.J., Tallquist, M.D., et al. (2016). Genetic lineage tracing defines myofibroblast origin and function in the injured heart. Nature Communications 2016 7:1 *7*, 1–14. 10.1038/ncomms12260.

128. Fu, X., Liu, Q., Li, C., Li, Y., and Wang, L. (2020). Cardiac Fibrosis and Cardiac Fibroblast Lineage-Tracing: Recent Advances. Front Physiol *11*. 10.3389/FPHYS.2020.00416.

129. Chen, W., Bian, W., Zhou, Y., and Zhang, J. (2021). Cardiac Fibroblasts and Myocardial Regeneration. Front Bioeng Biotechnol *9*. 10.3389/FBIOE.2021.599928.

130. Chi, C., and Song, K. (2023). Cellular reprogramming of fibroblasts in heart regeneration. J Mol Cell Cardiol *180*, 84–93. 10.1016/J.YJMCC.2023.03.009.

131. Hortells, L., Johansen, A.K.Z., and Yutzey, K.E. (2019). Cardiac Fibroblasts and the Extracellular Matrix in Regenerative and Nonregenerative Hearts. Journal of Cardiovascular Development and Disease 2019, Vol. 6, Page 29 *6*, 29. 10.3390/JCDD6030029.

132. Van Amerongen, M.J., Bou-Gharios, G., Popa, E.R., Van Ark, J., Petersen, A.H., Van Dam, G.M., Van Luyn, M.J.A., and Harmsen, M.C. (2008). Bone marrow-derived myofibroblasts contribute functionally to scar formation after myocardial infarction. Journal of Pathology *214*, 377–386. 10.1002/path.2281.

133. de Wit, L., Fang, J., Neef, K., Xiao, J., Doevendans, P.A., Schiffelers, R.M., Lei, Z., and Sluijter, J.P.G. (2020). Cellular and Molecular Mechanism of Cardiac Regeneration: A Comparison of Newts, Zebrafish, and Mammals. Biomolecules *10*, 1–20. 10.3390/BIOM10091204.

134. Sánchez-Iranzo, H., Galardi-Castilla, M., Sanz-Morejón, A., González-Rosa, J.M., Costa, R., Ernst, A., de Aja, J.S., Langa, X., and Mercader, N. (2018). Transient fibrosis resolves via fibroblast inactivation in the regenerating zebrafish heart. Proc Natl Acad Sci U S A *115*, 4188–4193. 10.1073/pnas.1716713115.

135. Kim, K.K., Sheppard, D., and Chapman, H.A. (2018). TGF-β1 Signaling and Tissue Fibrosis. Cold Spring Harb Perspect Biol *10*. 10.1101/CSHPERSPECT.A022293.

136. Shull, M.M., Ormsby, I., Kier, A.B., Pawlowski, S., Diebold, R.J., Yin, M., Allen, R., Sidman, C., Proetzel, G., Calvin, D., et al. (1992). Targeted disruption of the mouse transforming growth factor-β1 gene results in multifocal inflammatory disease. Nature *359*, 693. 10.1038/359693A0.

137. Zhang, H., Yang, K., Chen, F., Liu, Q., Ni, J., Cao, W., Hua, Y., He, F., Liu, Z., Li, L., et al. (2022). Role of the CCL2-CCR2 axis in cardiovascular disease: Pathogenesis and clinical implications. Front Immunol *13*. 10.3389/FIMMU.2022.975367.

138. Wenstrup, R.J., Florer, J.B., Brunskill, E.W., Bell, S.M., Chervoneva, I., and Birk, D.E. (2004). Type V collagen controls the initiation of collagen fibril assembly. Journal of Biological Chemistry *279*, 53331–53337. 10.1074/jbc.M409622200.

139. Pöschl, E., Schlötzer-Schrehardt, U., Brachvogel, B., Saito, K., Ninomiya, Y., and Mayer, U. (2004). Collagen IV is essential for basement membrane stability but dispensable for initiation of its assembly during early development. Development *131*, 1619–1628. 10.1242/DEV.01037.

140. Majaj, M., and Weckbach, L.T. (2022). Midkine—A novel player in cardiovascular diseases. Front Cardiovasc Med *9*, 1003104. 10.3389/FCVM.2022.1003104/BIBTEX.

141. Sato, W., Kadomatsu, K., Yuzawa, Y., Muramatsu, H., Hotta, N., Matsuo, S., and Muramatsu, T. (2001). Midkine Is Involved in Neutrophil Infiltration into the Tubulointerstitium in Ischemic Renal Injury. The Journal of Immunology *167*, 3463–3469. 10.4049/JIMMUNOL.167.6.3463.

142. Silva, A.C., Pereira, C., Fonseca, A.C.R.G., Pinto-do-Ó, P., and Nascimento, D.S. (2021). Bearing My Heart: The Role of Extracellular Matrix on Cardiac Development, Homeostasis, and Injury Response. Front Cell Dev Biol *8*, 621644. 10.3389/FCELL.2020.621644/BIBTEX.

143. González-Rosa, J.M., Martín, V., Peralta, M., Torres, M., and Mercader, N. (2011). Extensive scar formation and regression during heart regeneration after cryoinjury in zebrafish. Development *138*, 1663–1674. 10.1242/dev.060897.

144. Hasan, W. (2013). Autonomic cardiac innervation: Development and adult plasticity. Organogenesis *9*, 176–193. 10.4161/org.24892.

145. Kanazawa, H., and Fukuda, K. (2022). The plasticity of cardiac sympathetic nerves and its clinical implication in cardiovascular disease. Front Synaptic Neurosci *14*, 960606. 10.3389/FNSYN.2022.960606/BIBTEX.

146. Young, H.M., Cane, K.N., and Anderson, C.R. (2011). Development of the autonomic nervous system: A comparative view. Auton Neurosci *165*, 10–27. 10.1016/J.AUTNEU.2010.03.002.

147. Kalueff, A. V., Stewart, A.M., and Gerlai, R. (2014). Zebrafish as an emerging model for studying complex brain disorders. Trends Pharmacol Sci *35*, 63. 10.1016/J.TIPS.2013.12.002.

148. Panula, P., Chen, Y.C., Priyadarshini, M., Kudo, H., Semenova, S., Sundvik, M., and Sallinen, V. (2010). The comparative neuroanatomy and neurochemistry of zebrafish CNS systems of relevance to human neuropsychiatric diseases. Neurobiol Dis *40*, 46–57. 10.1016/J.NBD.2010.05.010.

149. Lymperopoulos, A., Cora, N., Maning, J., Brill, A.R., and Sizova, A. (2021). Signaling and function of cardiac autonomic nervous system receptors: Insights from the GPCR signalling universe. FEBS J *288*, 2645–2659. 10.1111/FEBS.15771.

150. Foster, S.R., Roura, E., Molenaar, P., and Thomas, W.G. (2015). G protein-coupled receptors in cardiac biology: old and new receptors. Biophys Rev *7*, 77. 10.1007/S12551-014-0154-2.

151. Ciccarelli, M., Sorriento, D., Coscioni, E., Iaccarino, G., and Santulli, G. (2017). Adrenergic Receptors. Endocrinology of the Heart in Health and Disease: Integrated, Cellular, and Molecular Endocrinology of the Heart, 285–315. 10.1016/B978-0-12-803111-7.00011-7.

152. Chhatar, S., and Lal, G. (2021). Role of adrenergic receptor signalling in neuroimmune communication. Current Research in Immunology *2*, 202. 10.1016/J.CRIMMU.2021.11.001.

153. Hanlon, C.D., and Andrew, D.J. (2015). Outside-in signaling - A brief review of GPCR signaling with a focus on the Drosophila GPCR family. J Cell Sci *128*, 3533–3542. 10.1242/JCS.175158/-/DC1.

154. Ang, R., Opel, A., and Tinker, A. (2012). The Role of Inhibitory G Proteins and Regulators of G Protein Signaling in the in vivo Control of Heart Rate and Predisposition to Cardiac Arrhythmias. Front Physiol *3*. 10.3389/FPHYS.2012.00096.

155. Saternos, H.C., Almarghalani, D.A., Gibson, H.M., Meqdad, M.A., Antypas, R.B., Lingireddy, A., and Aboualaiwi, W.A. (2018). Distribution and function of the muscarinic receptor subtypes in the cardiovascular system. Physiol Genomics *50*, 1–9. 10.1152/PHYSIOLGENOMICS.00062.2017/ASSET/IMAGES/LARGE/ZH70121742170002.JPEG.

156. Naga, V., Garikipati, S., Verma, S., and Kishore, R. The Nervous Heart: Role of Sympathetic Re-innervation in Cardiac Regeneration. 10.1161/CIRCRESAHA.115.307637.

157. Fujiu, K., and Manabe, I. (2022). Nerve-macrophage interactions in cardiovascular disease. Int Immunol *34*, 81–95. 10.1093/intimm/dxab036.

158. Joven, A., and Simon, A. (2018). Homeostatic and regenerative neurogenesis in salamanders. Prog Neurobiol *170*, 81–98. 10.1016/J.PNEUROBIO.2018.04.006.

159. Chavan, S.S., Pavlov, V.A., and Tracey, K.J. (2017). Mechanisms and Therapeutic Relevance of Neuro-immune Communication. Immunity *46*, 927–942. 10.1016/j.immuni.2017.06.008.

160. de Jonge, W.J. (2015). Neuronal Regulation of Mucosal Immune Responses. Mucosal Immunology: Fourth Edition *1–2*, 929–942. 10.1016/B978-0-12-415847-4.00046-X.

161. Pavlov, V.A., Chavan, S.S., and Tracey, K.J. (2018). Molecular and Functional Neuroscience in Immunity. Annu Rev Immunol *36*, 783–812. 10.1146/annurev-immunol-042617-053158.

162. Fonseca, F.A., and Izar, M.C. (2022). Role of Inflammation in Cardiac Remodeling After Acute Myocardial Infarction. Front Physiol *13*. 10.3389/FPHYS.2022.927163.

163. Scanzano, A., and Cosentino, M. (2015). Adrenergic regulation of innate immunity: A review. Front Pharmacol *6*, 171. 10.3389/fphar.2015.00171.

164. Sharma, D., and Farrar, J.D. (2020). Adrenergic regulation of immune cell function and inflammation. Semin Immunopathol *42*, 709–717. 10.1007/s00281-020-00829-6.

165. Woodcock, E.A., Du, X.J., Reichelt, M.E., and Graham, R.M. (2008). Cardiac α1-adrenergic drive in pathological remodelling. Cardiovasc Res *77*, 452–462. 10.1093/cvr/cvm078.

166. Freire, B.M., De Melo, F.M., and Basso, A.S. (2022). Adrenergic signaling regulation of macrophage function: do we understand it yet? Immunotherapy Advances *2*, 1–12. 10.1093/IMMADV/LTAC010.

167. Grisanti, L.A., Woster, A.P., Dahlman, J., Sauter, E.R., Combs, C.K., and Porter, J.E. (2011). α1-Adrenergic Receptors Positively Regulate Toll-Like Receptor Cytokine Production from Human Monocytes and Macrophages. J Pharmacol Exp Ther *338*, 648. 10.1124/JPET.110.178012.

168. Fujii, T., Mashimo, M., Moriwaki, Y., Misawa, H., Ono, S., Horiguchi, K., and Kawashima, K. (2017). Physiological functions of the cholinergic system in immune cells. J Pharmacol Sci *134*, 1–21. 10.1016/j.jphs.2017.05.002.

169. Di Lascio, S., Fornasari, D., and Benfante, R. (2022). The Human-Restricted Isoform of the α7 nAChR, CHRFAM7A: A Double-Edged Sword in Neurological and Inflammatory Disorders. Int J Mol Sci *23*. 10.3390/IJMS23073463.

170. Delgado-Vélez, M., and Lasalde-Dominicci, J.A. (2018). The Cholinergic Anti-Inflammatory Response and the Role of Macrophages in HIV-Induced Inflammation. Int J Mol Sci *19*. 10.3390/IJMS19051473.

171. Kelly, M.J., Breathnach, C., Tracey, K.J., and Donnelly, S.C. (2022). Manipulation of the inflammatory reflex as a therapeutic strategy. Cell Rep Med *3*. 10.1016/J.XCRM.2022.100696.

172. Tanaka, S., Abe, C., Abbott, S.B.G., Zheng, S., Yamaoka, Y., Lipsey, J.E., Skrypnyk, N.I., Yao, J., Inoue, T., Nash, W.T., et al. (2021). Vagus nerve stimulation activates two distinct neuroimmune circuits converging in the spleen to protect mice from kidney injury. Proc Natl Acad Sci U S A *118*. 10.1073/PNAS.2021758118/-/DCSUPPLEMENTAL.

173. Zumerle, S., Calì, B., Munari, F., Angioni, R., Di Virgilio, F., Molon, B., and Viola, A. (2019). Intercellular Calcium Signaling Induced by ATP Potentiates Macrophage Phagocytosis. Cell Rep *27*, 1-10.e4. 10.1016/J.CELREP.2019.03.011.

174. Zhu, L., Jones, C., and Zhang, G. (2018). The Role of Phospholipase C Signaling in Macrophage-Mediated Inflammatory Response. J Immunol Res *2018*. 10.1155/2018/5201759.

175. Desai, B.N., and Leitinger, N. (2014). Purinergic and Calcium Signaling in Macrophage Function and Plasticity. Front Immunol *5*. 10.3389/FIMMU.2014.00580.

176. Poon, K.L., and Brand, T. (2013). The zebrafish model system in cardiovascular research: A tiny fish with mighty prospects. Glob Cardiol Sci Pract *2013*, 4. 10.5339/gcsp.2013.4.

177. Teame, T., Zhang, Z., Ran, C., Zhang, H., Yang, Y., Ding, Q., Xie, M., Gao, C., Ye, Y., Duan, M., et al. (2019). The use of zebrafish (Danio rerio) as biomedical models. Animal Frontiers *9*, 68–77. 10.1093/af/vfz020.

178. Martins, R.R., Ellis, P.S., MacDonald, R.B., Richardson, R.J., and Henriques, C.M. (2019). Resident Immunity in Tissue Repair and Maintenance: The Zebrafish Model Coming of Age. Front Cell Dev Biol *7*, 12. 10.3389/fcell.2019.00012.

179. Kikuchi, K., Holdway, J.E., Werdich, A.A., Anderson, R.M., Fang, Y., Egnaczyk, G.F., Evans, T., MacRae, C.A., Stainier, D.Y.R., and Poss, K.D. (2010). Primary contribution to zebrafish heart regeneration by gata4(+) cardiomyocytes. Nature *464*, 601–605. 10.1038/NATURE08804.

180. Sánchez-Iranzo, H., Galardi-Castilla, M., Minguillón, C., Sanz-Morejón, A., González-Rosa, J.M., Felker, A., Ernst, A., Guzmán-Martínez, G., Mosimann, C., and Mercader, N. (2018). Tbx5a lineage tracing shows cardiomyocyte plasticity during zebrafish heart regeneration. Nature Communications 2018 9:1 *9*, 1–13. 10.1038/s41467-017-02650-6.

181. Schindler, Y.L., Garske, K.M., Wang, J., Firulli, B.A., Firulli, A.B., Poss, K.D., and Yelon, D. (2014). Hand2 elevates cardiomyocyte production during zebrafish heart development and regeneration. Development (Cambridge) *141*, 3112–3122. 10.1242/DEV.106336/-/DC1.

182. Jopling, C., Sleep, E., Raya, M., Martí, M., Raya, A., and Belmonte, J.C.I. (2010). Zebrafish heart regeneration occurs by cardiomyocyte dedifferentiation and proliferation. Nature *464*, 606. 10.1038/NATURE08899.

183. Lai, S.L., Marín-Juez, R., and Stainier, D.Y.R. (2019). Immune responses in cardiac repair and regeneration: a comparative point of view. Cell Mol Life Sci *76*, 1365–1380. 10.1007/S00018-018-2995-5.

184. Lai, S.L., Marín-Juez, R., Moura, P.L., Kuenne, C., Lai, J.K.H., Tsedeke, A.T., Guenther, S., Looso, M., and Stainier, D.Y.R. (2017). Reciprocal analyses in zebrafish and medaka reveal that harnessing the immune response promotes cardiac regeneration. Elife *6*, 1–20. 10.7554/eLife.25605.

185. Huang, W.C., Yang, C.C., Chen, I.H., Liu, Y.M.L., Chang, S.J., and Chuang, Y.J. (2013). Treatment of Glucocorticoids Inhibited Early Immune Responses and Impaired Cardiac Repair in Adult Zebrafish. PLoS One *8*, e66613. 10.1371/JOURNAL.PONE.0066613.

186. Schindelin, J., Arganda-Carreras, I., Frise, E., Kaynig, V., Longair, M., Pietzsch, T., Preibisch, S., Rueden, C., Saalfeld, S., Schmid, B., et al. (2012). Fiji: an open-source platform for biological-image analysis. Nat Methods *9*, 676–682. 10.1038/nmeth.2019.

187. Apaydin, D.C., Jaramillo, P.A.M.M., Corradi, L., Cosco, F., Rathjen, F.G., Kammertoens, T., Filosa, A., and Sawamiphak, S. (2020). Early-Life Stress Regulates Cardiac Development through an IL-4-Glucocorticoid Signaling Balance. Cell Rep *33*, 108404. 10.1016/j.celrep.2020.108404.

188. Luttrell, L.M., Ostrowski, J., Cotecchia, S., Kendall, H., and Lefkowitz, R.J. (1993). Antagonism of catecholamine receptor signaling by expression of cytoplasmic domains of the receptors. Science (1979) *259*, 1453–1457. 10.1126/science.8383880.

189. Wang, X., Zeng, W., Syombo, A.A., Tang, W., Ross, E.M., Barnes, A.P., Milgram, S.L., Penninger, J.M., Allen, P.B., Greengard, P., et al. (2005). Spinophilin regulates Ca2+ signalling by binding the N-terminal domain of RGS2 and the third intracellular loop of G-protein-coupled receptors. Nat Cell Biol *7*, 405–411. 10.1038/ncb1237.

190. Hague, C., Bernstein, L.S., Ramineni, S., Chen, Z., Minneman, K.P., and Hepler, J.R. (2005). Selective inhibition of α1A-adrenergic receptor signaling by RGS2 association with the receptor third intracellular loop. Journal of Biological Chemistry *280*, 27289–27295. 10.1074/jbc.M502365200.

191. Kjelsberg, M.A., Cotecchia, S., Ostrowski, J., Caron, M.G., and Lefkowitz, R.J. (1992). Constitutive activation of the alpha 1B-adrenergic receptor by all amino acid substitutions at a single site. Evidence for a region which constrains receptor activation. Journal of Biological Chemistry *267*, 1430–1433. 10.1016/S0021-9258(18)45962-5.

192. Scheer, A., Fanelli, F., Costa, T., De Benedetti, P.G., and Cotecchia, S. (1996). Constitutively active mutants of the α(1B)-adrenergic receptor: Role of highly conserved polar amino acids in receptor activation. EMBO Journal *15*, 3566–3578. 10.1002/j.1460-2075.1996.tb00726.x.

193. Ahles, A., and Engelhardt, S. (2014). Polymorphic variants of adrenoceptors: pharmacology, physiology, and role in disease. Pharmacol Rev *66*, 598–637. 10.1124/pr.113.008219.

194. Wu, C.C., Kruse, F., Vasudevarao, M.D., Junker, J.P., Zebrowski, D.C., Fischer, K., Noël, E.S., Grün, D., Berezikov, E., Engel, F.B., et al. (2016). Spatially Resolved Genome-wide Transcriptional Profiling Identifies BMP Signaling as Essential Regulator of Zebrafish Cardiomyocyte Regeneration. Dev Cell *36*, 36–49. 10.1016/j.devcel.2015.12.010.

195. Nieto-Arellano, R., and Sánchez-Iranzo, H. (2019). ZfRegeneration: A database for gene expression profiling during regeneration. Bioinformatics *35*, 703–705. 10.1093/bioinformatics/bty659.

196. Wang, T., Qin, Y., Lai, H., Wei, W., Li, Z., Yang, Y., Huang, M., and Chen, J. (2019). The prognostic value of ADRA1 subfamily genes in gastric carcinoma. Oncol Lett *18*, 3150–3158. 10.3892/ol.2019.10660.

197. Nakai Junichi , Ohkura Masamichi & Imoto Keiji, A. (2001). The measurement of intracellular Ca 2+ concentration, [Ca 2+] i. Nat Biotechnol *19*, 137–141.

198. Nowbar, A.N., Gitto, M., Howard, J.P., Francis, D.P., and Al-Lamee, R. (2019). Mortality From Ischemic Heart Disease. Circ Cardiovasc Qual Outcomes *12*. 10.1161/CIRCOUTCOMES.118.005375.

199. Nowbar, A.N., Gitto, M., Howard, J.P., Francis, D.P., and Al-Lamee, R. (2019). Mortality from ischemic heart disease: Analysis of data from the world health organization and coronary artery disease risk factors from NCD risk factor collaboration. Circ Cardiovasc Qual Outcomes *12*. 10.1161/CIRCOUTCOMES.118.005375.

200. Ryan, R., Moyse, B.R., and Richardson, R.J. (2020). Zebrafish cardiac regeneration—looking beyond cardiomyocytes to a complex microenvironment. Histochem Cell Biol *154*, 533–548. 10.1007/S00418-020-01913-6.

201. He, L., Nguyen, N.B., Ardehali, R., and Zhou, B. (2020). Heart Regeneration by Endogenous Stem Cells and Cardiomyocyte Proliferation. Circulation *142*, 275–291. 10.1161/CIRCULATIONAHA.119.045566.

202. He, L., Nguyen, N.B., Ardehali, R., and Zhou, B. (2020). Heart regeneration by endogenous stem cells and cardiomyocyte proliferation: Controversy, fallacy, and progress. Circulation *142*, 275–291. 10.1161/CIRCULATIONAHA.119.045566.

203. Becker, R.O., Chapin, S., and Sherry, R. (1974). Regeneration of the ventricular myocardium in amphibians. Nature 1974 248:5444 *248*, 145–147. 10.1038/248145a0.

204. Olofsson, P.S., Rosas-Ballina, M., Levine, Y.A., and Tracey, K.J. (2012). Rethinking inflammation: Neural circuits in the regulation of immunity. Immunol Rev *248*, 188–204. 10.1111/j.1600-065X.2012.01138.x.

205. Wilund, K.R., Rosenblat, M., Chung, H.R., Volkova, N., Kaplan, M., Woods, J.A., and Aviram, M. (2009). Macrophages from alpha 7 nicotinic acetylcholine receptor knockout mice demonstrate increased cholesterol accumulation and decreased cellular paraoxonase expression: A possible link between the nervous system and atherosclerosis development. Biochem Biophys Res Commun *390*, 148–154. 10.1016/J.BBRC.2009.09.088.

206. Tzahor, E., and Dimmeler, S. (2022). A coalition to heal-the impact of the cardiac microenvironment. Science *377*, eabm4443. 10.1126/science.abm4443.

207. Padro, C.J., and Sanders, V.M. (2014). Neuroendocrine regulation of inflammation. Semin Immunol *26*, 357–368. 10.1016/J.SMIM.2014.01.003.

208. Carnevale, D., and Lembo, G. (2021). Neuroimmune interactions in cardiovascular diseases. Cardiovasc Res *117*, 402–410. 10.1093/cvr/cvaa151.

209. Godinho-Silva, C., Cardoso, F., and Veiga-Fernandes, H. (2019). Neuro–Immune Cell Units: A New Paradigm in Physiology. Annu Rev Immunol *37*, 19–46. 10.1146/annurev-immunol-042718-041812.

210. Chrousos, G.P. (2009). Stress and disorders of the stress system. Nature Reviews Endocrinology 2009 5:7 *5*, 374–381. 10.1038/nrendo.2009.106.

211. Wendelaar Bonga, S.E. (1997). The stress response in fish. Physiol Rev *77*, 591–625. 10.1152/physrev.1997.77.3.591.

212. Brotman, D.J., Golden, S.H., and Wittstein, I.S. (2007). The cardiovascular toll of stress. Lancet *370*, 1089–1100. 10.1016/S0140-6736(07)61305-1.

213. Chrousos, G.P., and Gold, P.W. (1992). The Concepts of Stress and Stress System Disorders: Overview of Physical and Behavioral Homeostasis. JAMA: The Journal of the American Medical Association *267*, 1244–1252. 10.1001/jama.1992.03480090092034.

214. Casaletto, K.B., Staffaroni, A.M., Elahi, F., Fox, E., Crittenden, P.A., You, M., Neuhaus, J., Glymour, M., Bettcher, B.M., Yaffe, K., et al. (2018). Perceived Stress is associated with Accelerated Monocyte/Macrophage Aging Trajectories in Clinically Normal Adults. Am J Geriatr Psychiatry *26*, 952. 10.1016/J.JAGP.2018.05.004.

215. Viola, A., Munari, F., Sánchez-Rodríguez, R., Scolaro, T., and Castegna, A. (2019). The metabolic signature of macrophage responses. Front Immunol *10*, 466337. 10.3389/FIMMU.2019.01462/BIBTEX.

216. Barrett, T.J., Corr, E.M., van Solingen, C., Schlamp, F., Brown, E.J., Koelwyn, G.J., Lee, A.H., Shanley, L.C., Spruill, T.M., Bozal, F., et al. (2021). Chronic stress primes innate immune responses in mice and humans. Cell Rep *36*, 109595. 10.1016/J.CELREP.2021.109595.

217. Tymen, S.D., Rojas, I.G., Zhou, X., Fang, Z.J., Zhao, Y., and Marucha, P.T. (2013). Restraint stress alters neutrophil and macrophage phenotypes during wound healing. Brain Behav Immun *28*, 207–217. 10.1016/J.BBI.2012.07.013.

218. Andersson, U., and Tracey, K.J. (2012). Reflex principles of immunological homeostasis. Annu Rev Immunol *30*, 313–335. 10.1146/annurev-immunol-020711-075015.

219. Ordovas-Montanes, J., Rakoff-Nahoum, S., Huang, S., Riol-Blanco, L., Barreiro, O., and von Andrian, U.H. (2015). The Regulation of Immunological Processes by Peripheral Neurons in Homeostasis and Disease. Trends Immunol *36*, 578. 10.1016/J.IT.2015.08.007.

220. Gold, R., Archelos, J.J., and Hartung, H.P. (1999). Mechanisms of Immune Regulation in the Peripheral Nervous System. Brain Pathology *9*, 343. 10.1111/J.1750-3639.1999.TB00231.X.

221. Zhou, Z., Zhan, J., Luo, Q., Hou, X., Wang, S., Xiao, D., Xie, Z., Liang, H., Lin, S., and Zheng, M. (2022). ADRB3 induces mobilization and inhibits differentiation of both breast cancer cells and myeloid-derived suppressor cells. Cell Death & Disease 2022 13:2 *13*, 1–10. 10.1038/s41419-022-04603-4.

222. Liu, X.J., Zhang, Y., Liu, T., Xu, Z.Z., Park, C.K., Berta, T., Jiang, D., and Ji, R.R. (2014). Nociceptive neurons regulate innate and adaptive immunity and neuropathic

pain through MyD88 adapter. Cell Research 2014 24:11 *24*, 1374–1377. 10.1038/cr.2014.106.

223. Hanke, M.L., and Kielian, T. (2011). Toll-like receptors in health and disease in the brain: mechanisms and therapeutic potential. Clin Sci (Lond) *121*, 367. 10.1042/CS20110164.

224. Xiong, X.-Y.Y., Liu, L., Wang, F.-X.X., Yang, Y.-R.R., Hao, J.-W.W., Wang, P.-F.F., Zhong, Q., Zhou, K., Xiong, A., Zhu, W.-Y.Y., et al. (2016). Toll-Like Receptor 4/MyD88-Mediated Signaling of Hepcidin Expression Causing Brain Iron Accumulation, Oxidative Injury, and Cognitive Impairment after Intracerebral Hemorrhage. Circulation *134*, 1025–1038. 10.1161/CIRCULATIONAHA.116.021881.

225. Tracey, K.J. (2002). The inflammatory reflex. Nature *420*, 853–859. 10.1038/nature01321.

226. Nakamura, Y., Matsumoto, H., Wu, C.H., Fukaya, D., Uni, R., Hirakawa, Y., Katagiri, M., Yamada, S., Ko, T., Nomura, S., et al. (2023). Alpha 7 nicotinic acetylcholine receptors signaling boosts cell-cell interactions in macrophages effecting anti-inflammatory and organ protection. Communications Biology 2023 6:1 *6*, 1–15. 10.1038/s42003-023-05051-2.

227. Pavlov, V.A., Ochani, M., Gallowitsch-Puerta, M., Ochani, K., Huston, J.M., Czura, C.J., Al-Abed, Y., and Tracey, K.J. (2006). Central muscarinic cholinergic regulation of the systemic inflammatory response during endotoxemia. Proc Natl Acad Sci U S A *103*, 5219. 10.1073/PNAS.0600506103.

228. Yamada, M., and Ichinose, M. (2018). The cholinergic anti-inflammatory pathway: an innovative treatment strategy for respiratory diseases and their comorbidities. Curr Opin Pharmacol *40*, 18–25. 10.1016/J.COPH.2017.12.003.

229. Olofsson, P.S., Katz, D.A., Rosas-Ballina, M., Levine, Y.A., Ochani, M., Valdés-Ferrer, S.I., Pavlov, V.A., Tracey, K.J., and Chavan, S.S. (2012). α7 nicotinic acetylcholine receptor (α7nAChR) expression in bone marrow-derived non-T cells is required for the inflammatory reflex. Mol Med *18*, 539–543. 10.2119/molmed.2011.00405.

230. Sakabe, M., Thompson, M., Chen, N., Verba, M., Hassan, A., Lu, R., and Xin, M. (2022). Inhibition of β1-AR/Gαs signaling promotes cardiomyocyte proliferation in juvenile mice through activation of RhoAYAP axis. Elife *11*. 10.7554/ELIFE.74576.

231. Leor, J., Palevski, D., Amit, U., and Konfino, T. (2016). Macrophages and regeneration: Lessons from the heart. Semin Cell Dev Biol *58*, 26–33. 10.1016/J.SEMCDB.2016.04.012.

232. Honold, L., and Nahrendorf, M. (2018). Resident and Monocyte-Derived Macrophages in Cardiovascular Disease. Circ Res *122*, 113–127. 10.1161/CIRCRESAHA.117.311071.

233. Pelegrin, P., and Surprenant, A. (2009). Dynamics of macrophage polarization reveal new mechanism to inhibit IL-1β release through pyrophosphates. EMBO J *28*, 2114–2127. https://doi.org/10.1038/emboj.2009.163.

234. Nahrendorf, M., Swirski, F.K., Aikawa, E., Stangenberg, L., Wurdinger, T., Figueiredo, J.L., Libby, P., Weissleder, R., and Pittet, M.J. (2007). The healing myocardium sequentially mobilizes two monocyte subsets with divergent and complementary functions. Journal of Experimental Medicine *204*, 3037–3047. 10.1084/jem.20070885.

235. Sager, H.B., Hulsmans, M., Lavine, K.J., Moreira, M.B., Heidt, T., Courties, G., Sun, Y., Iwamoto, Y., Tricot, B., Khan, O.F., et al. (2016). Proliferation and Recruitment Contribute to Myocardial Macrophage Expansion in Chronic Heart Failure. Circ Res *119*, 853–864. 10.1161/CIRCRESAHA.116.309001/-/DC1.

236. Grisanti, L.A., Traynham, C.J., Repas, A.A., Gao, E., Koch, W.J., and Tilley, D.G. (2016). β2-Adrenergic receptor-dependent chemokine receptor 2 expression regulates leukocyte recruitment to the heart following acute injury. Proc Natl Acad Sci U S A *113*, 15126–15131. 10.1073/PNAS.1611023114/-/DCSUPPLEMENTAL.

237. Tanner, M.A., Maitz, C.A., and Grisanti, L.A. (2021). Immune cell b2-adrenergic receptors contribute to the development of heart failure. Am J Physiol Heart Circ Physiol *321*, H633–H649. 10.1152/AJPHEART.00243.2021/ASSET/IMAGES/LARGE/AJPHEART.00243.2021_F008.JPEG.

238. Vu, T.V.A., Lorizio, D., Vuerich, R., Lippi, M., Nascimento, D.S., and Zacchigna, S. (2022). Extracellular Matrix-Based Approaches in Cardiac Regeneration: Challenges and Opportunities. International Journal of Molecular Sciences 2022, Vol. 23, Page 15783 *23*, 15783. 10.3390/IJMS232415783.

239. Wang, J., Karra, R., Dickson, A.L., and Poss, K.D. (2013). Fibronectin is deposited by injury-activated epicardial cells and is necessary for zebrafish heart regeneration. Dev Biol *382*, 427–435. 10.1016/J.YDBIO.2013.08.012.

240. Chanthra, N., Abe, T., Miyamoto, M., Sekiguchi, K., Kwon, C., Hanazono, Y., and Uosaki, H. (2020). A Novel Fluorescent Reporter System Identifies Laminin-511/521 as Potent Regulators of Cardiomyocyte Maturation. Scientific Reports 2020 10:1 *10*, 1–13. 10.1038/s41598-020-61163-3.

241. Chute, M., Aujla, P., Jana, S., and Kassiri, Z. (2019). The Non-Fibrillar Side of Fibrosis: Contribution of the Basement Membrane, Proteoglycans, and Glycoproteins to Myocardial Fibrosis. J Cardiovasc Dev Dis *6*. 10.3390/JCDD6040035.

242. Murtha, L.A., Schuliga, M.J., Mabotuwana, N.S., Hardy, S.A., Waters, D.W., Burgess, J.K., Knight, D.A., and Boyle, A.J. (2017). The Processes and Mechanisms of Cardiac and Pulmonary Fibrosis. Front Physiol *8*, 777. 10.3389/FPHYS.2017.00777.

243. Xue, M., and Jackson, C.J. (2015). Extracellular Matrix Reorganization During Wound Healing and Its Impact on Abnormal Scarring. Adv Wound Care (New Rochelle) *4*, 119. 10.1089/WOUND.2013.0485.

244. Wight, T.N., and Potter-Perigo, S. (2011). The extracellular matrix: an active or passive player in fibrosis? Am J Physiol Gastrointest Liver Physiol *301*, G950. 10.1152/AJPGI.00132.2011.

245. Engler, A.J., Carag-Krieger, C., Johnson, C.P., Raab, M., Tang, H.Y., Speicher, D.W., Sanger, J.W., Sanger, J.M., and Discher, D.E. (2008). Embryonic cardiomyocytes beat best on a matrix with heart-like elasticity: scar-like rigidity inhibits beating. J Cell Sci *121*, 3794. 10.1242/JCS.029678.

246. Richardson, W.J., Clarke, S.A., Alexander Quinn, T., and Holmes, J.W. (2015). Physiological Implications of Myocardial Scar Structure. Compr Physiol *5*, 1877. 10.1002/CPHY.C140067.

247. Zhao, W., Lu, L., Chen, S.S., and Sun, Y. (2004). Temporal and spatial characteristics of apoptosis in the infarcted rat heart. Biochem Biophys Res Commun *325*, 605–611. 10.1016/J.BBRC.2004.10.064.

248. Kühn, B., Del Monte, F., Hajjar, R.J., Chang, Y.S., Lebeche, D., Arab, S., and Keating, M.T. (2007). Periostin induces proliferation of differentiated cardiomyocytes and promotes cardiac repair. Nature Medicine 2007 13:8 *13*, 962–969. 10.1038/nm1619.

249. Lockhart, M., Wirrig, E., Phelps, A., and Wessels, A. (2011). Extracellular Matrix and Heart Development. Birth Defects Res A Clin Mol Teratol *91*, 535. 10.1002/BDRA.20810.

250. Bassat, E., Mutlak, Y.E., Genzelinakh, A., Shadrin, I.Y., Baruch Umansky, K., Yifa, O., Kain, D., Rajchman, D., Leach, J., Riabov Bassat, D., et al. (2017). The extracellular matrix protein agrin promotes heart regeneration in mice. Nature *547*, 179. 10.1038/NATURE22978.

251. Song, R., and Zhang, L. (2020). Cardiac ECM: Its Epigenetic Regulation and Role in Heart Development and Repair. Int J Mol Sci *21*, 1–20. 10.3390/IJMS21228610.

252. Männer, J., and Yelbuz, T.M. (2019). Functional Morphology of the Cardiac Jelly in the Tubular Heart of Vertebrate Embryos. J Cardiovasc Dev Dis *6*. 10.3390/JCDD6010012.

253. Kular, J.K., Basu, S., and Sharma, R.I. (2014). The extracellular matrix: Structure, composition, age-related differences, tools for analysis and applications for tissue engineering. J Tissue Eng *5*. 10.1177/2041731414557112.

254. Frantz, C., Stewart, K.M., and Weaver, V.M. (2010). The extracellular matrix at a glance. J Cell Sci *123*, 4195. 10.1242/JCS.023820.

255. Singh, D., Rai, V., and Agrawal, D.K. (2023). Regulation of Collagen I and Collagen III in Tissue Injury and Regeneration. Cardiol Cardiovasc Med *7*, 5. 10.26502/FCCM.92920302.

256. Hong, J., Chu, M., Qian, L., Wang, J., Guo, Y., and Xu, D. (2017). Fibrillar Type I Collagen Enhances the Differentiation and Proliferation of Myofibroblasts by Lowering α2β1 Integrin Expression in Cardiac Fibrosis. Biomed Res Int *2017*. 10.1155/2017/1790808.

257. Lindsey, M.L., Iyer, R.P., Zamilpa, R., Yabluchanskiy, A., DeLeon-Pennell, K.Y., Hall, M.E., Kaplan, A., Zouein, F.A., Bratton, D., Flynn, E.R., et al. (2015). A Novel Collagen Matricryptin Reduces Left Ventricular Dilation Post-myocardial Infarction by Promoting Scar Formation and Angiogenesis. J Am Coll Cardiol *66*, 1364. 10.1016/J.JACC.2015.07.035.

258. Senk, A., and Djonov, V. (2021). Collagen fibers provide guidance cues for capillary regrowth during regenerative angiogenesis in zebrafish. Scientific Reports 2021 11:1 *11*, 1–17. 10.1038/s41598-021-98852-6.

259. Smith, M., Dalurzo, M., Panse, P., Parish, J., and Leslie, K. (2013). Usual interstitial pneumonia-pattern fibrosis in surgical lung biopsies. Clinical, radiological and histopathological clues to aetiology. J Clin Pathol *66*, 896–903. 10.1136/JCLINPATH-2013-201442.

260. Marro, J., Pfefferli, C., De Charles, A.S.P., Bise, T., and Jaźwiñska, A. (2016). Collagen XII Contributes to Epicardial and Connective Tissues in the Zebrafish Heart during Ontogenesis and Regeneration. PLoS One *11*. 10.1371/JOURNAL.PONE.0165497.

261. Bader, H.L., Keene, D.R., Charvet, B., Veit, G., Driever, W., Koch, M., and Ruggiero, F. (2009). Zebrafish collagen XII is present in embryonic connective tissue sheaths (fascia) and basement membranes. Matrix Biol *28*, 32–43. 10.1016/J.MATBIO.2008.09.580.

262. Young, B.B., Zhang, G., Koch, M., and Birk, D.E. (2002). The roles of types XII and XIV collagen in fibrillogenesis and matrix assembly in the developing cornea. J Cell Biochem *87*, 208–220. 10.1002/JCB.10290.

263. Kanisicak, O., Khalil, H., Ivey, M.J., Karch, J., Maliken, B.D., Correll, R.N., Brody, M.J., Lin, S.C.J., Aronow, B.J., Tallquist, M.D., et al. (2016). Genetic lineage tracing defines myofibroblast origin and function in the injured heart. Nat Commun *7*, 1–14. 10.1038/ncomms12260.

264. Kikuchi, K., Gupta, V., Wang, J., Holdway, J.E., Wills, A.A., Fang, Y., and Poss, K.D. (2011). Tcf21+ epicardial cells adopt non-myocardial fates during zebrafish heart development and regeneration. Development *138*, 2895–2902. 10.1242/dev.067041.

265. González-Rosa, J.M., Peralta, M., and Mercader, N. (2012). Pan-epicardial lineage tracing reveals that epicardium derived cells give rise to myofibroblasts and perivascular cells during zebrafish heart regeneration. Dev Biol *370*, 173–186. 10.1016/J.YDBIO.2012.07.007.

266. Wang, Y., Shi, R., Zhai, R., Yang, S., Peng, T., Zheng, F., Shen, Y.N., Li, M., and Li, L. (2022). Matrix stiffness regulates macrophage polarization in atherosclerosis. Pharmacol Res *179*, 106236. 10.1016/J.PHRS.2022.106236.

267. Travers, J.G., Kamal, F.A., Robbins, J., Yutzey, K.E., and Blaxall, B.C. (2016). Cardiac Fibrosis: The Fibroblast Awakens. Circ Res *118*, 1021. 10.1161/CIRCRESAHA.115.306565.

268. Lin, L., and Hu, K. (2014). LRP-1: Functions, Signaling and Implications in Kidney and Other Diseases. Int J Mol Sci *15*, 22887. 10.3390/IJMS151222887.

269. He, Z., Wang, G., Wu, J., Tang, Z., and Luo, M. (2021). The molecular mechanism of LRP1 in physiological vascular homeostasis and signal transduction pathways. Biomedicine & Pharmacotherapy *139*, 111667. 10.1016/J.BIOPHA.2021.111667.

270. Potere, N., Del Buono, M.G., Niccoli, G., Crea, F., Toldo, S., and Abbate, A. (2019). Developing LRP1 Agonists into a Therapeutic Strategy in Acute Myocardial Infarction. Int J Mol Sci *20*. 10.3390/IJMS20030544.

271. Bres, E.E., and Faissner, A. (2019). Low Density Receptor-Related Protein 1 Interactions With the Extracellular Matrix: More Than Meets the Eye. Front Cell Dev Biol *7*. 10.3389/FCELL.2019.00031.

272. Gaultier, A., Hollister, M., Reynolds, I., Hsieh, E. hui, and Gonias, S.L. (2010). LRP1 regulates remodeling of the extracellular matrix by fibroblasts. Matrix Biol *29*, 22. 10.1016/J.MATBIO.2009.08.003.

273. Arai, A.L., Migliorini, M., Au, D.T., Hahn-Dantona, E., Peeney, D., Stetler-Stevenson, W.G., Muratoglu, S.C., and Strickland, D.K. (2020). High-affinity binding of LDL

receptor–related protein 1 to matrix metalloprotease 1 requires protease:inhibitor complex formation. Biochemistry *59*, 2922. 10.1021/ACS.BIOCHEM.0C00442.

274. Toldo, S., Austin, D., Mauro, A.G., Mezzaroma, E., Van Tassell, B.W., Marchetti, C., Carbone, S., Mogelsvang, S., Gelber, C., and Abbate, A. (2017). Low-Density Lipoprotein Receptor–Related Protein-1 Is a Therapeutic Target in Acute Myocardial Infarction. JACC Basic Transl Sci *2*, 561. 10.1016/J.JACBTS.2017.05.007.

275. Mueller, P.A., Zhu, L., Tavori, H., Huynh, K., Giunzioni, I., Stafford, J.M., Linton, M.F., and Fazio, S. (2018). Deletion of Macrophage Low-Density Lipoprotein Receptor-Related Protein 1 (LRP1) Accelerates Atherosclerosis Regression and Increases C-C Chemokine Receptor Type 7 (CCR7) Expression in Plaque Macrophages. Circulation *138*, 1850–1863. 10.1161/CIRCULATIONAHA.117.031702.

276. Grivas, D., González-Rajal, Á., and de la Pompa, J.L. (2021). Midkine-a Regulates the Formation of a Fibrotic Scar During Zebrafish Heart Regeneration. Front Cell Dev Biol *9*. 10.3389/FCELL.2021.669439/FULL.

277. Lien, C.L., Schebesta, M., Makino, S., Weber, G.J., and Keating, M.T. (2006). Gene Expression Analysis of Zebrafish Heart Regeneration. PLoS Biol *4*, 1386–1396. 10.1371/JOURNAL.PBIO.0040260.

278. Luo, J., Uribe, R.A., Hayton, S., Calinescu, A.A., Gross, J.M., and Hitchcock, P.F. (2012). Midkine-A functions upstream of Id2a to regulate cell cycle kinetics in the developing vertebrate retina. Neural Dev *7*, 33. 10.1186/1749-8104-7-33.

279. Horiba, M., Kadomatsu, K., Yasui, K., Lee, J.K., Takenaka, H., Sumida, A., Kamiya, K., Chen, S., Sakuma, S., Muramatsu, T., et al. (2006). Midkine plays a protective role against cardiac ischemia/reperfusion injury through a reduction of apoptotic reaction. Circulation *114*, 1713–1720. 10.1161/CIRCULATIONAHA.106.632273.

280. Gramage, E., D'Cruz, T., Taylor, S., Thummel, R., and Hitchcock, P.F. (2015). Midkine-a Protein Localization in the Developing and Adult Retina of the Zebrafish and Its Function During Photoreceptor Regeneration. PLoS One *10*, e0121789. 10.1371/JOURNAL.PONE.0121789.

281. Ishiguro, H., Horiba, M., Takenaka, H., Sumida, A., Opthof, T., Ishiguro, Y.S., Kadomatsu, K., Murohara, T., and Kodama, I. (2011). A Single Intracoronary Injection of Midkine Reduces Ischemia/Reperfusion Injury in Swine Hearts: A Novel Therapeutic Approach for Acute Coronary Syndrome. Front Physiol *2*. 10.3389/FPHYS.2011.00027.

282. Tang, Y., Kwiatkowski, D.J., and Henske, E.P. (2022). Midkine expression by stem-like tumor cells drives persistence to mTOR inhibition and an immune-suppressive microenvironment. Nature Communications 2022 13:1 *13*, 1–22. 10.1038/s41467-022-32673-7.

283. Tsai, S.L., Baselga-Garriga, C., and Melton, D.A. (2020). Midkine is a dual regulator of wound epidermis development and inflammation during the initiation of limb regeneration. Elife *9*. 10.7554/ELIFE.50765.

284. Filippou, P.S., Karagiannis, G.S., and Constantinidou, A. (2019). Midkine (MDK) growth factor: a key player in cancer progression and a promising therapeutic target. Oncogene 2019 39:10 *39*, 2040–2054. 10.1038/s41388-019-1124-8.

285. Fukui, S., Kitagawa-Sakakida, S., Kawamata, S., Matsumiya, G., Kawaguchi, N., Matsuura, N., and Sawa, Y. (2008). Therapeutic Effect of Midkine on Cardiac Remodeling in Infarcted Rat Hearts. Annals of Thoracic Surgery *85*, 562–570. 10.1016/j.athoracsur.2007.06.002.

286. Weckbach, L.T., Groesser, L., Borgolte, J., Pagel, J.I., Pogoda, F., Schymeinsky, J., Müller-Höcker, J., Shakibaei, M., Muramatsu, T., Deindl, E., et al. (2012). Midkine acts as proangiogenic cytokine in hypoxia-induced angiogenesis. Am J Physiol Heart Circ Physiol *303*, 429–438. 10.1152/AJPHEART.00934.2011/ASSET/IMAGES/LARGE/ZH40161204970006.JPEG.

287. Ikutomo, M., Sakakima, H., Matsuda, F., and Yoshida, Y. (2014). Midkine-deficient mice delayed degeneration and regeneration after skeletal muscle injury. Acta Histochem *116*, 319–326. 10.1016/J.ACTHIS.2013.08.009.

288. Woulfe, K.C., and Sucharov, C.C. (2017). Midkine's Role in Cardiac Pathology. J Cardiovasc Dev Dis *4*. 10.3390/JCDD4030013.

289. Narita, H., Chen, S., Komori, K., and Kadomatsu, K. (2008). Midkine is expressed by infiltrating macrophages in in-stent restenosis in hypercholesterolemic rabbits. J Vasc Surg *47*, 1322–1329. 10.1016/J.JVS.2007.12.037.

290. Weckbach, L.T., Gola, A., Winkelmann, M., Jakob, S.M., Groesser, L., Borgolte, J., Pogoda, F., Pick, R., Pruenster, M., Müller-Höcker, J., et al. (2014). The cytokine midkine supports neutrophil trafficking during acute inflammation by promoting adhesion via β2 integrins (CD11/CD18). Blood *123*, 1887–1896. 10.1182/BLOOD-2013-06-510875.

291. Weckbach, L.T., Preissner, K.T., and Deindl, E. (2018). The Role of Midkine in Arteriogenesis, Involving Mechanosensing, Endothelial Cell Proliferation, and Vasodilation. Int J Mol Sci *19*. 10.3390/IJMS19092559.

Publications

1. Apaydin, O., Altaikyzy, A., Filosa, A., Sawamiphak, S. (accepted to be published in November 2023). Alpha-1 adrenergic signaling drives cardiac regeneration via an extracellular matrix remodeling transcriptional program in zebrafish macrophages. Dev. Cell

2. Apaydin, D.C., Zakarauskas-Seth, B.I., Carnevale, L., Apaydin, O., Perrotta, M., Carnevale, R., Kotini, M.P., Kotlar-Goldaper, I., Belting, H.G., Carnevale, D., Filosa, A., Sawamiphak, S. (2023). Interferon-γ drives macrophage reprogramming, cerebrovascular remodelling, and cognitive dysfunction in a zebrafish and a mouse model of ion imbalance and pressure overload. Cardiovasc Res 119, 1234–1249. 10.1093/CVR/CVAC188.

.

Abbreviations

ACE	Angiotensinogen Converting Enzyme
ADRA	Adrenergic Receptor Alpha
ADRB	Adrenergic Receptor Beta
AFOG	Acid Fuchsin Orange G
ANS	Autonomic Nervous System
BSA	Bovine Serum Albumin
cAMP	Cyclic AMP
cDNA	Complementary DNA
CCL	C-C Motif Chemokine Ligand
CCR	C-C Motif Chemokine Receptor
CHP	Collagen Hybridizing Peptide
CHRNA7	Cholinergic Receptor Nicotinic Alpha 7 Subunit
CD	Cluster Of Differentiation
CNS	Central Nervous System
DAG	Diacylglycerol
DAMPs	Damage Associated Molecular Patterns
DAPI	4′,6-Diamidin-2-Phenylindol
DC	Dendritic Cell
DMSO	Dimethylsulfoxide
dpf	Days Post Fertilization
dpi	Days Post Injury
ECM	Extracellular Matrix
EdU	5-Ethynyl-2′-Deoxyuridine
ELISA	Enzyme-Linked Immunosorbent Assay
FACS	Fluorescence-Activated Cell Sorting
FBS	Fetal Bovine Serum
GO	Gene Ontology
GPCR	G Protein-Coupled Receptor
HBSS	Hank's Balanced Salt Solution
HCR-FISH	Hybridization Chain Reaction Fluorescent *In Situ* Hybridization
hpf	Hour Post Fertilization
hpi	Hour Post Injury
HRP	Horseradish Peroxidase
HSC	Hematopoietic Stem Cell
IFN	Interferon
Ig	Immunoglobulin
IL	Interleukin
IP3	Inositol Triphosphate

MEF	Myocyte Enhancer Factor-2
LRP1	Ldl Receptor-Related Protein
MDK	Midkine
MI	Myocardial Infarction
MMP	Matrix Metalloproteases
MP	Macrophage
mpi	Minutes Post-Injury
mRNA	Messenger RNA
NK	Natural Killer
PBS	Phosphate Buffered Saline
PCNA	Proliferating Cell Nuclear Antigen
PCR	Polymerase Chain Reaction
PFA	Paraformaldehyde
PKA	Protein Kinase A
PKC	Protein Kinase C
PLC	Phospholipase C
PTU	1-Phenyl-2-Thiourea
RNA	Ribonucleic Acid
RT-PCR	Real Time Pcr
scRNAseq	Single-Cell Rna-Sequencing
SDS-PAGE	Sodium Dodecyl Sulfate-Polyacrylamide Gel Electrophoresis
SEM	Standard Error Of The Mean
SMA	Smooth Muscle Actin
SSC	Sodium Chloride Sodium Citrate
TLR	Toll-Like Receptor
TNF	Tumor Necrosis Factor
tSNE	T-Stochastic Neighbor Embedding
UAS	Upstream Activation Sequence
UMAP	Uniform Manifold Approximation And Projection
VEGF	Vascular Endothelial Growth Factor

List of Figures and Tables